Performance assessment of self-adaptive cooling devices under unsteady and non-uniform heat loads

Gerard Laguna Benet

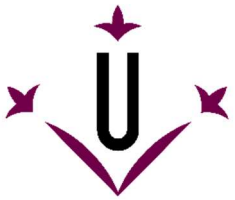

Universitat de Lleida

Ph.D. Thesis

Performance assessment of self-adaptive cooling devices under unsteady and non-uniform heat loads

Thesis presented for the degree of Doctor by Universitat de Lleida in Engineering and Information Technologies

By

Gerard Laguna Benet

Thesis supervisor

Jérôme Barrau

Manel Ibañez Plana

Academic supervisor

Jérôme Barrau

Lleida, April 2020

“There is nothing like looking, if you want to find something.
You certainly usually find something, if you look,
but it is not always quite the something you were after.”

– Gandalf, from The Hobbit, by J. R. R. Tolkien

Acknowledgements

This thesis would not have been done without the work and support of many people who had the bad luck to suffer me during these three years, and whom I would really like to thank:

To my supervisors Jérôme, Joan Ignasi and Manel for their patience, help, and for showing me that I still have a great capacity to improve my writing skills (because there is a lot of room for improvement).

To Luc Fréchette for the opportunity to do my research stage at Université de Sherbrooke (UdeS), and for all his dedication and advice. I want to thank the MICROS research group from UdeS for its hospitality, especially Amrid and Rajesh for having the patience to introduce me to the cleanroom world, even if it was just as a bystander. Also, thanks to Étienne for his practical contributions, but especially for showing me his (shared) passion for destructive tests (of course, always intended for academic purposes…).

To Gemma and Desideri for their crucial work in the lab and for convincing me not to start running the destructive tests every now and then.

And last, but not least, to my office colleagues, Laia and Montse, friends and family for all their support during all the ups and downs of this intense journey.

Thank you all. I could not have done it, or survived it, without you.

Summary

With the end of Dennard scaling, the power and the power density required by chips start to increase. If this trend were to continue, the microelectronics power consumption needed to satisfy efficiency requirements and for thermal management would be prohibitive. To meet the efficiency and thermal management requirements, the chip improvement is limited by restricting the number of cores and their operation frequency. This trend implies the need for a cooling solution that is able to extract the non-uniform and time-dependent high power density heat flux and reduce the temperature non-uniformity, which reduces the electronic reliability.

This thesis is developed in the framework of the Horizon 2020 Project STREAMS (Smart Technologies for eneRgy Efficient Active cooling in advanced Microelectronics Systems), which aims to develop a cooling device that is able to satisfy the microelectronics cooling needs. The main objective of this thesis is to design a microfluidic cell cooling system and assess its impact on the microelectronics and concentrating photovoltaic receivers.

The cooling device is formed by an array of microfluidic cells, each one responsible for removing the local heat flux. Coolant flow is fed in parallel to the cells by interdigitated cold and warm flow channels connected to manifolds. Each cell therefore has a cold inlet flow, irrespective of its location. Heat is removed by the flow through each cell, which can contain microchannels to enhance the heat transfer and self-adaptive valves capable of tailoring the flow rate of each cell to its cooling needs.

In the design stage, the MC6T microfluidic cell is designed and numerically assessed under a non-uniform and time-dependent heat load scenario, reducing the flow rate by 42.5 % and the pressure drop by 81.0 % with respect to the microchannel cooling device under the same boundary conditions. The combination of both low flow rates and pressure drops implies an average pumping power reduction of 89.1 % in comparison to microchannels, while the temperature uniformity is improved by the use of the self-adaptive microfluidic valves.

The impact of this novel cooling solution on the performance of dense array CPV receivers is numerically assessed. Depending on the electrical configuration and the non-uniformity of the illumination profile, the increase in power generation of the dense array CPV receiver can reach up to 9.7 %, compared with the same CPV receiver cooled by microchannels.

Once the concept is validated numerically, and after identifying and resolving the challenges inherent in the microfabrication procedure of self-adaptive cooling devices, selected designs are fabricated in order to assess experimentally the performance of the self-adaptive microfluidic cell cooling device, with and without

self-adaptive valves. A control algorithm tailors the total flow rate to the heat extraction needs. Compared to conventional microchannels with fixed flow rates, the microfluidic cell array without valves improves the pumping power by 83.7 % and improves a 10.8 % in terms of temperature uniformity. However, the array of microfluidic cells with self-adaptive valves reduces the pumping power by 74.7 %, while the temperature non-uniformity is reduced by 31.7 %. When applying the flow rate control algorithm to the microchannels, the pumping power needs of the array of microfluidic cells with and without self-adaptive valves are, respectively, 15.5 % and 45.6 %, compared to microchannels. In these conditions, the temperature uniformity of the microfluidic cell without self-adaptive valves presents a similar behaviour as the flow rate controlled microchannels, however the microfluidic cell with self-adaptive valves improves the temperature uniformity a 23.9 %.

Resum

Degut a la fi de l'escalament de Dennard, la potència i la densitat de potència requerides pel funcionament dels xips comencen a augmentar. Si aquesta tendència continués en augment, el consum d'energia seria prohibitiu tant per criteris d'eficiència com per a la gestió tèrmica. Per tal de complir els criteris d'eficiència i gestió tèrmica, la millora dels xips es va limitar restringint el nombre de nuclis i la seva freqüència de funcionament. Aquesta tendència implica la necessitat d'una solució de refrigeració capaç d'extreure un flux de calor heterogeni d'alta densitat de potència i variant en el temps, a més de reduir el gradient de temperatura que redueix la fiabilitat de l'electrònica.

Aquesta tesi es desenvolupa en el marc del projecte Europeu Horitzó 2020 STREAMS (Smart Technologies for eneRgy Efficient Active cooling in advanced Microelectronics Systems), que té com a objectiu desenvolupar un dispositiu capaç de satisfer les necessitats de refrigeració de la microelectrònica. L'objectiu principal d'aquesta tesi és desenvolupar un sistema de refrigeració de cel·les microfluídiques i avaluar el seu impacte en la microelectrònica i en els receptors fotovoltaics de concentració.

El dispositiu de refrigeració desenvolupat està format per una matriu de cel·les microfluídiques, cadascuna de les quals és responsable de l'extracció del flux de calor local. El refrigerant es subministra a les cel·les de forma paral·lela mitjançant canals de subministrament i de recollida connectats als col·lectors. Per tant, cada cel·la té l'entrada de refrigerant fred independentment de la seva localització. La calor és extreta per cada cel·la, la qual pot contenir microcanals que milloren la transferència de calor i vàlvules autoadaptatives capaces d'ajustar el cabal a les seves necessitats de refrigeració.

En l'etapa de disseny, la cel·la microfluidica MC6T és dissenyada i avaluada numèricament en un escenari de càrrega de calor no uniforme i variable en el temps, reduint el cabal en un 42.5 % i la caiguda de pressió en un 81.0 % comparat amb un dispositiu de microcanals sotmès a les mateixes condicions. La combinació de la reducció de cabal i la caiguda de pressió suposa una disminució de la potència mitjana de bombeig en un 89.1 % comparat amb un dispositiu de microcanals. Tanmateix també es millora la uniformitat de temperatura gràcies a l'ús de les vàlvules microfluídiques.

Altrament, s'avalua numèricament l'impacte d'aquest nou dispositiu de refrigeració sobre els receptors fotovoltaics de concentració solar (CPV) de matriu densa. Segons la configuració elèctrica dels receptors i de la no uniformitat del perfil d'irradiació, l'increment de potència pot arribar a un 9.7 % comparat amb el mateix receptor CPV refrigerat amb microcanals.

Un cop validat numèricament el concepte i després de la identificació i resolució dels reptes inherents al procediment de microfabricació dels dispositius autoadaptatius de refrigeració, es fabriquen els dispositius dissenyats per tal d'avaluar experimentalment el rendiment del sistema de cel·les microfluídiques, amb vàlvules autoadaptatives i sense. A més a més, s'aplica un algoritme de control que adapta el cabal total del dispositiu a les necessitats d'extracció d'aquest. Si es compara el nou disseny amb un dispositiu de microcanals convencionals amb cabal constant, la matriu de cel·les microfluidiques sense vàlvules redueix la potència de bombeig en un 83.7 % i presenta una millora del 10.8 % en uniformitat de temperatura. Tot i això, la matriu de cel·les amb vàlvules autoadaptatives redueix la potència de bombeig en un 74.7 %, al mateix temps que també millora la uniformitat de temperatura en un 31.7 %. Altrament, quan s'aplica l'algoritme de control de cabal al dispositiu de microcanals, la potència de bombeig requerida pels dispositius de cel·les microfluídiques amb vàlvules autoadaptatives i sense és, respectivament, del 15.5 % i del 45.6 % en comparació amb microcanals. En aquestes condicions, la uniformitat de temperatura de les cel·les microfluídiques sense vàlvula és semblant a la dels microcanals amb cabal controlat, però el dispositiu de cel·les amb vàlvules millora la uniformitat de temperatura en un 23.9 %.

Resumen

Con el fin del escalamiento de Dennard, la potencia y la densidad de potencia requeridas por chip empiezan a aumentar. Si esta tendencia continuara, el consumo de energía sería prohibitivo tanto por criterios de eficiencia como para la gestión térmica. Para cumplir los criterios de eficiencia y gestión térmica la mejora de los chips se limitó restringiendo el número de núcleos y su frecuencia de funcionamiento. Esta tendencia implica la necesidad de una solución de refrigeración capaz de extraer un flujo de calor heterogéneo de alta densidad de potencia y variando en el tiempo, además de reducir el gradiente de temperatura que reduce la fiabilidad de la electrónica.

Esta tesis se desarrolla en el marco del proyecto europeo Horizonte 2020 STREAMS (Smart Technologies for eneRgy Efficient Active cooling in advanced Microelectronics Systems), que tiene como objetivo desarrollar un dispositivo de refrigeración capaz de satisfacer las necesidades de refrigeración en la microelectrónica. El objetivo principal de esta tesis es desarrollar un sistema de refrigeración de celdas microfluídicas y evaluar su impacto en microelectrónica y en receptores fotovoltaicos de concentración.

El dispositivo de refrigeración está formado por una matriz de celdas microfluídicas, cada una de las cuales es responsable de la extracción del flujo de calor local. El refrigerante se suministra a las celdas paralelamente mediante canales de suministro y recogida conectados a los colectores. Por lo tanto, cada celda tiene la entrada de refrigerante frío independientemente de su localización. El calor es extraído por cada celda la cual puede contener microcanales para mejorar la transferencia de calor y válvulas autoadaptativas capaces de adaptar el caudal de cada celda a sus necesidades de refrigeración.

En la etapa de diseño, la celda microfluídica MC6T es diseñada y evaluada numéricamente en un escenario de carga de calor no uniforme y variable en el tiempo, reduciendo el caudal un 42.5 % y la caída de presión un 81.0 % comparado con un dispositivo de microcanales sometido a las mismas condiciones. La combinación de la reducción de caudal y caída de presión supone una reducción de la media de potencia de bombeo de un 89.1 % en comparación con microcanales, mientras se mejora la uniformidad de temperatura gracias al uso de las válvulas microfluídicas.

En otro caso, se evalúa numéricamente el impacto de este nuevo dispositivo de refrigeración sobre los receptores fotovoltaicos de concentración solar (CPV) en matriz densa. Según la configuración eléctrica de los receptores y de la no uniformidad del perfil de irradiación, el incremento de potencia puede llegar a un 9.7 %, comparado con el mismo receptor CPV refrigerado con microcanales.

Una vez validado numéricamente el concepto y tras la identificación y resolución de retos inherentes al procedimiento de microfabricación de los dispositivos autoadaptativos de refrigeración, se fabrican los dispositivos diseñados para evaluar experimentalmente el rendimiento del sistema de celdas microfluídicas, con y sin válvulas autoadaptativas. Además, se aplica un algoritmo de control que adapta el caudal total del dispositivo a las necesidades de extracción del dispositivo. Comparando con microcanales convencionales con caudal constante, la matriz de celdas microfluídicas sin válvulas reduce la potencia de bombeo en un 83.7 % y presenta una mejora del 10.8 % en uniformidad de temperatura. Sin embargo, la matriz de celdas con válvulas autoadaptativas reducen la potencia de bombeo en un 74.7 %, al tiempo que también mejora la uniformidad de temperatura en un 31.7 %. De lo contrario, cuando se aplica el algoritmo de control de caudal también al dispositivo de microcanalas, la potencia de bombeo requerida por los dispositivos de celdas microfluídicas con y sin válvulas autoadaptativas es, respectivamente, el 15.5 % y el 45.6 % comparado con microcanales. En estas condiciones, la uniformidad de temperatura de las celdas microfluídicas sin válvula es similar a la de los microcanales con caudal controlado, pero el dispositivo de celdas con válvulas mejora la uniformidad de temperatura en un 23.9%.

Table of contents

Nomenclature

ΔP	Pressure drop [Pa]
ΔT	Increase of temperature [ºC]
ΔT_{chip}	Temperature difference on the chip base [ºC]
ΔTq	Normalized temperature difference [ºC]
μ	Fluid's dynamic viscosity [Pa·s]
ρ	Density [kg/m^3]
σ_m	Standard deviation of the mean irradiation of the modules [suns]
b	Valve width [µm]
C	Sun concentration [suns]
C_0	Reference solar concentration [suns]
C_1	Equivalent band gap [J]
COP	Coefficient of performance [-]
C_p	Specific heat capacity at constant stress [J/(kg·K)]
e	Valve eccentricity [µm]
e^-	Electron charge [C]
Eg	Energy gap [eV]
F	Volume force vector [N/m^3]
FF	Fill Factor [-]
h	Valve thickness [µm]
I	Current [A]
I_0	Temperature dependence of the equivalent reverse diode current [A]
$I_{0'}$	Reverse current factor independent of the voltage [A/K^3]
I_L	Short-circuit current [A]
J_{mp}	Current density at maximum power point [A/cm^2]
J_{sc}	Current density at short circuit [A/cm^2]
k	Thermal conductivity [W/(m·K)]
K_B	Boltzman constant [J/K]
L	Valve length [mm]
n	Ideality reduced factor [-]
n_m	Number of modules [-]
P	Power [W]
p	Pressure [Pa]
P_{mp}	Power density at the maximum power point [W/cm2]
P_{pump}	Hydraulic power [W]
Q	Flow rate [ml/min]
q"	Heat flux [W/cm^2]
Q_{hs}	Contains additional heat sources [W/m^3]
Q_{max}	Maximum flow rate [ml/min]
Q_p	Work done by pressure changes [W/m^3]
Q_{vd}	Viscous dissipation [W/m^3]
R	Thermal resistance [m^2·K/W]
$\bar{R}_S$	Mean irradiation of the entire CPV receiver [suns]
R_{si}	Mean solar irradiation of the module *i* [suns]
T	Absolute temperature [K]
t	time [s]
T_{chip}	average temperature on the chip base [ºC]

$T_{chip,max}$	maximum temperature on the chip base [ºC]
T_{in}	temperature inlet [ºC]
u	velocity vector of translational motion [m/s]
V	Potential [V]
V_{mp}	Potential at the maximum power point [V]
V_{oc}	Potential at open circuit [V]
V_T	thermal voltage [V]

1. Introduction

1.1. Cooling, the challenge in microelectronics

Gordon Moore observed in 1965 that the number of components on an integrated circuit (IC) had doubled every year on average since the beginning of this technology in 1959. He estimated, based on economic considerations of cost and yield, that this rate would continue for at least 10 years. He also pointed out that reducing the dimensions of an integrated structure led to increasing the operation speed, demanding identical power density [1].

In 1975, 10 years later, Gordon Moore re-evaluated his analysis which, as predicted, took an exponential growth but decomposed the trend of the IC complexity curve into various components (die size, dimension reduction, the product of size and dimensions and the cleverness of the device and the circuit). He determined that the increase of complexity would approximately double every two years rather than every year [2]. This prediction was named Moore's law. In 2015, the logic gate's energy efficiency continues to scale, but the data-carrying capacity and the wire's efficiency are not improving at the same rate. This, associated with the change of paradigm from computation-centric to data-centric programming, could change the trend and break Moore's law [3].

Robert H. Dennard observed that, with the reduction of the component area by a factor of K^2, the electrode spacing is decreased by a factor of K, so the capacitances are reduced by the same factor. The reduced capacitances are the result of the unchanged device resistances V/I. Due to the reduced voltage and current levels, the power dissipation of each circuit is reduced by K^2. Therefore, the decreasing size and increasing performance of MOSFET devices in IC lead to a constant power density. So, if many more circuits are placed on a given chip, the cooling problem is essentially unchanged.

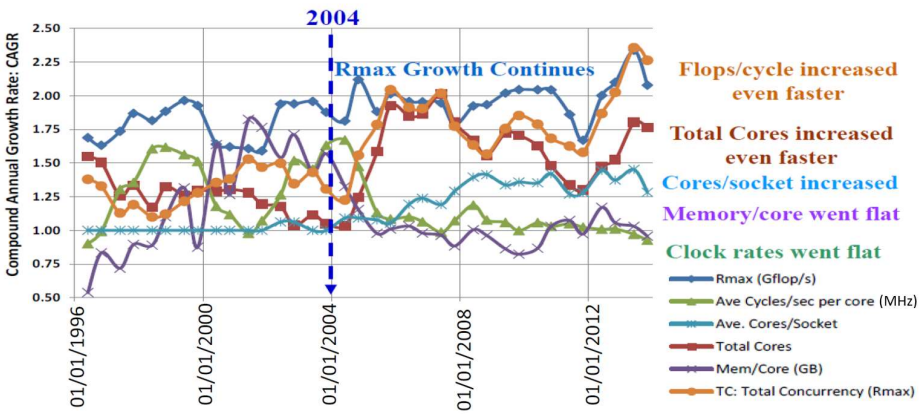

Figure 1: The evolution of CPU characteristics 1996-2012 [4]

This prediction was called Dennard scaling [5]. However, around 2004, the IC was reduced to a size for which it was not possible to reduce the voltage, so the power

density could reach unsustainable levels. The industry faces this challenge with multi-core processors achieving improvements in the maximum computer performance (R_{max}). However, the clock rates are not increasing due to the power restriction limiting the computational improvement [3,6] (Figure 1)

If chip architects only operate the chips at maximum operation frequency and continue adding more cores to the chips, the power consumption needed to satisfy efficiency requirements and for thermal management will be prohibitive (Figure 2). To operate within reasonable bounds, the chip improvement must be limited by restricting the number of cores and their operation frequency [7]. Also, the multicore scaling and the power constraints have led to the concept of "dark silicon", silicon that is underutilized [6,8]. The end of Dennard scaling caused a change in the microelectronics thermal management paradigm, evolving to an increase of the power density extraction requirements. Further, the multicore scaling and the dark silicon boost the power non-uniformities, which lead to temperature gradients in the package, increasing the thermal stress in the chip to substrate or heatsink interface, and so reducing the electronic reliability [9,10].

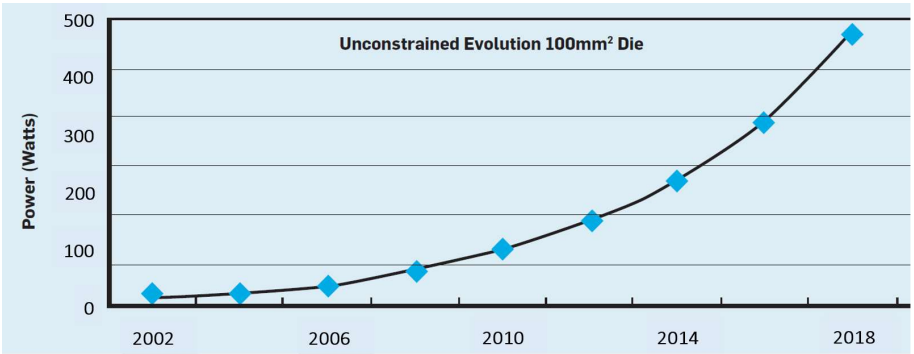

Figure 2: Unconstrained evolution of microprocessor results in excessive power consumption [7]

The increase in power demand has a direct impact on energy consumption worldwide. Data centres are infrastructures housing hundreds of IT (Information Technology) servers running 24 hours a day, 7 days a week and 365 days a year [11].

IT consumes around 10 % of the worldwide energy generation, around 1500 TWh per year. From this, data centres consume up to 23 % of the energy, 350 TWh in 2013. In the US the data centre energy consumption is expected to grow by over 50 % from 2013 to 2020 [12].

A large part of the data centre's energy consumption is for the thermal management and therefore the power dissipation has to be managed skillfully. In 2009, it was estimated that the energy consumption due to thermal management was similar to the energy used by the servers [13]. The thermal management in some new data centres was optimised to be approximately 33 % of the total energy consumption

of the facility. Despite the increase of data centres' efficiencies, these facilities generate a massive amount of heat through their continuous operation. This paradigm leads to a demand for efficient cooling solutions that are able to dissipate power densities that have risen to unprecedented levels in recent years [11].

1.2. Objectives of this thesis

The objectives of this thesis are the following:

1. Design and validate a cooling device for microelectronic systems based on an array of microfluidic cells, reducing the pressure drop by 25 % compared with the state of the art, while maintaining the same temperature limitation in a non-uniform and time-dependent heat load scenario.
2. Design and demonstrate a cooling system that is able to self-adapt its distribution of local heat extraction capacity to non-uniform and time-dependent heat load scenarios, in order to improve the temperature uniformity with lower energy consumption than the current solutions.
3. Design and fabricate a microelectronics cooling system which reduces energy consumption by 50 % compared to the state of the art.
4. Design, build and develop the control software for a test bench in order to test experimentally the devices developed.
5. Assess the proposed cooling solution impact in other fields requiring high heat flux extraction capacities.

In order to assess these objectives, microchannels are taken as the state of the art reference technology.

1.3. Outline of this thesis

1.3.1. Thesis overview

The present thesis is structured as a collection of papers organised in the three central chapters.

After the introductory chapter 1, the objectives 1 to 3 are numerically addressed in chapter 2, focused on the designs and simulation of the microfluidic cell cooling system with the aim of improving both the cooling efficiency and the temperature uniformity of the chip. This chapter is organised in two blocks, an introductory section with the numerical models applied and a second part with the results published in three papers.

Chapter 3, devoted to objective 5, evaluates the impact of the proposed cooling solution on the performance of a dense array CPV receiver. This chapter is structured in three blocks: a brief introduction to current CPV cooling solutions, the description of the electrical model applied in simulations and the three published papers with the results.

Chapter 4, focused on the experimental tasks, is structured in three parts: a description of the experimental setup, fabrication of the cooling devices and the experimental results obtained. Finally, discussion and conclusions are considered in chapter 5.

1.3.2. Publications in this thesis

Articles published from chapter 2:

1. “Microfluidic cell cooling system for electronics” published in January 2017 at THERMINIC 2017 - 23rd Int. Work. Therm. Investig. ICs Syst.
   Authors: Gerard Laguna, Hassan Azarkish, Montse Vilarrubí, Manel Ibañez, Joan Rosell, Yina Betancourt, Josep Illa, Louis-Michel Collin, Jérôme Barrau, Luc Fréchette, Perceval Coudrain and Guillaume Savelli.
   https://doi.org/10.1109/THERMINIC.2017.8233790
2. “Numerical parametric study of a hotspot-targeted microfluidic cooling array for microelectronics” published in November 2018 in Applied Thermal Engineering, volume 144.
   Authors: Gerard Laguna, Montse Vilarrubí, Manel Ibañez, Yina Betancourt, Josep Illa, Hassan Azarkish, Amrid Amnache, Louis-Michel Collin, Perceval Coudrain, Luc Fréchette and Jérôme Barrau.
   https://doi.org/10.1016/j.applthermaleng.2018.08.030

3. “Impact of the self-adaptive valve behavior on an array of microfluidic cells under unsteady and non-uniform heat load distributions” published in January 2019 in the Journal of Applied Fluid Mechanics, volume 12.
   Authors: Gerard Laguna, Montse Vilarrubí, Manel Ibañez, Joan Rosell, Ferran Badia, Hassan Azarkish, Louis-Michel Collin, Luc Fréchette and Jerome Barrau.

Articles published from chapter 3:

4. “Distributed and self-adaptive microfluidic cell cooling for CPV dense array receivers” published in September 2017 in AIP Conference Proceedings, volume 1881.
   Authors: Gerard Laguna, Jérôme Barrau, Luc Fréchette, Joan Rosell, Manel Ibañez, Montse Vilarrubí, Yina Betancourt, Hassan Azarkish, Louis-Michel Collin, Alvaro Fernandez and Gonzalo Sisó.
   https://doi.org/10.1063/1.5001444
5. “Dense array CPV receivers: Impact of the cooling device on the net PV output for different illumination profiles” published in September 2018 in AIP Conference Proceedings, volume 2012.
   Authors: Gerard Laguna, Montse Vilarrubí, Alvaro Fernandez, Gonzalo Sisó, Joan Rosell, Manel Ibañez, Josep Illa, Ferran Badia, Luc Fréchette, Maxime Darnon, Louis-Michel Collin, Alain Dollet and Jérôme Barrau.
   https://doi.org/10.1063/1.5053536
6. “Assessment of the impact of non-uniform illumination and temperature profiles on a dense array CPV receiver performance” published in September 2018 in Solar Energy, volume 171.
   Authors: Álvaro Fernández, Gerard Laguna, Joan Rosell, Montse Vilarrubí, Manel Ibañez, Gonzalo Sisó, Josep Illa and Jérôme Barrau.
   https://doi.org/10.1016/j.solener.2018.07.001

Article from chapter 5:

7. “Experimental study of a microfluidic cell cooling for microelectronics” unpublished.
   Authors: Gerard Laguna, Desideri Regany, Gemma Antoni, Rajesh Pandiyan, Amrid Amnache, Manel Ibañez, Luc Fréchette and Jérôme Barrau

1.4. Streams H2020 Project

This thesis is developed in the framework of the Horizon 2020 Project STREAMS (Smart Technologies for eneRgy Efficient Active cooling in advanced Microelectronics Systems), studying mainly the implementation of the microfluidic cell system in microelectronics systems but also in other applications [14].

The consortium of the STREAMS project is composed of one of the leading European industrial manufacturers in the electronics area (STMicroelectronics), three research and technology organisations (Commissariat à l'énergie atomique et aux énergies alternatives (CEA), Centre National de la Recherche Scientifique - Laboratoire Nanotechnologies Nanosystèmes (CNRS - LN2) and Hahn-Schickard-Gesellschaft (HSG)), and two academic bodies (University of Lleida (UdL) and Albert-Ludwigs University of Freiburg (UFR-IMTEK)).

The active cooling proposal in STREAMS consists of a generic, smart, adaptable and embedded thermal management solution, targeting a 50 % reduction in power consumption, a 70 % drop in footprint with no efficiency reduction compared to the state of the art.

The European project will strive to achieve three functionalities from low technological readiness (TRL 2 or 3 [15]) to reach the laboratory demonstration (TRL4):

- Functionality 1: Versatile microfluidic actuation (starting at TRL2), to be able to adapt to variable and time-dependent scenarios in an energy-efficient way.
- Functionality 2: Anticipating the thermal map (starting at TRL3) to be able to detect the heat extraction needs and respond in real time to the non-uniform and time-dependent thermal management problem.
- Functionality 3: Thermal energy harvesting (starting at TRL2), to be able to generate enough energy to power the control of the thermal management solution.

In order to successfully integrate these three new functionalities in a system on package, the project team focuses on accomplishing these specific objectives:

- O1: Lay out advanced functionalities of realistic and representative use-cases with non-uniform and time-dependent heat load distributions including hotspot areas (150 to 300 W/cm^2) and background zones (20 W/cm^2).
- O2: Reduce by 25 % the pressure loss and the fluid flow rate, keeping the temperature below 15 % of the acceptable limits of each component for non-uniform time- and space-dependent heat loads by developing self-adaptive and controlled microfluidic actuators.

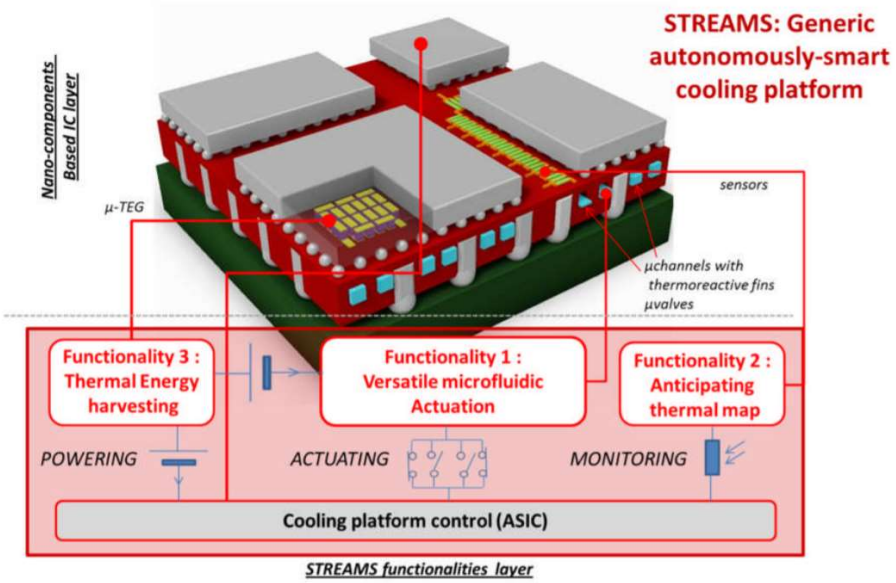

Figure 3: STREAMS concept [14]

- O3: Integrate on-chip passive heat flux sensors, with sensitivity up to 100 mV/K, at the interposer level in order to anticipate the alteration of the thermal map (time response ~200 ms, lateral spatial resolution = 500 µm).
- O4: Take advantage of the existing thermal gradients with integrated nanostructured thermoelectric generators to harvest up to 10 mW to power local functionalities (power management and read-out circuits, control ASIC).
- O5: Incorporate the developed functionalities into a silicon-based interposer to demonstrate a smart, adaptable and embedded active cooling thermal management solution with a reduced footprint (reducing the thickness by 70 %) and reduced consumption (50 % energy reduction).
- O6: Evaluate the reliability and performance of the developed thermal management solution on real future high performance applications in micro-servers (dissipating 50 W) and network use cases (dissipating 200 W).

The performance of the thermal management solution is determined by three main physical indicators:

- Cooling efficiency: Liquid cooling is worthwhile because, compared to air cooling, it increases by up to three orders of magnitude the transfer coefficient (h). However, the existing liquid solutions which prevent overheating well, tend to overcool. The STREAMS objective is to perform a similar cooling efficiency to the existing solutions but with

configurations that are adaptable to widely time-dependent and non-uniform heat distributions, avoiding both overheating and overcooling.

- Compactness: in order to extract the required heat, solutions with low heat extraction capacities like passive air cooling have the disadvantage of using large contact areas and becoming large cooling systems. As liquid cooling has a high heat extraction capacity value compared to air cooling, it tends to be more compact. By developing an integrated liquid cooling, STREAMS reduces the active cooling footprint in terms of package thickness by 70 % compared to the state of the art.
- Consumption: STREAMS reduces 50 % of the cooling thermal management solution energy consumption through smart control, tailoring the activation of the cooling system to the cooling requirements.

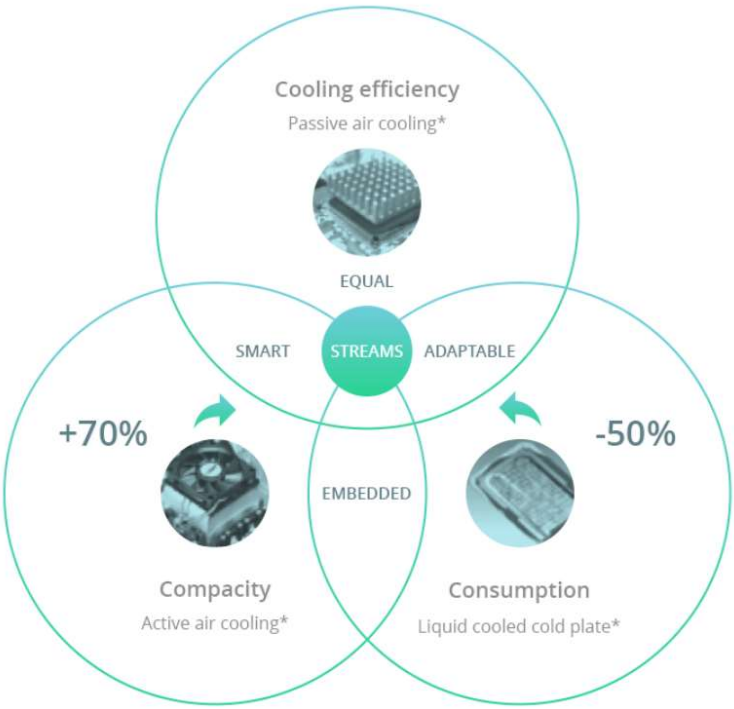

Figure 4: STREAMS strategy and positioning versus actual state-of-the-art cooling technologies low points [14]

This thesis is focused on designing and testing the devices to accomplish the first functionality (versatile microfluidic actuation) with fixed structures and microfluidic valves [16]. The impact of this self-adaptive cooling solution in other application fields is also an object of study.

1.5. Microfluidic device development

In order to be able to assess the cooling system with the upcoming generations of microelectronics, an element to simulate the non-uniform and high-density heat flux in the STREAMS project is needed. For this purpose, a resistance pattern is used to create a non-uniform heat flux distribution, called the Thermal Test Chip (TTC). This pattern is composed of four RTDs (resistance temperature detectors): the central heater, one hotspot on each side of the central heater, and the peripheral heater surrounding the central and the hotspots heaters (Figure 5a). The set of RTDs is able to generate a non-uniform and time-dependent heat flux. But each RTD can be used to detect the temperature, so the thermal map is known at each instant (Figure 5b).

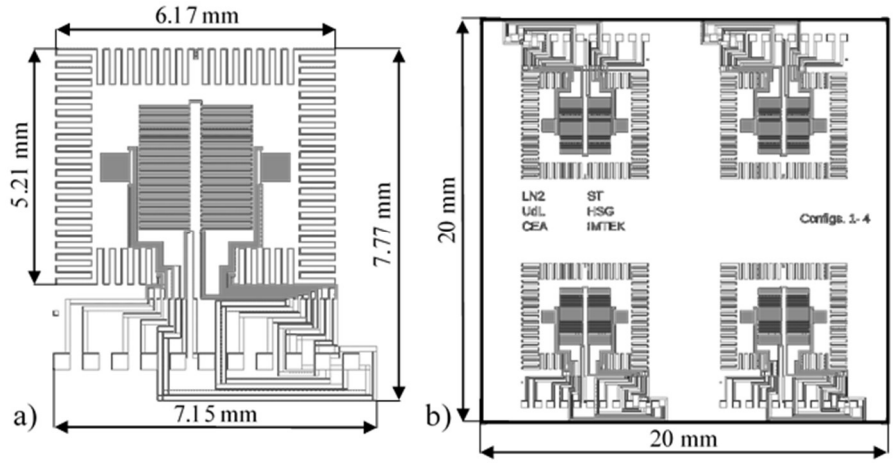

Figure 5: a) Thermal test chip (TTC) composed of 4 RTDs, b) scheme of the configuration of the 4 TTCs placed on each device

The design of the STREAMS device is based on an array of microfluidic cells. A distributor, in charge of feeding and collecting the coolant from the cells, is located on the opposite side from the heaters, the cold side of the cell (Figure 6a and Figure 6b). Compared to the microchannel cooling solution (nowadays, the reference in liquid cooling), the shorter flow path length of this system presents a lower pressure drop and therefore lower pumping power needs (Figure 6c). Also, this system tailors the flow rate distribution in the array of microfluidic cells through the use of microfluidic valves which are able to open and close by thermal expansion as a function of their own temperature [16] (Figure 7). This smart behaviour allows the cooling device to match the distribution of the local heat extraction capacity to time-dependent and non-uniform cooling needs.

In the first steps of the STREAMS device design, the microfluidic cell was just an empty cavity (MC0) of 1200 x 2000 μm^2 with a microvalve (125 µm wide by 1000 µm long) placed as close as possible to the heat source (Figure 6c). The cell's

inlets and outlets were hydraulically connected to a distributor designed to be fed by a central channel and to take the fluid from the sides of the device (Figure 6a and Figure 6b). This distributor was designed in order to lower the pressure drop by reducing the flow path length, being fed by the middle of the device.

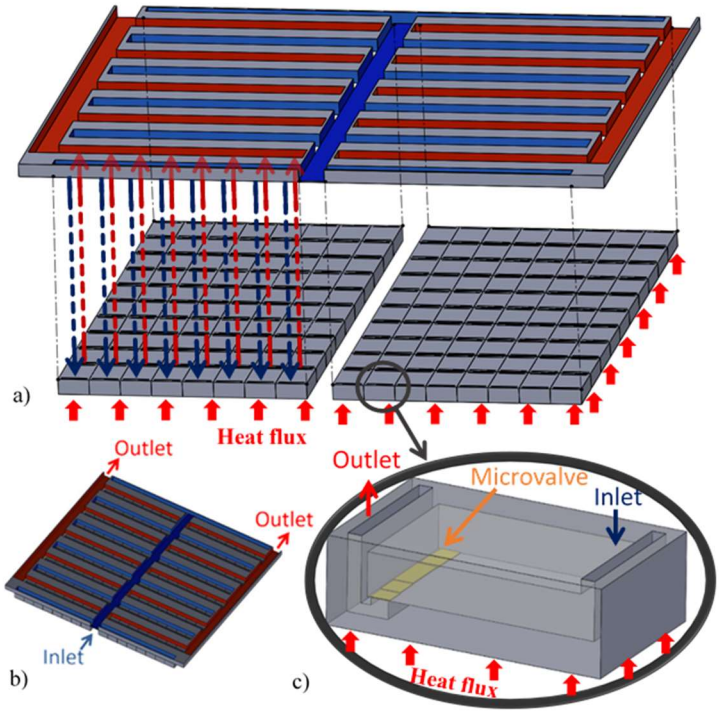

Figure 6: First iteration in the design of the STREAMS cooling device: a) microfluidic cell matrix and distributor assembly b) distributor above cell array c) microfluidic cell MC0 [17]

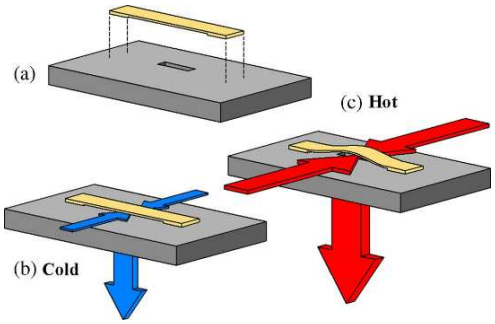

Figure 7: Microvalve a) placement, b) cold position and c) hot position [16]

This first iteration presented two main problems: on the one hand, the microfluidic cell presents a low heat transfer coefficient so it requires a huge flow rate to meet the cooling performance requirements, even higher than microchannels [17]. On the other hand, the central location of the inlet channel implied an uncooled zone in the middle of the chip.

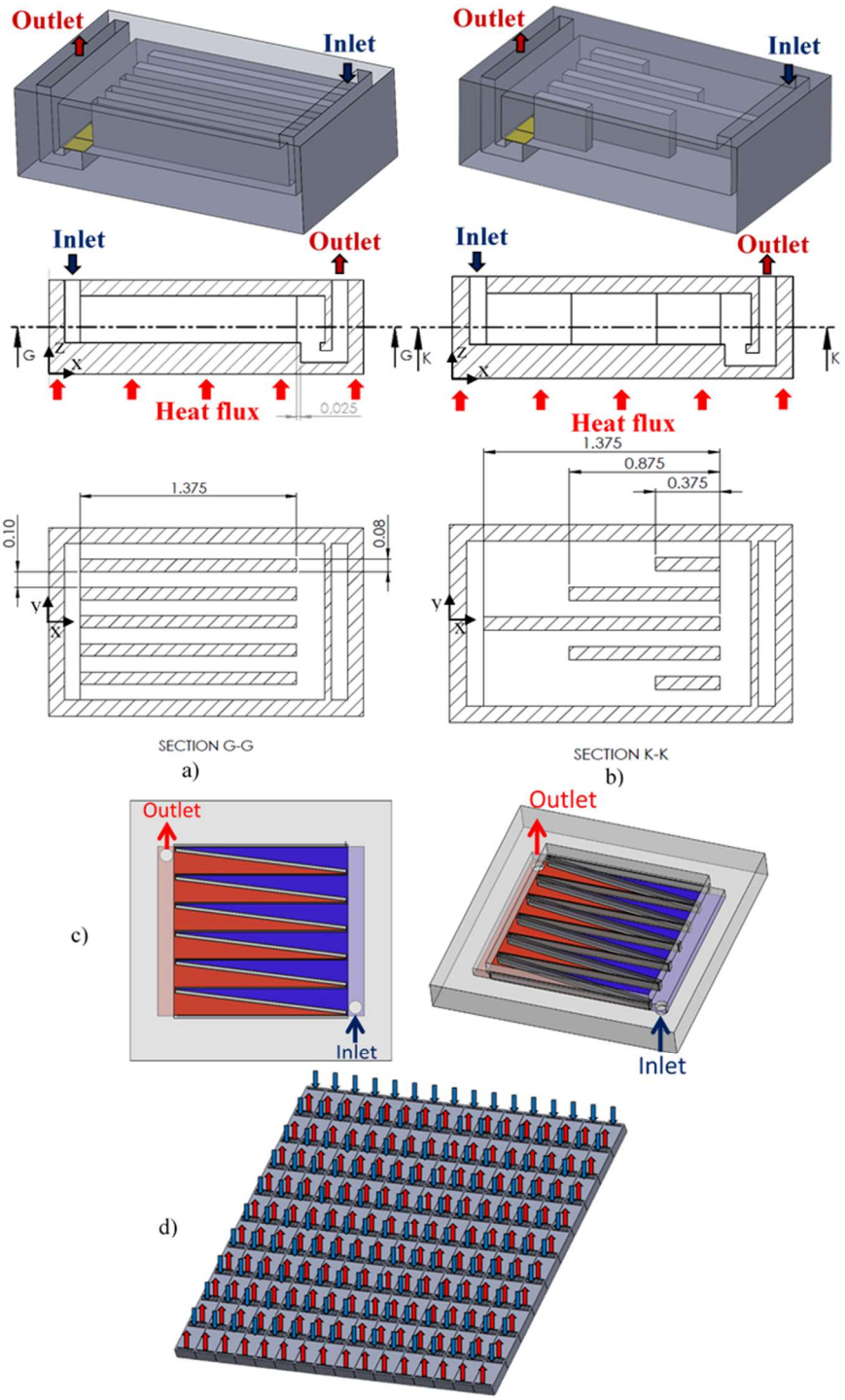

Figure 8: Second iteration of microfluidic cell: a) MC6, b) MC6T [17,18], c) distributor, d) microfluidic cell matrix

To address these drawbacks, some internal geometries were studied in order to enhance the cell's heat transfer coefficient. First of all, the MC6 microfluidic cell was proposed. This cell was similar to MC0, but including 6 microchannels along the microfluidic cell (Figure 8a). With the addition of these microchannels inside the microfluidic cell, the heat transfer was boosted, having a competitive system compared to the microchannels. However, there was room for improvement in the temperature uniformity and pumping power needs. In order to accomplish these goals, the MC6T cell was proposed. This cell uses the same concept as MC6, but the microchannels inside the cell present a tailored length to decrease the heat transfer next to the inlet, reducing the pressure drop and the temperature non-uniformity along the flow path (Figure 8b). The distributor (Figure 8c) was redesigned in order to be able to refrigerate the entire 20 x 20 mm^2 chip surface with a continuous microfluidic cell array of 16 x 10 cells (Figure 8d). Also, the channels used to feed and collect the coolant from the microfluidic cells present a variable width in order to hydraulically equilibrate the circuit.

From the studied configurations, the device composed of 16 x 10 MC6T microfluidic cells is selected for fabrication because of its better performance results from simulations [17]. However, after the experimental characterisation of the microvalves, the system was redesigned in order to fit longer microvalves (1720 x 260 μm^2), so as to increase the flow rate that can be fed into the cell. Moreover, the valve was moved to the top layer for fabrication concerns, leading to the creation of a second cavity in order to place the valve (Figure 9). These modifications required an adjustment of the cell size to 3250 x 1950 µm, which also reduces the cell array to a 6 x 10 cell matrix in order to fit in the 20 x 20 mm^2 device area.

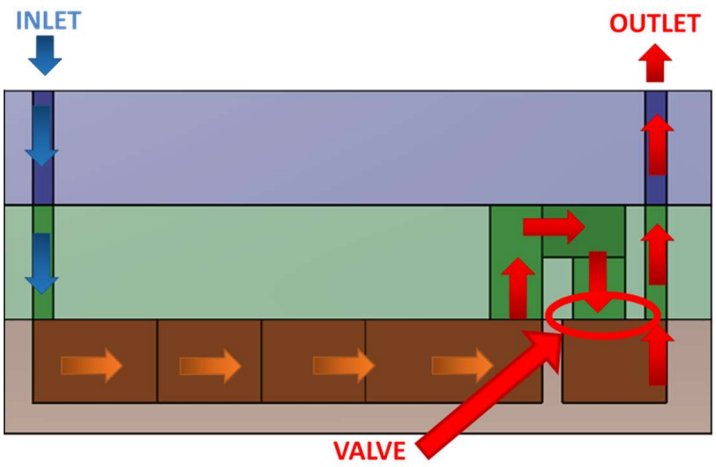

Figure 9: Redesign of the MC6T cell

Additionally, some studies showed a relevant thermal spreading effect between the microfluidic cells. The chip surface of a 3 x 3 MC6T microfluidic cell array at 150 W/cm^2, applying to the 9 cells the flow rate needed for an isolated cell at this heat flux to stay below 85 ºC, has a temperature gradient along the long side of the cell (Figure 10).

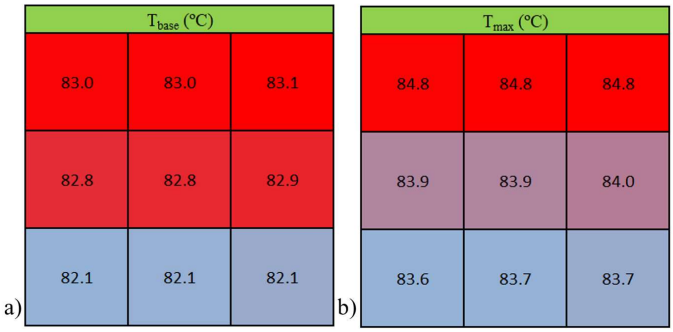

Figure 10: Temperature distribution of the microfluidic cells submitted to a uniform 150 W/cm^2 with the V60 valve: a) average base temperature, b) maximum temperature

For this thermal gradient the conduction of the microfluidic cell placed in rows, forming a single cell to 10 cells, was studied. All these cells are submitted to a 20 W/cm^2 heat flux (background) and cooled with the 50 ºC flow rate required to maintain the isolated cell's maximum temperature below 85 ºC (Figure 11).

The power absorbed by the first cells is lower than the power delivered to them because of the thermal conduction in the Y axis (Figure 11). The power absorbed by the last cells is higher than the power delivered to them. This effect causes the variation in temperature between the individual cells and the arrays. Also, the power absorbed by the first and the last cell on the 6 to 10 cells arrays is stabilised. This is due to the uniformity of the boundary conditions on the central cells. The cells from the middle of the array have the same heat flux input from the previous cell as the output heat flux to the next cell in the array. For this reason, the central cell absorbs approximately 0.48 W delivered by the cell.

This effect contradicts one of the goals of the microfluidic cell system, the decoupling of the cell temperature and its position. With this thermal gradient, the cells which have the inlet on the border of the device will be colder than the ones which have the outlet on the corner of the device. For this reason, the scheme of the microfluidic cell was changed to a flip configuration (Figure 12b) in order to break the Y-axis thermal gradient (Figure 12a).

With the application of the flip cell distribution, the initial assumption of no thermal spreading is valid when no hotspots are used. When hotspots are used (hotspot at 300 W/cm^2 and background at 20 W/cm^2), around 10 % of the power delivered to

the hotspot is absorbed by the surrounding cells by spreading so, in this case, it should be considered as spreading.

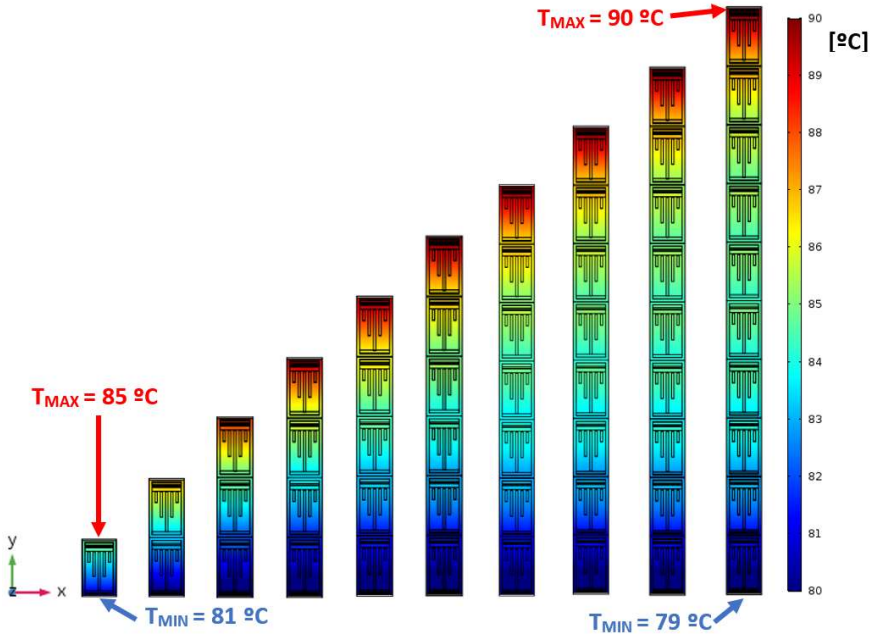

Figure 11: Base temperature of cell rows, from a single cell to ten, all with the same flow rate and submitted to 20 W/cm²

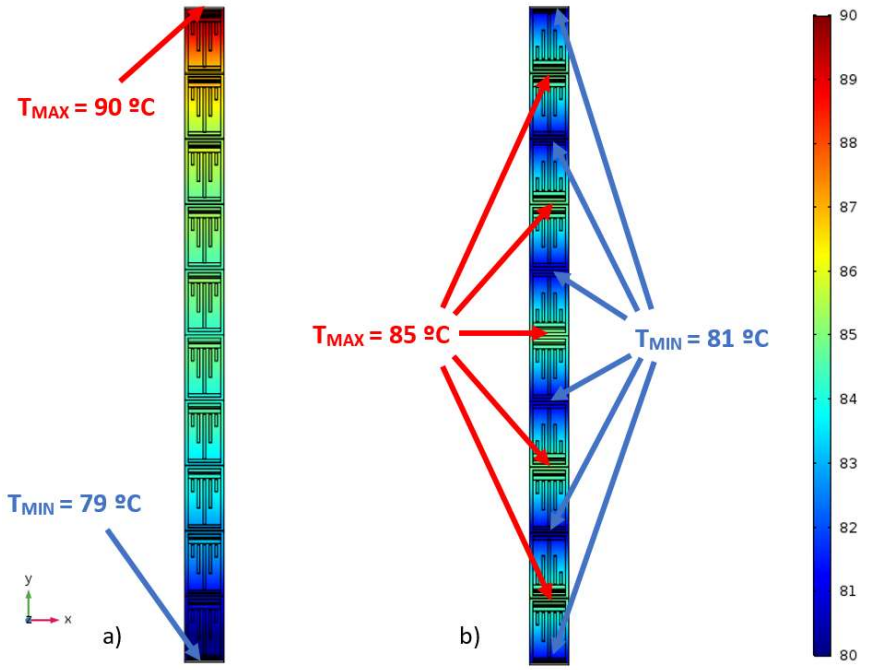

Figure 12: Temperature comparison between 10-cell row: a) initial placement configuration, b) flipped cell

This change of configuration also had a direct effect on the distributor geometry. Also, it was decided to 3D print the distributor, which was initially planned to be built with PDMS. Taking into account the 3D print resolution and tolerances, 7 channels were designed, which each one feeding or collecting the flow rate of two microfluidic cells rows, except the ones on the corners which collect the flow rate of only one row of cells (Figure 13a). Placing 7 microchannels instead of the 12 of the previous distributor, with the same available surface, allows them to be made wider, reducing in this way the pressure drop in the distributor.

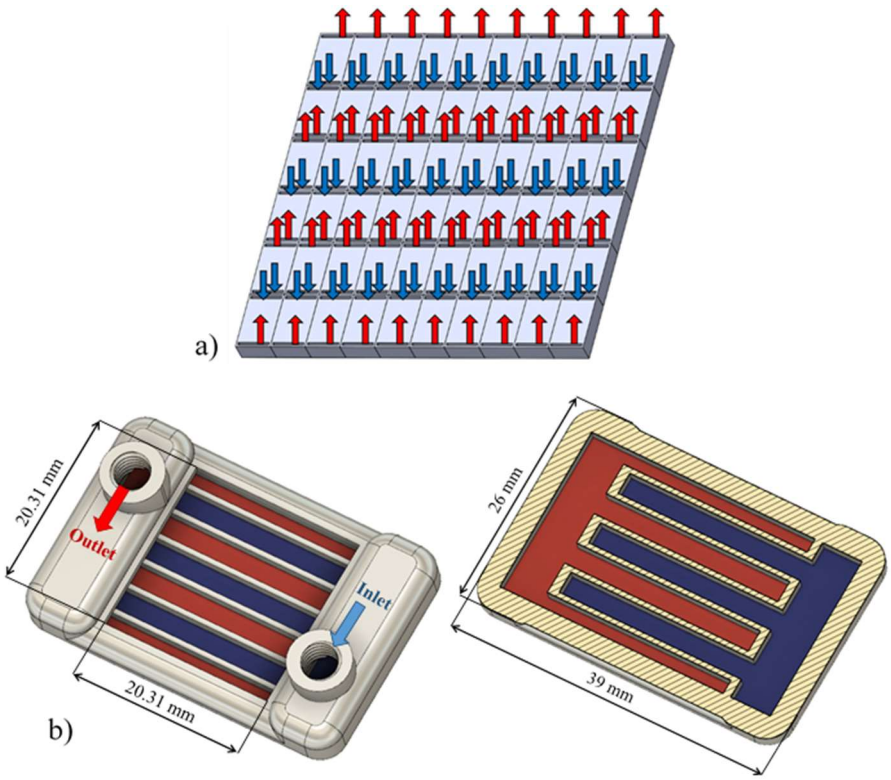

Figure 13: a) MC6T flip cell array, b) STREAMS microfluidic cell distributor

2. Microfluidic cell cooling device for microelectronics

This chapter presents the CFD studies focused on the assessment of the behaviour of both the microfluidic cells themselves and the array of cells under different boundary conditions. These simulations have been used to detect the weaknesses of the system and redesign it in order to reduce both the pumping power and the temperature non-uniformities of the chip surface.

At this stage, as no previous studies on this type of cooling solution have been previously developed, it has been impossible to validate experimentally the numerical model. However, the order of magnitude of the impact of the proposed cooling solutions assessed in this chapter has been validated through the experimental results (chapter 4).

2.1. Numerical methodology

The simulations are done with COMSOL Multiphysics®, a finite element analysis, solver and multiphysics simulation software, applying the Heat Transfer Module and the CFD Module using the Laminar Flow interface.

The Heat Transfer Module used [19] is based on Fourier's law of heat conduction (Eq. 1) and the heat transfer in solids (Eq. 2) and in fluids (Eq. 3).

$$q = -k\nabla T \tag{1}$$

$$\rho C_p u \cdot \nabla T + \nabla \cdot q = Q_{hs} \tag{2}$$

$$\rho C_p u \cdot \nabla T + \nabla \cdot q = Q_{hs} + Q_p + Q_{vd} \tag{3}$$

where

- q is the heat flux by conduction [W/m^2]
- k is the thermal conductivity [W/(m·K)]
- T is the absolute temperature [K]
- ρ is the density [kg/m^3]
- C_p is the specific heat capacity at constant stress [J/(kg·K)]
- u is the velocity vector of translational motion [m/s]
- Q_{hs} contains additional heat sources [W/m^3]
- Q_p is the work done by pressure changes [W/m^3]
- Q_{vd} is the viscous dissipation [W/m^3]

Fourier's law (Eq. 1) determines the heat flux density through a material by the conductivity of the material and the negative local temperature gradient. The heat transfer in solids and fluids expressions (Eq. 2, 3) are composed of a first term of energy convection by flow and a second term of net heat flux. The difference between the solid and the fluid heat transfer equations is the terms of heat generation; on the one hand, the solid heat transfer only has heat generation added

by constraints, but on the other hand, the fluid heat transfer has heat generation by constraints, pressure changes and viscous dissipation.

The CFD Module [20] using the Laminar Flow interface is used to compute the velocity and pressure fields for single-phase fluids in laminar regime. This module is based on the Navier–Stokes equations for the conservation of momentum (Eq. 4) and also the continuity equation for the conservation of mass (Eq. 5).

$$\rho(u \cdot \nabla)u = -\nabla pI + \nabla\left[\mu(\nabla u + (\nabla u)^T - \frac{2}{3}u(\nabla \cdot u)I\right] + F \tag{4}$$

$$\nabla \cdot (\rho u) = 0 \tag{5}$$

where

- ρ is the density [kg/m^3]
- u is the velocity vector of translational motion [m/s]
- p is pressure [Pa]
- I is the identity tensor
- μ is the fluid's dynamic viscosity [Pa·s]
- F is the volume force vector [N/m^3]

The Navier–Stokes equation (Eq. 4) is composed of a first term corresponding to the inertial forces, a second one corresponding to the pressure forces, a third one corresponding to the viscous forces and finally, the fourth corresponding to the external forces applied to the fluid.

With the application of the presented models with a proper mesh applied to the studied 3D geometries, the behaviour of the cooling solution can be evaluated.

2.2. Microfluidic Cell Cooling System for Electronics

This chapter is the published conference paper "Microfluidic cell cooling system for electronics" published in January of 2017 at THERMINIC 2017 - 23rd Int. Work. Therm. Investig. ICs Syst.

The authors of this article are: Gerard Laguna[1], Hassan Azarkish[2], Montse Vilarrubí[1], Manel Ibañez[1], Joan Rosell[1], Yina Betancourt[1], Josep Illa[1], Louis-Michel Collin[2], Jérôme Barrau[1], Luc Fréchette[2], Perceval Coudrain[3] and Guillaume Savelli[4].

[1]University of Lleida, 25001 Lleida, Spain

[2]UMI-LN2, Institut Interdisciplinaire d'Innovation Technologique (3IT), Université de Sherbrooke, Sherbrooke, Canada

[3]STMicroelectronics, 850 rue Jean Monnet, Crolles, France

[4]CEA, Liten, Thermoelectricity Laboratory, 17 rue des Martyrs, 38000 Grenoble, France

Abstract

Poor temperature uniformities and high pumping powers due to large pressure drops are the major drawbacks of the conventional microchannel cooling solutions. In this work, a liquid cooling device based on a matrix of microfluidic cells is presented. The coolant flow rate in each microfluidic cell is individually tailored, through thermally activated microvalves, to the local heat extraction needs in order to improve the temperature uniformity and avoid overcooling. A numerical study is implemented to assess the thermo-hydraulic performance of the cooling device. The analysis is performed in a steady state CFD study and integrated along a time dependent and non-uniform heat load scenario. The results show an enhancement of the temperature uniformity along the whole system while reducing the energy needed for the pumping power by 89.2 % compared to the conventional microchannel technology.

2.2.1.Introduction

Thermal viability of advanced micro- and nanoelectronic systems is one of the major challenges of the ICT community. Liquid cooling devices based on microchannels reach very low thermal resistance coefficients. Nevertheless, this technology has two main drawbacks: their large pressure drop, which involves high pumping powers, and the poor temperature uniformity of the cooled object, which implies reliability issues.

As a consequence, many papers and review articles are focused on enhanced microchannels [21–23] in order to deal with these drawbacks. Also, other solutions, based on hybrid jet impingement/microchannel techniques have been proposed and tested experimentally [24–27]. Such cooling schemes have demonstrated their capacity to obtain prefixed temperature profiles along the coolant flow path (even uniform) when tailoring, at the design stage, their internal geometry to the heat loads. Furthermore, the hybrid jet impingement/microchannels devices generate less pressure losses than conventional microchannels and, as a consequence, need lower pumping powers [28,29].

However, these investigations are carried out through constant and uniform boundary conditions while heat load scenarios are, for example in electronic applications, usually unsteady and non-uniform. As a consequence, cooling devices with constant and uniform flow rate distributions are overly conservatives and lead to oversized pumping powers.

In this work, the thermo-hydraulic performance of a cooling device formed by a matrix of microfluidic cells with individually variable coolant flow rate is assessed. The main objective of this device is to avoid overcooling and, as a consequence, to reduce the pumping power, by tailoring the distribution of the local heat extraction capacity to the time dependent and non-uniform heat flux distributions.

2.2.2.Description of the thermal device

A matrix of microfluidic cells (Figure 14) has been designed to both reduce the length of the coolant flow path, in order to reduce the pressure losses and to locally control the flow rate in each of the cells through self-regulated microvalves [16].

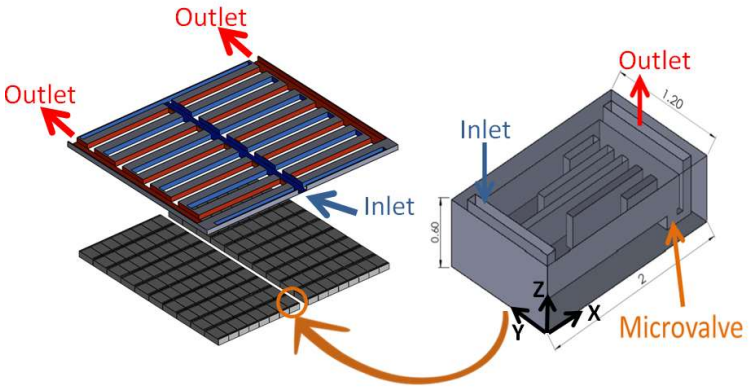

Figure 14: a) Matrix of microfluidic cells with distributor b) MC6T microfluidic cell (dimensions in mm)

The aperture of these valves, located at the hot side of the cell, near the coolant outlet (hottest point of the cooled object, in order to protect it from overheating), depends on their own temperature (Figure 15).

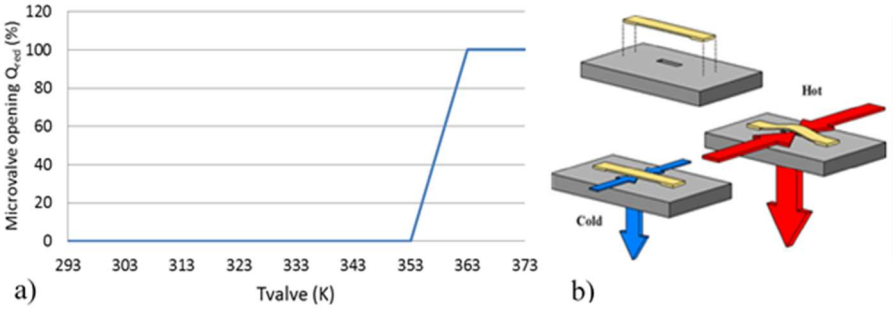

Figure 15: Self-adaptive microvalve a) opening function b) placement, hot and cold positions (from [16]*)*

A non-uniform and time dependent heat load scenario is applied, with several power densities from 20 to 300 W/cm^2 in the background and hotspot areas, respectively (Figure 16).

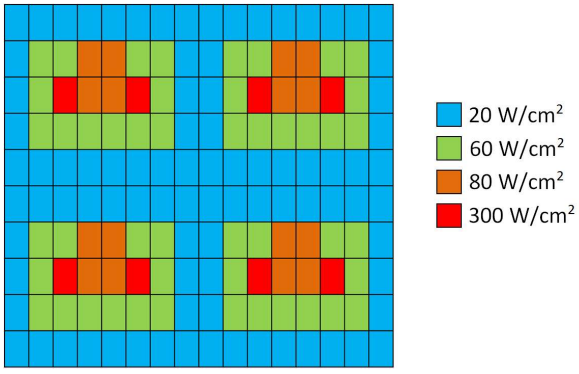

Figure 16: Power density applying the hypothesis

This area is cooled by a matrix of 16 x 10 microfluidic cells. The following assumptions are assumed [30]:

- No thermal inertia.
- When two loads are located on the same cell, only the highest is considered.
- When one load does not fit with the whole surface of a cell, a uniform heat load, with the same heat flux (in W/cm^2) is applied on this cell.
- The 4 chips of the interposer are activated in the same way.

At a first stage, a numerical study is carried out to determine, for a given microfluidic cell geometry, the flow rate needed to maintain the maximum temperature of the cooled object below 100 ºC when submitted to the different boundary conditions (heat flux: 300 W/cm^2, 80 W/cm^2, 60 W/cm^2, 20 W/cm^2; inlet coolant temperature: 50 ºC). The pressure drop, the pumping power and the chip surface temperature uniformity are also assessed.

Finally, the steady state results are spatially integrated along a 5 minutes time period function, as shown in Figure 17. Figure 18 presents the heat flux distribution for t_3.

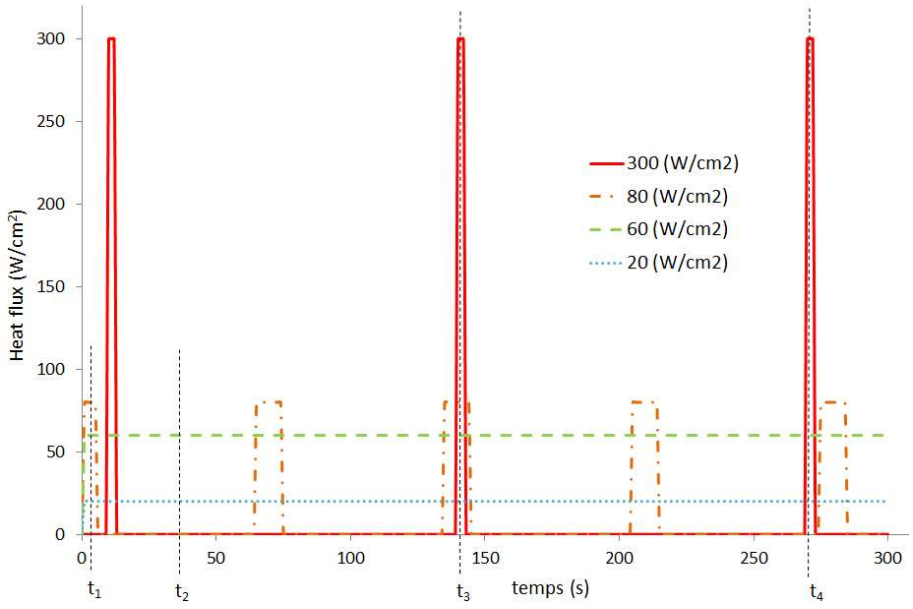

Figure 17: Time dependence of the heat loads

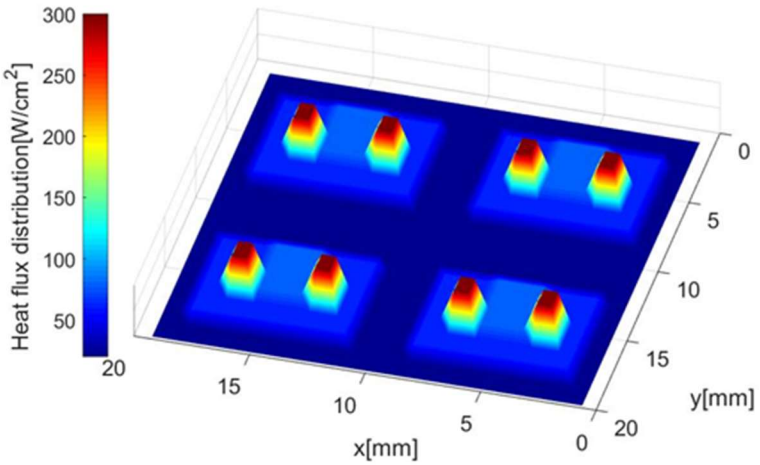

Figure 18: Heat flux distribution for t_3

2.2.3.Results

The performance of the matrix of microfluidic cells is compared with a microchannel cooling device submitted to the same boundary conditions.

The required total flow rate to maintain the device below 100 ºC is, on average, much higher for the microchannels than for the matrix of microfluidic cells (Figure 19). The flow rate in microchannels is constant because it is not tailored to the heat extraction demand. Otherwise, both the total flow rate of the matrix of microfluidic cells and its spatial distribution vary along the five minutes time period.

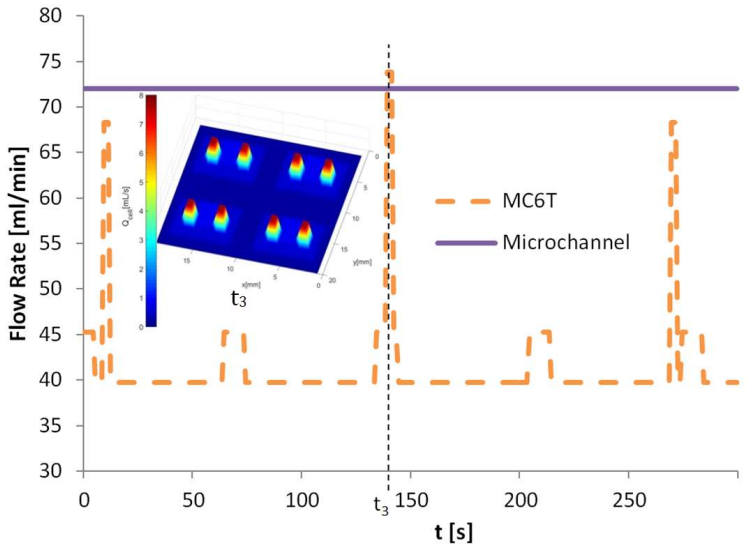

Figure 19: Flow rate over time and spatial distribution at t_3

Figure 20 shows the pressure drop over the 5 minutes time period in both systems. Due to its short length, the pressure drop of the microfluidic cell matrix is around 90 Pa when hotspots are not active. With microchannels, the pressure drop is around 6800 Pa.

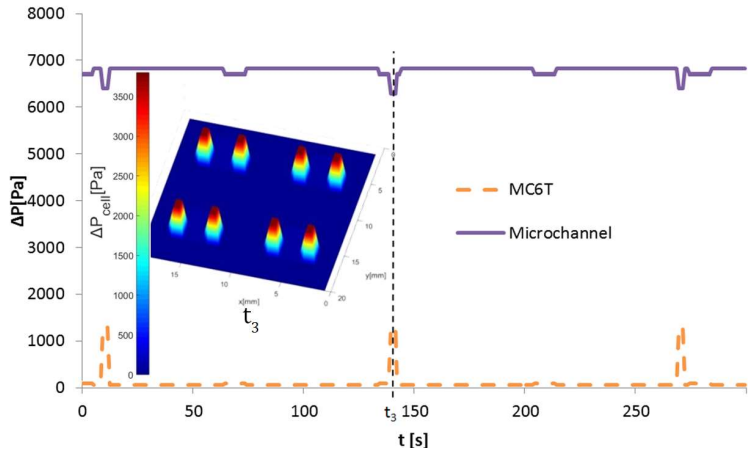

Figure 20: Pressure drop over time and spatial distribution at t_3

The tailored microchannels geometry within the microfluidic cells allow to reach a high temperature uniformity along the flow path (Figure 21). The temperature non uniformity through the whole cooling device is lower than 4 ºC.

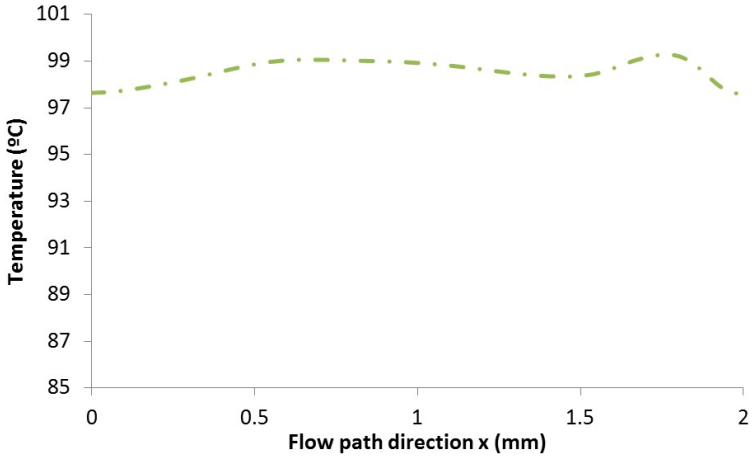

Figure 21: Temperature distribution along the coolant flow path of a microfluidic cell at chip surface, when submitted to 300 W/cm² (at z = 0 mm, y = 0.6 mm)

Also, as the microvalves of the matrix of microfluidic cells tailor the flow rate in function of their own temperature, the maximum temperature is stable around 100 ºC (Figure 22). In the case of microchannels, the maximum temperature oscillates between 82 ºC and 100 ºC along the time period, generating a thermal cycling that affects the reliability of the system.

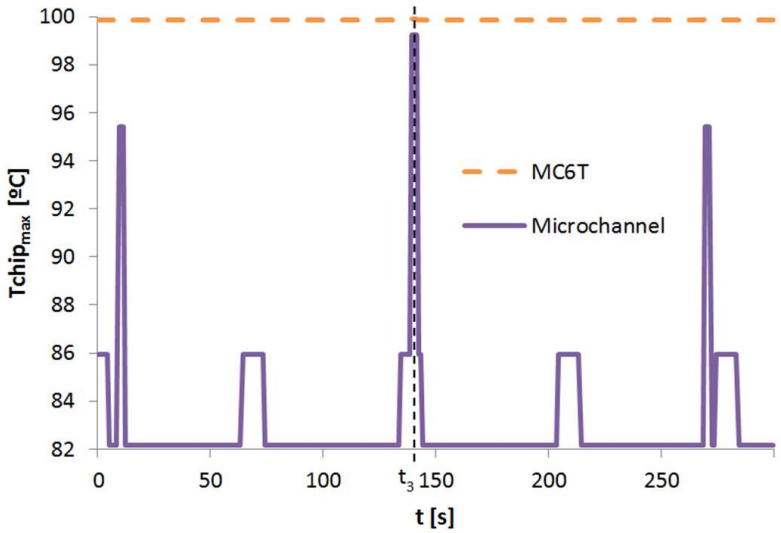

Figure 22: Chip maximum temperature over time

The hydraulic pumping power required for both cooling devices is integrated along the 5 minutes time period, and the average value for the matrix of microfluidic cell represents only 10.8 % of the one of microchannels.

The global performance of the studied cooling device, assessed with the quotient between the pumping power and the chip power (P_{pump}/P_{chip}) and the temperature uniformity, expressed through the normalized value ΔTq [9], are represented in Figure 23 and compared to previous studies. The temperature uniformity is comparable with the one obtained by the hotspot targeted design [9] but the P_{pump}/P_{chip} relation is widely reduced (around 250 times).

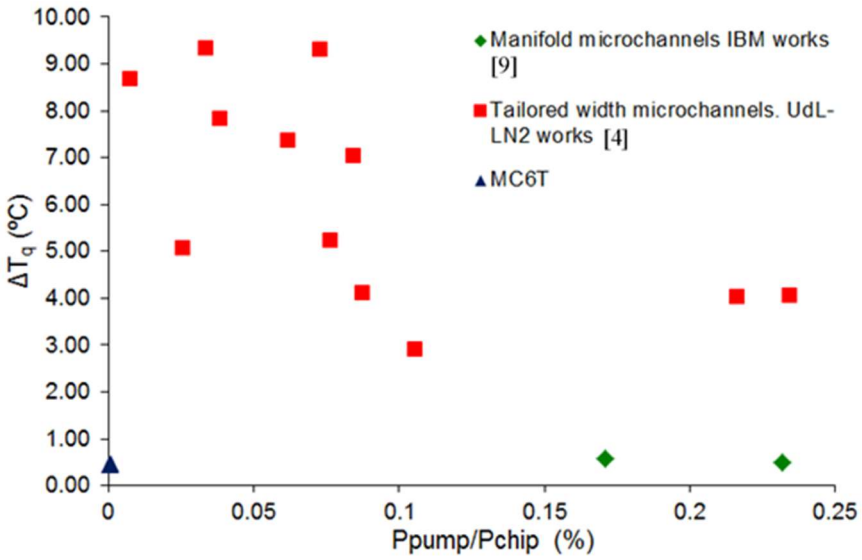

Figure 23: Comparison of the overall pumping performance

2.2.4. Conclusions

The performance of a matrix of microfluidic cells with individually tailored coolant flow rates is numerically assessed.

The short coolant flow path of the studied cooling device and its capacity to provide a distribution of the coolant flow rate tailored to the local heat extraction needs imply, respectively, low pressure drops and low total coolant flow rates with respect to conventional microchannels.

These characteristics allow assuming the safe function and providing good temperature uniformity, even for non-uniform and time dependent heat load scenarios at a low cost in terms of pumping power. Indeed, for a given heat load scenario, the matrix of microfluidic cells saves 89.2 % of energy for pumping with respect to conventional microchannels.

Acknowledgements

The research leading to these results has been performed within the STREAMS project and received funding from the European Community's Horizon 2020 program under Grant Agreement N° 688564.

2.3. Numerical parametric study of a hotspot-targeted microfluidic cooling array for microelectronics

This chapter is the published paper "Numerical parametric study of a hotspot-targeted microfluidic cooling array for microelectronics" published in August of 2018 at Applied Thermal Engineering.

The authors of this article are: Gerard Laguna[1], Montse Vilarrubí[1], Manel Ibañez[1], Yina Betancourt[1], Josep Illa[1], Hassan Azarkish[2], Amrid Amnache[2], Louis-Michel Collin[2], Perceval Coudrain[3], Luc Fréchette[2] and Jérôme Barrau[1].

[1]Dynamic Systems Applied to Solar Energy Research Group, University of Lleida, Lleida, Spain

[2]UMI-LN2, Institut Interdisciplinaire d'Innovation Technologique (3IT), Université de Sherbrooke, Sherbrooke, Canada

[3]STMicroelectronics, 850 rue Jean Monnet, 38926 Crolles Cedex, France

Abstract

Thermal management in integrated chips is one of the major challenges on advanced microelectronics. The increase in power density is raising the need for microchannel liquid cooling solutions. Although this technology can accommodate high heat rates, it has poor temperature uniformity and may require significant pumping power. In this work, a cooling scheme aiming for high temperature uniformity and low pumping power is numerically studied. The cooling scheme consists in a matrix of microfluidic cells with thermostatic microvalves, fed by an interdigitated manifold. The flow through each cell is controlled with the self-adaptive microvalves to only deliver the flow rate required to maintain a design temperature. This system is assessed with steady state CFD and heat transfer studies of various microfluidic cell designs combined with a time-dependent and non-uniform heat load scenario of a chip with hotspots. The studied cooling scheme practically eliminates chip temperature non-uniformity while also reducing the pumping power by nearly one order of magnitude compared to traditional microchannel configurations for similar applications.

2.3.1.Introduction

Cooling of microelectronic components has been extensively studied since the 1980s. Today's advanced information and communication technology (ICT) trends involve further integration, at the die and the package level. Die stacking and heterogeneous integration of temperature sensitive components are the technological paths ahead for a large share of ICT applications. Thermal viability of advanced micro- and nanoelectronic systems is one of the major challenges of the ICT community [31]. Until now, microelectronics thermal management has been based on continuous air cooling, using passive approaches by natural convection or active air cooling with a fan and heat sink depending on the power level. However, Integrated Circuit (IC) stacking and compact assemblies make conventional air heat dissipation challenging, raising the interest in liquid cooling technologies, preferred for their cooling capacities, compactness and high performance. Single-phase liquid cooling has long been identified as an effective and feasible approach for cooling high heat flux density chips. Starting with the landmark work of Tuckerman and Pease [32], liquid cooling of chips has been analyzed in great detail including investigations on traditional microchannel heat sinks [33], manifold microchannel heat sinks [34,35] and spray and jet cooling [36]. Most of the research on liquid cooling of chips has been focused on maximum temperature reduction under uniform heat flux dissipation conditions. However, it is also necessary for the chip temperature to be as spatially uniform as possible (i.e. approaching the isothermal chip condition). Indeed, large temperature gradients in the package increase thermal stresses in the heat sink interface, reduce electronic reliability in high temperature regions and create circuit imbalances in CMOS devices [37]. Some studies have focused on reducing chip temperature non-uniformity under a uniform heat flux map, including the use of flow boiling of dielectric liquid [38], single phase liquid cooling with variable pin fin density [39], variable microchannel width in the streamwise direction [40–42] and double-layer microchannel structures [43]. Hybrid jet impingement/microchannel cooling schemes have shown their capacity to provide low thermal resistances, good temperature uniformities and lower pressure drops than conventional microchannel devices for specific heat flux distributions [24,25].

In high performance chips, the large difference in heat dissipation between hotspot and background regions makes the goal of isothermal junction temperatures even more challenging. Several approaches have been proposed to achieve an isothermal chip condition by preferential cooling of hotspots (henceforth referred as hotspot-targeted cooling). For effective hotspot-targeted cooling, Dang *et al.*[44] and Kandlikar *et al.* [45] reported that thermal resistance can be reduced by circulating the coolant through microchannels, etched into the backside of the chip (also termed as embedded or direct chip backside microchannel cooling). Attempts using single phase liquid cooling have also been reported with different degree of

success [46]. Among the major findings in the literature, one can note that power densities larger than 400 W/cm² can be extracted with micro-channel single-phase conditions [22,47]. However, they are not able to provide a good temperature uniformity that preserves the reliability and efficiency of the cooled device. Furthermore, microchannel cooling designed for thermal performance tends to sacrifice pumping power, using high flow rates and pressure drop. An optimum thermal management approach should therefore provide higher cooling rates at the hot spot to achieve a uniform temperature while minimizing the overall flow rate and pressure drop of coolant fluid. The pressure losses are the main drawback of conventional microchannels and they must be lowered for pumping power reduction.

Conventional heat sinks with uniform distribution of microchannels or pin fins present the disadvantage of undercooling hotspot areas due to both the insufficient local heat transfer coefficient and the inadequate heat exchange area. Different approaches have been suggested in recent years to address this issue [48]. Sharma *et al.* [49] presented a numerical study to assess the concept of hotspot-targeted manifold microchannel heat sinks with multiple inlets and outlets using water as coolant, in which narrow channels are defined in the hotspot areas, while wider channels are used to cool background zones. Model predictions suggested the capability of this design to remove hotspot heat fluxes up to 300 W/cm^2, the microchannel design is based in the worst operating conditions with maximum heat flux on each hot spot simultaneously, in combination with a background heat flux of 20 W/cm^2 and a pressure drop below 35 kPa. Localized microchannels where shown by Collin *et al.* [47] to achieve high local heat flux of 1185 W/cm^2 with a pressure drop below 20 kPa. Nevertheless, these cooling devices do not tailor their behavior to the time-dependent heat load scenarios. As a consequence, their constant flow rate distributions are overly conservative and lead to oversized pumping powers for varying operating conditions.

Azarkish *et al.* [50] introduced a self-adaptive microfluidic system for thermal management of microelectronic chips with non-uniform thermal maps. The smart and self-adaptive microfluidic system, formed by an array of microfluidic cells with individually variable coolant flow rates, is designed to achieve an adequate cooling with minimum pumping power as well as appropriate surface temperature uniformity. The coolant mass flow rate of each zone is controlled independently based on its temperature by using temperature-regulated microvalves. The local cooling is adapted to the local heat flux. In the present work, a numerical parametric study of this smart and self-adaptive microfluidic system is developed to assess the impact of the internal geometry of the cooling cells on its thermo-hydraulic performance under non-uniform and both steady-state and time dependent heat load scenarios.

2.3.2.Description of the cooling device

The proposed approach consists of an array of microfluidic cells, each one responsible for removing the local heat flux. Coolant flow is fed in parallel to the cells by interdigitated cold and warm flow channels connected to manifolds (Figure 24). Each cell, therefore, has a cold inlet flow, irrespective of its location. Heat is removed by the flow through each cell, which can contain microchannels to enhance the heat transfer. Pressure drop is minimized due to the short length of the cells, compared to traditional microchannels that would span the entire chip. Furthermore, the local flow rate is controlled by integrating a self-adaptive microvalve in each cell that tailors its aperture to the local temperature (Figure 25).

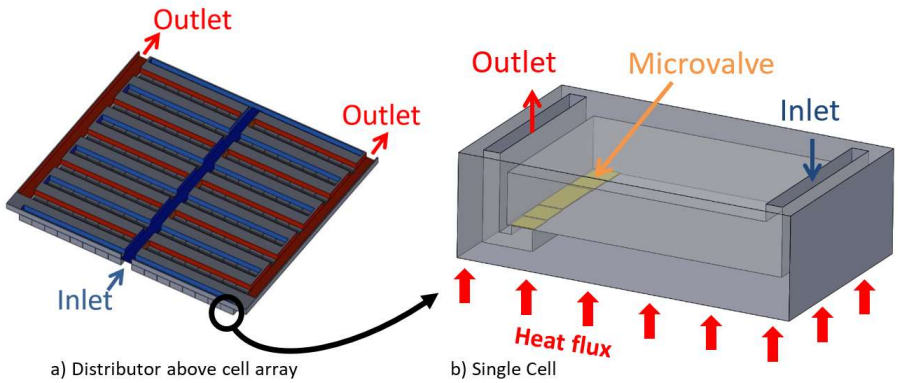

Figure 24: Array of microfluidic cooling cells, fed by interdigitated distributor channels above the cell array (a), and details of single microfluidic cell (b).

This type of valve has been designed and demonstrated experimentally as an effective passive flow control mechanism based on the flow temperature [16]. The beams are formed by depositing metal (Ni) on a silicon substrate, with the ends clamped to the substrate but the central portion released by depositing it over a sacrificial layer. The coefficient of thermal expansion (CTE) of the beam being greater than that of the substrate, the beam will be subject to compression as the cell heats up. It will tend to buckle and deflect away from the substrate, opening the gap and allowing more coolant flow through the cell.

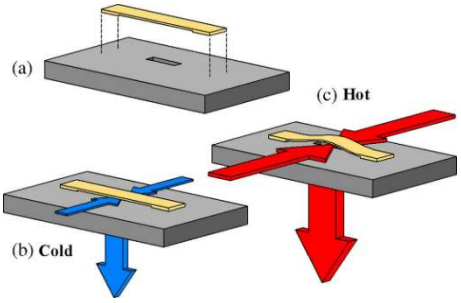

Figure 25: Thermostatic microvalve formed from a buckling beam over a slot [16]

Depending on its shape, the deflection behavior versus temperature can be tuned to vary sharply once a critical temperature is reached or gradually over a desired temperature range. Since the microvalve is thermostatic, large arrays can be implemented (using microfabrication) without the need for sensors nor control logic.

The microfluidic cell array has been conceived in order to provide the following advantages compared to the conventional microchannel cooling systems:

- Local control: The microvalve opening, which depends on its own temperature, allows tailoring of the mass flow rate of each microfluidic cell to the local cooling needs. As a consequence, the overall cooling can be managed easily with low pumping power costs.
- Low pressure drop: The length of each cell is short. Therefore, if a high local coolant flow rate is needed near the hotspot zones, the corresponding pressure drop is not very significant.
- Versatile microfluidic actuation: With microchannels or other cooling schemes, the design is optimized for a given heat load at a given flow rate or is adapted to the worst case scenario. The self-adaptive local coolant flow rate provides versatility in order to adapt to varying spatial and temporal heat load scenarios.

To evaluate the benefits and performance of this self-adaptive cell array configuration, this paper will evaluate it for different heat loads, as well as consider the effect of using microchannels in the cells to enhance the heat transfer.

In this paper, three geometries of the microfluidic cells are numerically studied. The first one consists on a cell with an external size of 2 x 1.2 mm^2 without fins inside (cell MC0, Figure 26). The coolant, water in this study, enter the cell from the coolant distribution layer through an inlet slot located on the cold side of the cell (opposite face to the heat load) and exits through the outlet slot on the same side, which also connects to the distribution layer. The outlet flow path allows the microvalve, which regulates the coolant flow rate for each microfluidic cell, to be located near to the chip zone where its temperature is maximum (end of the coolant flow path), in order to narrow the relationship between the valve temperature (and so its opening) and the maximum chip surface temperature.

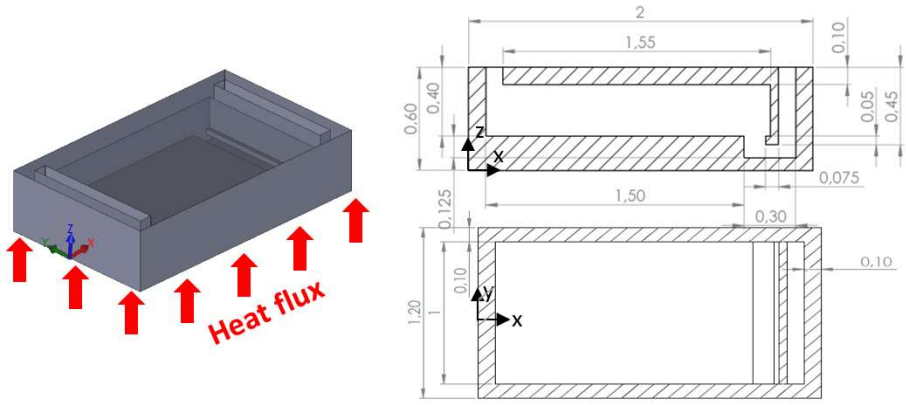

Figure 26: MC0 design (dimensions in mm)

In a second design, fins are included within the microfluidic cell to build a 6 microchannel configuration (cell MC6, Figure 27a). Their length corresponds to the distance between the inlet and the microvalve. They are expected to improve the heat transfer, hence require lower flow rates to keep the chip below the temperature limit, but on the other hand, the narrow flow paths will generate more pressure drop.

Based on previous studies [24,25], a tailored fin design is proposed (cell MC6T, Figure 27b). The aim of this solution is to keep the heat extraction capacity to values relatively close to those of the MC6 model, but with lower pressure drop and higher temperature uniformity across the chip area above the fluidic cell.

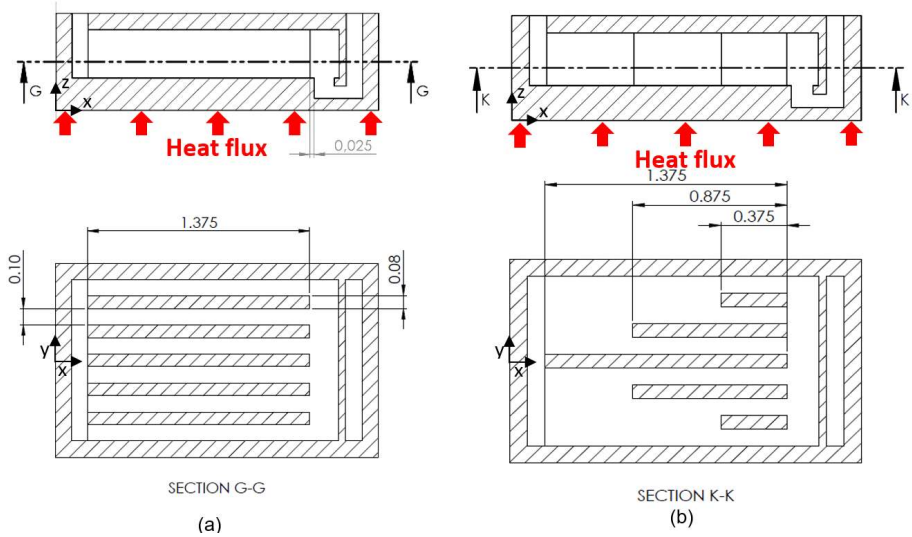

Figure 27: a) MC6 and b) MC6T cell designs (dimensions in mm)

2.3.3. Cooling cell steady state performance assessment

Numerical model

A numerical model is used to develop a parametric study and assess the performance of each cell individually as a function of the cell dimensions and the internal geometry of the cells for several heat fluxes with a given coolant inlet temperature. The maximum chip temperatures ($T_{chip,max}$), temperature non-uniformities (ΔT_{chip}), pressure drop (ΔP), flow rate (Q) and hydraulic pumping power (P_{pump}) are analyzed for each of the 3 designs considered and compared those obtained with conventional microchannels. A commercial finite element solver (COMSOL) is used to model the steady-state fluid flow and heat conduction in a single cell (conjugate heat transfer), taking into account the temperature dependent properties of water and silicon.

Due to longitudinal symmetry, only half of the cooling cell is considered in the numerical model with a symmetry boundary condition at the mid-plane. The boundary conditions of the numerical models considered in this steady-state study are as indicated in Figure 28.

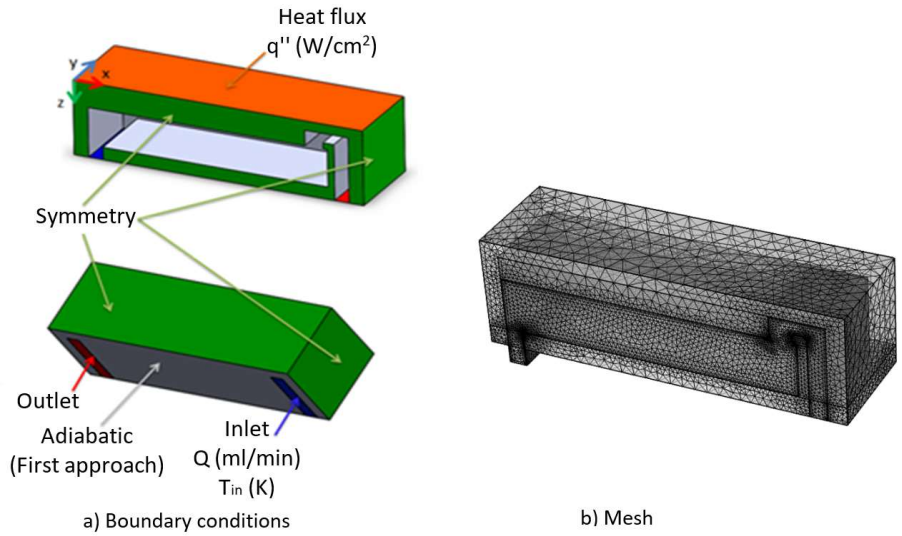

Figure 28: Numerical model of a microfluidic cell

In order to fix the maximum flow rate needed to maintain the chip temperature in the adequate range, the worst case is considered with a heat flux of 300 W/cm^2 along the entire chip surface of the cooling cell. The coolant inlet temperature is 50 ºC and the optimization criterion for the determination of the cell coolant flow rate is a maximum allowable chip temperature ($T_{chip,max}$) of 100 ºC (±1 ºC).

The flow is considered laminar since the maximum Reynolds number is 420 at the inlet of MC0 cell (highest value of all cases studied). The mesh sensitivity analysis has been carried out showing convergence as a function of mesh refinement with a

final account of 603921 elements with an error lower than 0.15 % on chip temperature compared with a mesh with 1369807 elements.

Thermo-hydraulic Performance

Table 1 shows the thermo-hydraulic performance of the 3 microfluidic cell geometry when submitted to the most demanding boundary conditions. The flow rate was varied until the maximum allowable temperature was reached. The thermal resistance coefficient R is assessed through (Eq. 6):

$$R = \frac{\left(T_{chip,average} - T_{in}\right)}{q^{"}} \tag{6}$$

Table 1: Thermo-hydraulic performance of the cooling cell in the most demanding conditions.

Model	Q_{cell} *[ml/min]*	$T_{chip,average}$ *[ºC]*	$T_{chip,max}$ *[ºC]*	R *[cm² ºC/W]*	ΔT_{chip} *[ºC]*	ΔP *[Pa]*	P_{pump} *[W]*	COP *[-]*
MC0	7.68	93.7	99.7	0.145	13.2	3791	$4.85 \cdot 10^{-4}$	$1.48 \cdot 10^{5}$
MC6	3.48	93.8	99.1	0.146	10.1	1331	$7.72 \cdot 10^{-5}$	$9.33 \cdot 10^{5}$
MC6T	3.72	98.6	100.0	0.167	4.0	1291	$8.00 \cdot 10^{-5}$	$9.00 \cdot 10^{5}$

To achieve the same thermal resistance across all designs, the pumping power varies significantly. The high pressure drop caused by the low heat extraction capacity at cell MC0, that requires high flow rates (Q_{cell}) to reach the maximum allowable temperature, imply that heat transfer enhancement structures are beneficial to reduce the pumping power, as shown for models MC6 and MC6T. However, the tailored microchannel cell (MC6T) reaches a non-uniformity of 4.0 ºC that improves largely the 10.1 ºC obtained by the uniform microchannel cell (MC6) and 13.2 ºC for the empty cell.

The temperature distribution across the chip surface is shown in Figure 29 for the three models. MC6 presents a temperature increase along the longitudinal direction from the inlet to the valve position (x = 1.7 mm), typical from straight microchannels. The tailored microchannels MC6T shows a rather constant temperature distribution, this confirms the usefulness of increasing the fins density (reducing thermal resistance) along the coolant flow path to compensate for the increase in fluid temperature. MC0 temperature profile reaches its maximum before the outlet (x = 1.2 mm), due to the relatively low heat exchange capacity within the microfluidic cell and to the fact that most of the heat transfer is occurring near the inlet and outlet.

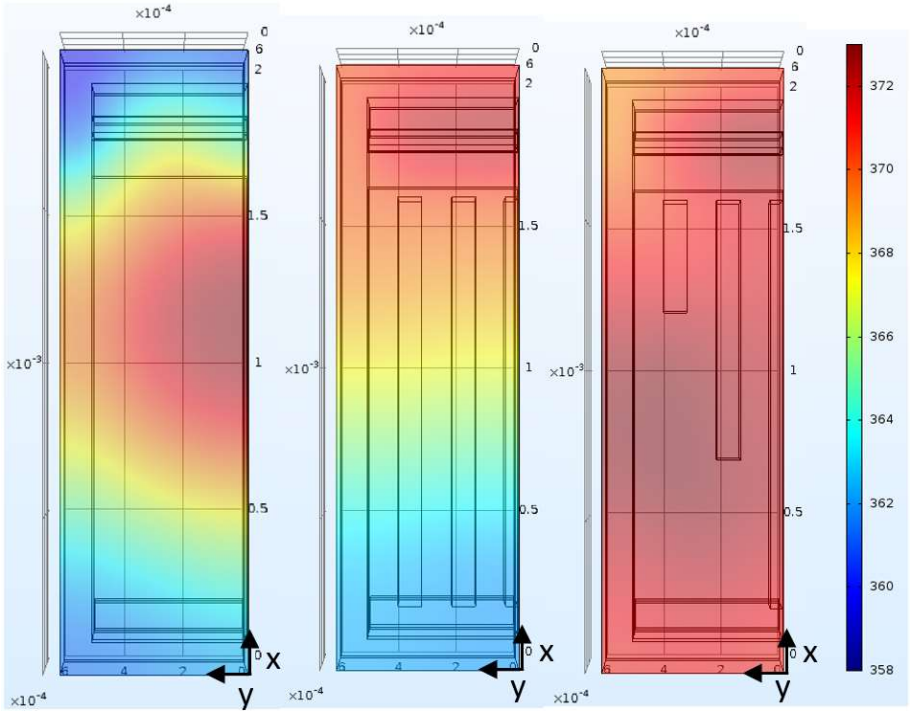

Figure 29: Thermal map of the chip surface (z = 0)

2.3.4. Performance assessment in the cell array under unsteady and non-uniform heat loads

This study is now done at the chip level: an array of cells with their own self-adaptive microvalves and covering the entire chip surface is considered. The performance of the three proposed designs is assessed for non-uniform and time dependent heat flux scenarios. For all the heat loads considered, the flow rate of each of the cells is assessed to reach a given $T_{chip,max}$. Tailoring of the local flow rate is carried out through the microvalve opening and closing, which depends on its own temperature.

For each of the three designs, as well as regular microchannels, a spatial and time dependent integration of quasi-steady state results has been used to determine the temperature distribution obtained along the heat load scenarios considered. Heat spreading between cells can be considered insignificant in our cooling device because the microvalve behaviour allows the microfluidic cell thermal resistances to be tailored to the local heat extraction need and so to provide a homogeneous temperature profile. This assumption is based on a previous study by Sharma *et al.* [51]. Indeed, the authors highlighted that the isothermal condition is one of the conditions that allow assessing the thermal behaviour through a one dimensional modelling approach.

Inputs and case study

In this analysis, the flow rate of each microvalve is defined from the quasi-steady flow rate, Q_{max}, required to respect the temperature limits under maximum heat load. This value is used as an input for the temperature dependent flow rate, defined as follows (Eq. 7):

$$Q(T) = \begin{cases} 0.01 \cdot Q_{max}, & T < 80ºC \\ \dfrac{T-80}{10} \cdot Q_{max}, & 80ºC < T < 90ºC \\ Q_{max}, & T \geq 90 \end{cases} \quad (7)$$

The microvalve starts to open at a control value, 80 ºC, and it is completely open at 90 ºC. Below the control value, a residual flow rate (1 % of Q_{max}) enters the cooling cell, since this kind of microvalve can't close completely since it is fabricated with a small clearance under the beam to allow its deflection. This general trend of valve response corresponds to the 'S' shape behaviour observed previously by McCarthy *et al.* [16]. The impact of the microvalve response function is further studied by Azarkish *et al.* [50].

Here we consider the case of a virtual 20 x 20 mm^2 circuit, with power characteristics derived from various realistic applications. Multimedia processors composed of CPU, GPU, Graphic accelerators, memories, power management unit, exhibit spatial and temporal power distribution variations, but with amplitudes of less than 15 W. On the other hand high performance computing chips and networking ASICs are typically active 100 % of the time with powers from 50 to 200 W for surfaces of 200 to 500 mm^2. In order to study the dynamical performance of the microfluidics cell array, the power profile is based on a virtual hybrid chip holding mixed characteristics form the two precedent scenarios. Power peaks frequencies corresponds to GPU, CPU and graphic accelerators requests in a multimedia processor while the amplitude of power peaks and hot spot densities are scaled on high performance computing or networking scenario. This virtual object mimics future versatile high performance silicon interposers in which independent high performance computing tasks could be co-integrated.

The spatial distribution includes four peripheral zones with heat flux of 60 W/cm^2, four central zones with 80 W/cm^2, eight hotspots zones with 300 W/cm^2 and all rounded by background areas with 20 W/cm^2 (Figure 30a). Heat load is mapped onto cell array (Figure 30b).

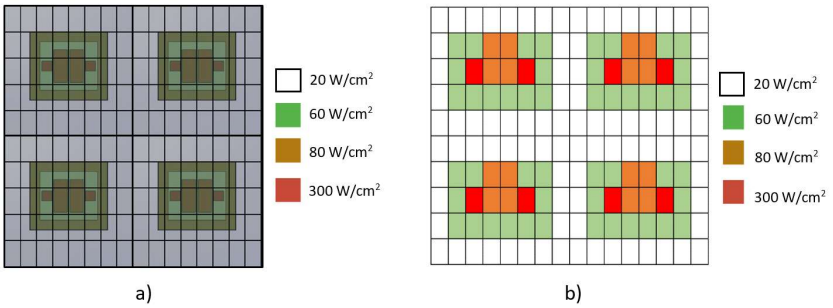

Figure 30: Baseline heat load map and its relationship with the microfluidic cell array

In order to study the dynamical performance of the microfluidic cell array, the power profile over time is based on realistic power dissipation profiles of commercial SoC during web browsing sessions. Power peaks corresponds to GPU, CPU and graphic accelerators requests, while the other blocks of the circuit are considered as a static background. The different constituting blocks have a fluctuating power dissipation, which makes the power map change over time. The time dependence of the heat loads is described in Figure 31. Four different heat load maps occur during the 5 minutes time period being captured as t_1, t_2, t_3 and t_4 in Figure 31. The timescale of change in the operating conditions (seconds) is sufficiently long compared to the thermal diffusion timescale (less than a msec) and the flow through time (also less than a msec) to assume quasi-steady behaviour of convection and conduction at the cell level as well as in the valve.

Behaviour of the cooling devices under different heat load scenarios

Conventional microchannels

A conventional microchannel device has been modeled in order to provide a baseline to compare the improvements provided by the microfluidic cell array cooling configurations. These models are formed by parallel microchannels of 300 µm high, 200 µm width and 100 µm of wall thickness. The parallel microchannels span the entire device width (20 mm). The inlet temperature is equal to the one imposed in the microfluidic cells models and the heat flux is assessed to provide, at each instant of the 5 minutes time period, the total dissipated heat defined in the heat load scenario. The flow rate is adjusted to maintain the chip temperature below 100 ºC. As conventional microchannel devices don't have the capacity to tailor their flow rate to variable heat flux scenarios, the flow rate applied is constant all along the 5 minutes time period.

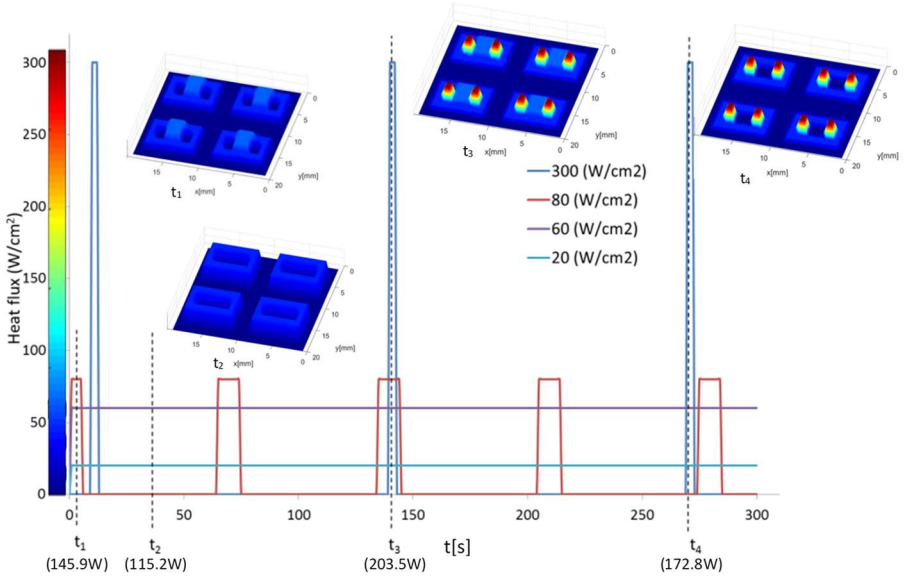

Figure 31: Heat load scenario

Maximum temperature

For the three microfluidic cell models, the chip maximum temperature is maintained below 100 ºC (Figure 32). When the heat flux decreases, microvalves close and the flow rates go down reducing the pumping power and avoiding cells overcooling. For the microchannel models, the flow rate is constant. As a consequence, the temperature decreases down to lower values compared to the microfluidic cells when the heat flux decreases. When measuring the performance of the cooling device through the pumping power, these lower temperatures are not required and correspond to additional pumping power.

However, some electronic applications need to work at lower temperatures. In this case, the lower thermal resistances of the microfluidic cell cooling approach could be leveraged to reach lower chip temperatures than microchannel cooling devices, for a fixed pumping power.

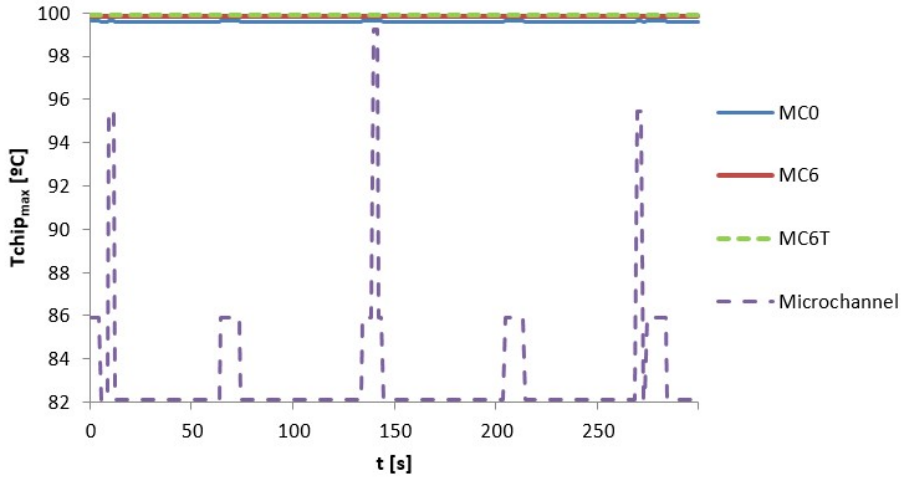

Figure 32: Chip maximum temperature over time

Flow rate

The time dependent total flow rates of the microfluidic cooling devices are represented in Figure 33. The flow rate is, at t_3, concentrated in the hotspot cells, so the microvalve effectively provides the flow rate only where needed. It is noticed that MC0, due to its poor heat extraction capacity, needs nearly two times the flow rate of the other cells to reach the temperature limit for the high heat flux condition (t_3).

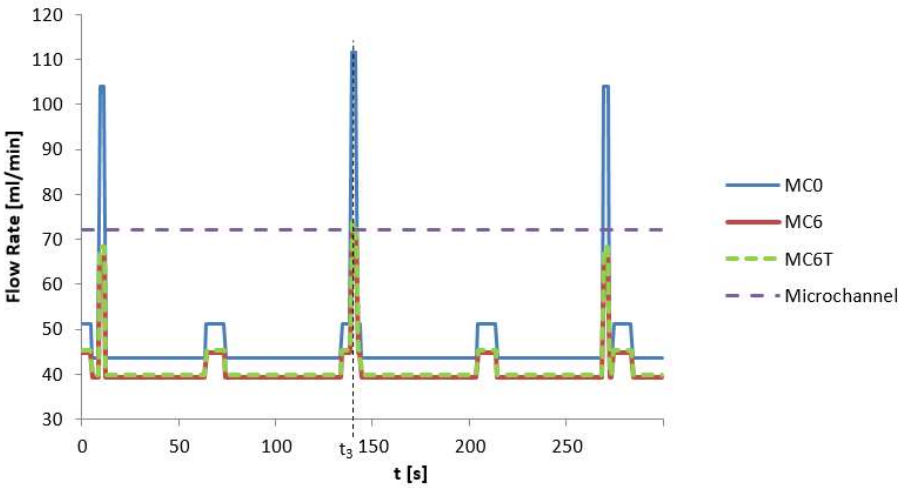

Figure 33: Total flow rate along the time period

In the case of microchannels, the flow rate can't be tailored to the time dependent heat flux distribution. As a consequence, the flow rate is constant in time and corresponds to the flow rate needed to reach the temperature limitations when submitted to the highest heat rate.

Furthermore, the total flow rate of the cooling device is, except at t_3, lower for the microfluidic cells than for the conventional microchannels.

The average flow rate, over the 5 minutes time period, for the MC0, MC6 and MC6T configurations is, respectively, 64.7 %, 56.9 % and 57.5 % of the flow rates required with conventional microchannels.

Pressure loss

To evaluate the pumping power for a complete cell, the valve pressure drop should be included. By design, the microvalves will close to restrict the flow rate in cooler zones, inducing an additional flow resistance across that cell. Since all the cells have a common inlet and outlet, they will effectively be subjected to the same pressure difference. In the proposed cooling devices, the valves provide the missing pressure drop that once added to the cell pressure drop will equate the applied pressure difference. The required pressure difference is hence defined by the cell with the highest pressure drop.

Although the pressure drop along the distribution channels is not the subject of this study, it has been assessed. It represents, for the MC6T model and in the most demanding operating conditions (t_3, highest flow rate), an additional pressure drop of 2250 Pa for distribution channels heights of 300 microns, suggesting that it should be considered in eventual array designs.

The microfluidic cells present a lower pressure drop than the microchannel. For an identical flow rate, MC0 generates less pressure drop than the other cells. But MC0 needs a higher flow rate to reach the temperature limitation, and its maximum pressure drop for the high heat flux conditions is higher than the ones for MC6 and MC6T. The pressures drop for the conventional microchannels is nearly constant given the constant flow rate. The slight variations are due to a decrease in viscosity at higher temperatures.

Assuming that the pump provides constant pressure over time, based on the cell with maximum pressure drop, we find that the pressure drops for MC0, MC6 and MC6T are respectively 55.5 %, 19.5 % and 19.0 % of the pressure drop in conventional microchannels.

Pumping power

The pumping power of the cooling devices, assessed with constant pressure over time (Figure 34), show similar trends than the flow rate.

For similar conditions, the MC0, MC6 and MC6T microfluidic cells pumping power, here expressed as the energy needed for pumping along the 5 minutes time period is, respectively, 35.9 %, 11.1 % and 10.9 % of the conventional microchannels.

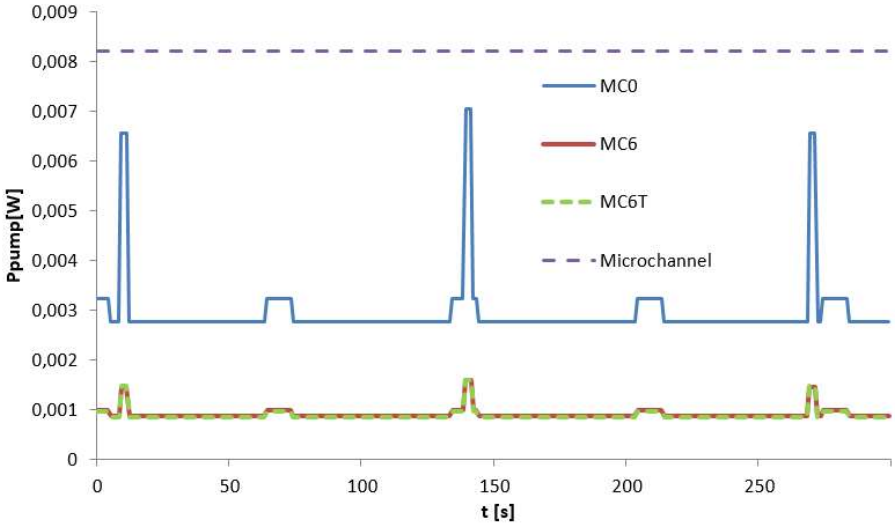

Figure 34: Pumping power of the whole cooling device along the time period

Overall performance

As the pumping power and the temperature uniformity are the main performance indicators, the results obtained for the microfluidic cell designs considered in this study are presented for each of the instants corresponding to the 4 heat load maps during the 5 minutes time period (Figure 35).

For a consistent comparison of various solutions, the pumping performance is expressed through the ratio (P_{pump}/P_{chip}) between the pumping power and the chip power integrated along the 5 minutes time period. The temperature non-uniformity depends on the non-uniformity of the thermal load distribution. In order to compare the temperature uniformity results with other studies uses various levels of heat flux non-uniformity, a normalized value (ΔT_q), introduced by Sharma *et al.* [40], is used (Eq. 8):

$$\Delta T_q = \frac{\Delta T_{s,max}}{\left(\frac{q''_{hs}}{q''_{bg}}\right)} \tag{8}$$

where $\Delta T_{s,max}$ is the chip wide temperature difference and q''_{hs} and q''_{bg} are the heat fluxes applied at the hotspot and background zones, respectively. Eq. (8) implies that a design is better if it achieves lower temperature non-uniformity $\Delta T_{s,max}$ for higher levels of power map non-uniformity q''_{hs}/q''_{bg}.

The average pumping power along the 5 minutes time period for MC0, MC6 and MC6T are widely below the accepted criteria for similar applications (P_{pump}< 1 % P_{chip}, [40]). MC6 and MC6T configurations present a ratio P_{pump}/P_{chip} between

$0.80 \cdot 10^{-3}$ % to $0.65 \cdot 10^{-3}$ % (COP from 1250 to 1538) depending on heat flux conditions.

In addition, the normalized difference of temperature (ΔT_q) of all the cells is below 1 ºC. These values are in the same range as manifold microchannels [40], with the advantage that this low temperature non-uniformity is maintained when the heat load map varies in the case of the microfluidic cell arrays. For MC6, the temperature increase along the flow path generates higher temperature non-uniformity. For MC0, when hotspots are active, the high flow rates needed to keep the temperature below 100 ºC generate both relatively high pumping power and higher normalized temperature non-uniformity (0.9 ºC). For lower heat loads (t_1 and t_2), the normalized temperature non-uniformity decreases down to 0.3 ºC.

When compared to previous studies, a significant reduction of pumping power is observed (Figure 35). The normalized values of temperature of MC6T is 0.46, below 0.49 ºC that represents the lowest of the compared studies.

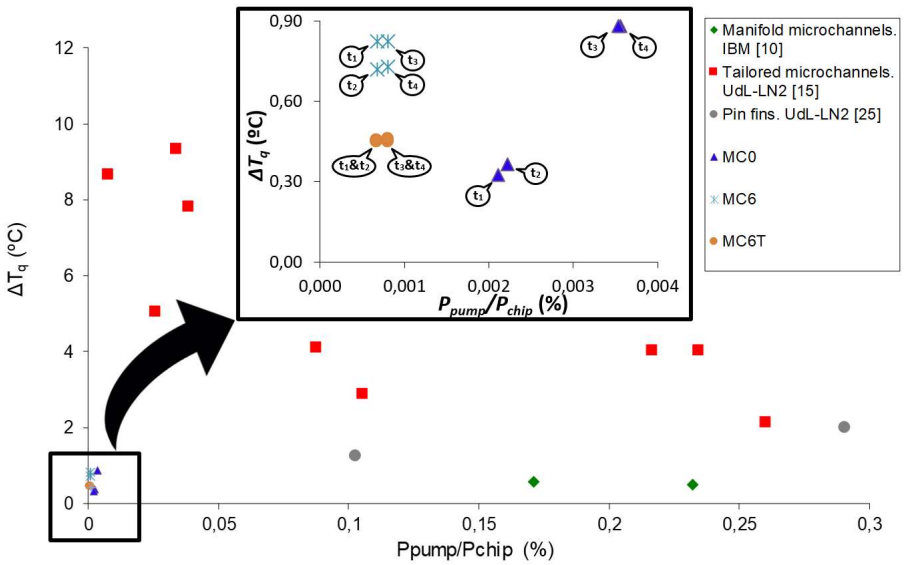

Figure 35: Comparison of the overall pumping performance with previous studies, for the 4 different heat load maps (t_1, t_2, t_3, t_4) of the heat load scenario considered

2.3.5. Conclusions

In this paper, a novel concept for cooling integrated chips in an energy-efficient way is numerically demonstrated under non-uniform and time-dependent heat load scenarios. The coolant is distributed towards an array of microfluidic cells where each cell's self-adaptive microvalve provides the required coolant flow rate as a function of its own temperature. Three internal geometries of the microfluidic cell are assessed. This assessment is made with the most demanding boundary

conditions, a maximum chip temperature allowed of 100 ºC with hotspots of 300 W/cm^2 and a coolant inlet temperature of 50 ºC.

Relevant temperature homogeneity and low pumping powers, which improve those of previous studies, are achieved by the studied configurations. The tailored microchannel device (MC6T) reaches, due to its internal geometry, a temperature uniformity of 4 ºC with a pumping power lower than 0.001 % of the chip power.

For identical performance (temperature limitation) and comparable boundary conditions, the pumping power of the microfluidic cell matrix with the best internal geometry (MC6T) reduces the energy needed for pumping along the 5 minutes time period to 10.9 % of microchannel configuration.

This work confirms the interest and capacity of the microfluidic cell array cooling strategy for improving the hotspot targeted cooling performance both in terms of temperature uniformity and pumping power.

Acknowledgement

The research leading to these results has been performed within the STREAMS project and received funding from the European Community's Horizon 2020 program under Grant Agreement N° 688564.

2.3.6. Velocity field analysis

Beyond the results presented in this article, in order to further improve the characterization of the microfluidic cell geometry, the coolant flow path has been assessed. The flow direction along the MC6T cell with 3.72 ml/min creates a jet impact just after the inlet (Figure 36a). This jet impact increases the heat transfer below the inlet zone, creating a cold zone as seen in Figure 29 with the MC0 and MC6 microfluidic cells. With the MC6T cell, the fluid velocity increases along the flow path from 0.15 m/s just before the microchannels to 0.26 m/s when the flow is at the end of the tailored microchannels. The progressive rise of velocity and increase of surface area along the flow path enhances gradually the heat transfer coefficient counterbalancing the increase of fluid temperature in order to get a better temperature uniformity (Figure 36b).

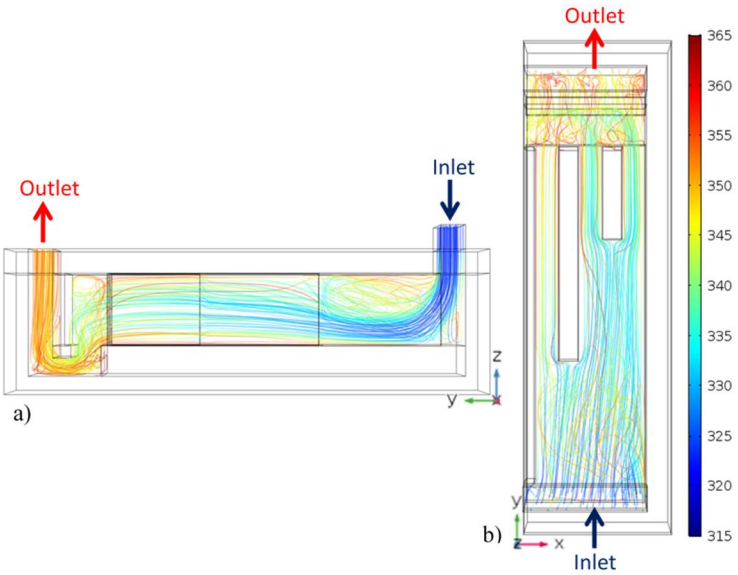

Figure 36: MC6T fluid velocity represented with streamlines when is applied 3.72 ml/min a) lateral view b) top view.

2.4. Impact of the self-adaptive valve behaviour on an array of microfluidic cells under unsteady and non-uniform heat load distributions

This chapter is the published paper "Impact of the self-adaptive valve behaviour on an array of microfluidic cells under unsteady and non-uniform heat load distributions" published in January 2019 at the Journal of Applied Fluid Mechanics.

The authors of this article are: Gerard Laguna[1], Montse Vilarrubí[1], Manel Ibañez[1], Joan Rosell[1], Ferran Badia[1], Hassan Azarkish[2], Louis-Michel Collin[2], Luc Fréchette[2] and Jerome Barrau[1].

[1]*University of Lleida, Lleida, 25001, Spain*

[2]*UMI-LN2, Institut Interdisciplinaire d'Innovation Technologique (3IT), Université de Sherbrooke, Sherbrooke, Canada*

Abstract

Previous studies have demonstrated that the performance of a cooling scheme based on a matrix of microfluidic cells with self-adaptive valves under unsteady and non-uniform heat load scenarios improves, in terms of pumping power and temperature uniformity, the ones from conventional microchannels and hybrid jet impingement/microchannel cooling devices. The behavior of the thermally dependent self-adaptive valves varies as a function of some design parameters. In this work, the impact of the valve's characteristic curve on the cooling device is assessed to establish the basic rules for the valve design. The performance of a 3×3 array of microfluidic cells is numerically studied under an unsteady and non-uniform heat load scenario. The results show that the valves which open at the most elevated temperature (control temperature of 90 ºC) reduce by 15.5 % the pumping power with respect to the valves opening at 60 ºC while improving by 25.0 % the temperature uniformity and reducing both the overcooling and the fatigue.

2.4.1.Introduction

Many applications, such as electronic devices or solar concentration receivers, are submitted to increasing heat flux densities, which implies the need for cooling devices that ensure their temperature control (safe function) without decreasing drastically their compactness. Liquid cooling devices based on microchannels [32] reach these goals as they provide very low thermal resistance coefficients. Nevertheless, this technology has two main drawbacks: large pressure drops, leading to high pumping powers, and poor temperature uniformity of the cooled object, implying reliability issues [37].

As a consequence, many papers and review articles are focused on enhanced microchannels [22,23,52] in order to deal with these drawbacks. Also, other solutions, based on hybrid jet impingement/microchannel techniques have been proposed and tested experimentally [24–27]. Such cooling schemes have demonstrated their capacity to obtain prefixed temperature profiles along the coolant flow path (even uniform) when tailoring at the design stage their internal geometry to the heat loads. Furthermore, the hybrid jet impingement/microchannels devices generate less pressure losses than conventional microchannels and, consequently, need lower pumping powers [28,29].

These investigations have been carried out through constant and uniform boundary conditions while heat load scenarios are, for example in electronic applications, usually unsteady and non-uniform. Riera *et al.* [53] demonstrated that, at the design stage, the internal geometry can be tailored to both uniform and non-uniform heat loads in order to generate a wide range of temperature profiles. However, as the geometry is fixed, the cooling device performance is not optimum when the heat load changes, for example in a transient heat load scenario. Therefore, cooling devices are overly conservatives and lead to oversized pumping powers.

In recent works, a cooling device formed by a matrix of microfluidic cells with individually variable coolant flow rate has been assessed under non-uniform and time dependent heat load scenarios [50,54]. The cooling scheme (Figure 37) consists in a matrix of microfluidic cells (dimensions 1.2 x 2.0 mm^2) with thermally activated microvalves (Figure 38, [16]), which tailor the local coolant flow rate to the local need of heat extraction capacity, avoiding overcooling and improving the temperature uniformity [54].

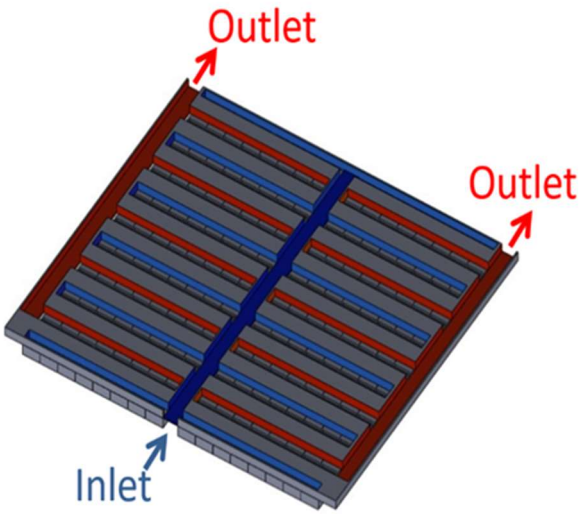

Figure 37: Microfluidic cells matrix with distributor

The self-adaptive valves are doubly-clamped beams, made with a high thermal expansion material with respect to the base on which they are fixed, that buckle when their temperature increases and therefore let the coolant flow through a slot located below them.

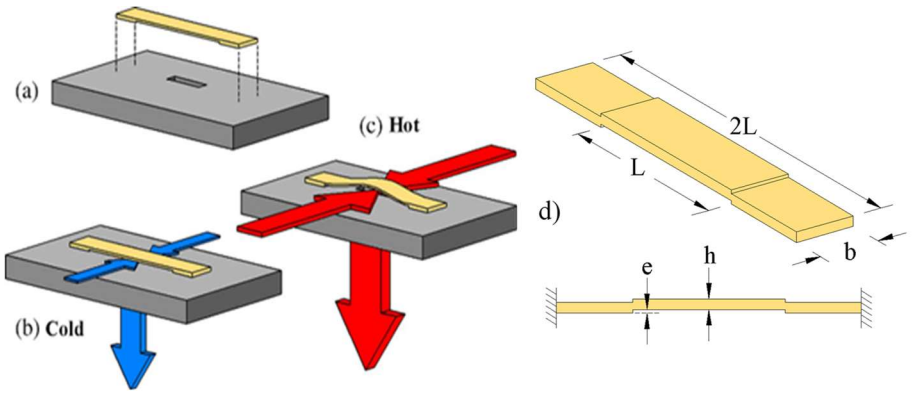

Figure 38: Microvalve a) placement, b) cold position c) hot position and d) valve parameters [16]

The authors demonstrated that the performance further enhance the one of conventional microchannels. Indeed, the temperature non-uniformities were reduced by a factor of 3 while the pumping power was reduced by 89.1 % [54]. These studies have been performed in ideal conditions, assuming the one dimensional approach presented by [55] and a theoretical valve with an aperture, and therefore a local flow rate, that maintains the maximum temperature of the cooled object below a given critical temperature.

However, as demonstrated by [56] the characteristic curves of the self-adaptive valves depend on their geometry (Figure 39).

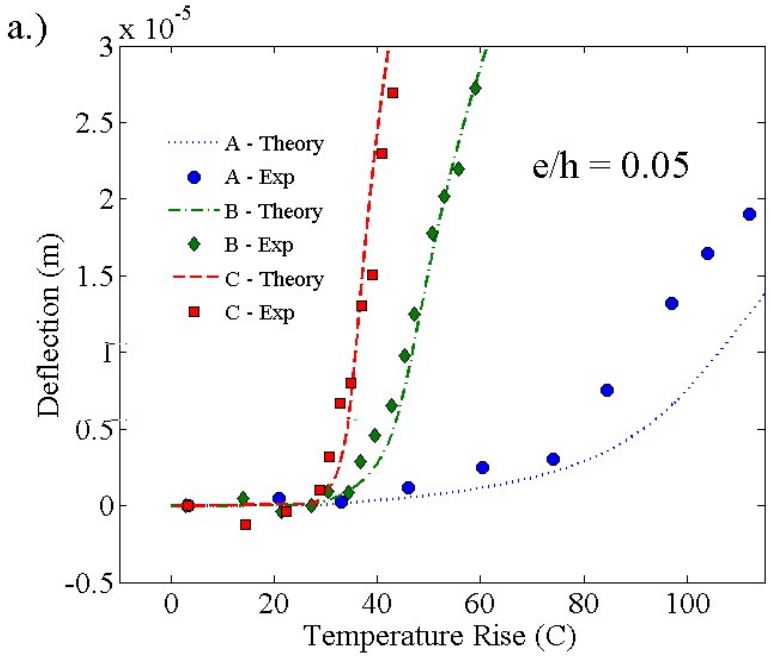

Figure 39: Valve deflection results with h = 30 µm, e = 1.5 µm and L = 1 mm (A), L = 2 mm (B) L = 3 mm (C) [56]

This behavior implies that the flow rate provided by the self-adaptive valve for a given set of boundary conditions does not correspond to the optimum one, which corresponds to the flow rate at which the maximum temperature of the cooled object is equal to the critical one. Therefore, the hypothesis of the one direction model, based on the isothermal assumption, is not verified.

In this study, a numerical model is developed to assess the performance of the matrix of microfluidic cells with self-adaptive microvalves. This model, which includes the conduction between adjacent cells, allows the assessment of the impact of spreading on the overall performance. Furthermore, the impact of the microvalve characteristic curves is evaluated to establish design criteria for this component.

2.4.2.Description of the cooling device

Geometry

In this work, a microfluidic cell with an external size of 2 x 1.2 mm^2 is used (Figure 40). Its internal geometry consists in 6 tailored microchannels that increase the local heat extraction capacity along the flow path, according to previous studies [54], counteracting the coolant temperature increase in the same direction.

The coolant (water in this study) enters from a distributor through a 1 x 0.1 mm^2 inlet slot located on the cell's cold side (heat load opposite side) and exits by the outlet slot, with the same dimensions as the inlet, connected to the exit path of the distributor. The valve is located at the outlet, near the heat load surface (hereafter chip surface), to approximate its temperature to the chip one (x, y, $z = 0$) and, therefore, to tailor the flow rate to this parameter.

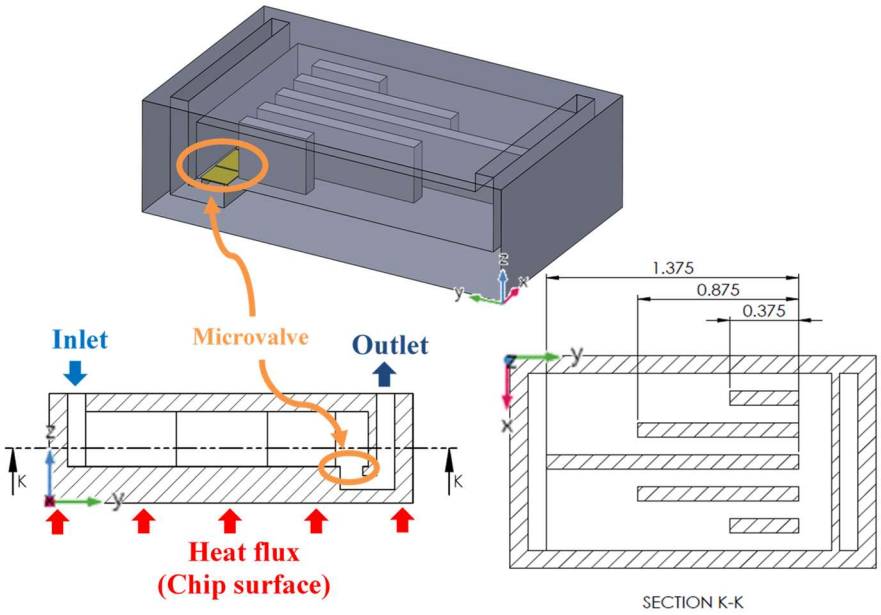

Figure 40: MC6T design (dimensions in mm)

Numerical Models

For all the numerical simulations, the coupling between heat transfer and fluid flow is included in the COMSOL Multiphysics CFD model in a steady state study with laminar flow model (maximum Reynolds number: 89).

At a first stage, a numerical study is carried out to assess the maximum flow rate needed to maintain the chip temperature below 100 ºC at the most demanding boundary conditions (heat flux: 300 W/cm^2; inlet coolant temperature: 50 ºC). For this steady-state study, the boundary conditions of the numerical models considered are indicated in Figure 41.

A mesh sensitivity analysis has been carried out and the final model accounts with 603921 elements.

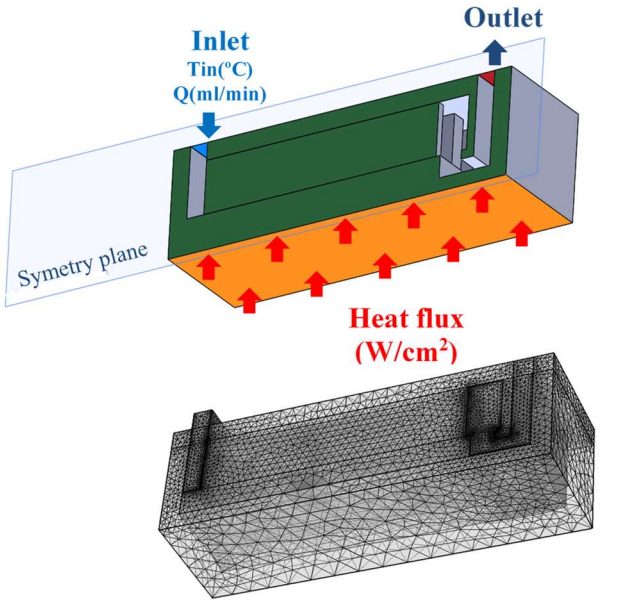

Figure 41: Numerical model. a) Boundary conditions, b) Mesh used

At a second stage, a numerical study is carried out with 9 microfluidic cells in a 3 x 3 cell matrix (Figure 42). This model has been implemented in order to take into account the conduction between adjacent microfluidic cells. Indeed, for non-uniform heat load scenarios, the characteristic curve of the valve generates some temperature uniformities that cause spreading.

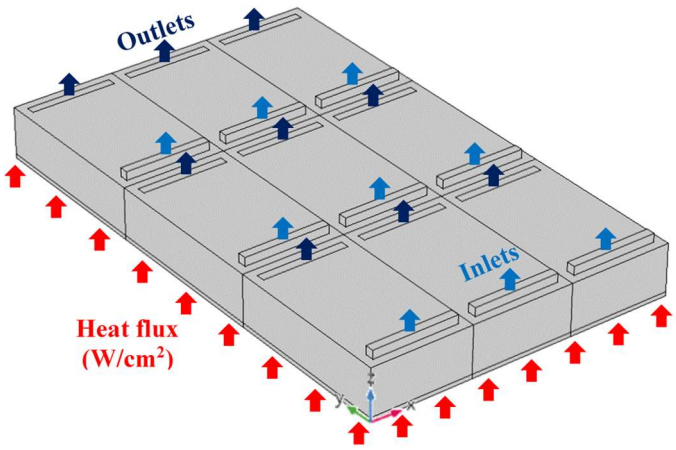

Figure 42: Boundary conditions of the numerical model.

The performance of the microfluidic cell array is assessed for three microvalve models. For the three models, (hereafter, V60, V75 and V90) the microvalves open linearly from control temperature (60 ºC, 75 ºC and 90 ºC, respectively) until complete opening is reached at 100 ºC (Figure 43). The maximum cell flow rate

(Q_{max}) corresponds to the one obtained in the previous simulation in the most demanding situation. When the boundary conditions vary with respect to the worst ones, the flow rate is tailored to the base temperature through the temperature dependent microfluidic valve function (hereafter characteristic curve). Below the control value, a residual flow rate (1 % of Q_{max}) enters the cooling cell, as this kind of microvalve can't close completely. This general trend of valve function corresponds to the results obtained previously (Figure 39, [56]).

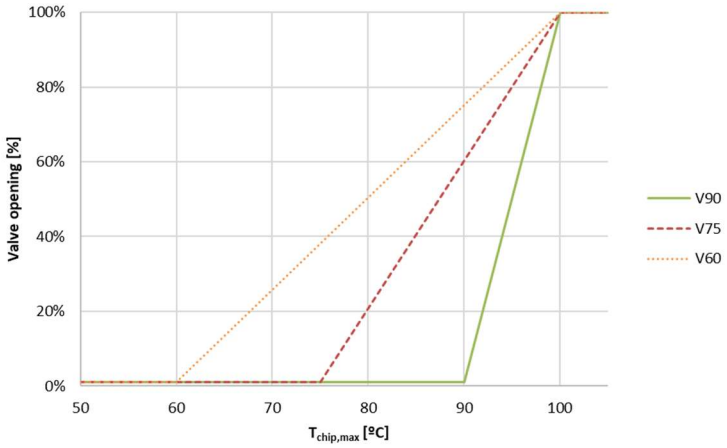

Figure 43: Microvalves aperture percentage versus temperature (characteristic curves).

Unsteady and non-uniform heat load scenario

A non-uniform and time dependent heat load scenario, including hotspot and base heat flux zones, is applied to the 3 x 3 microfluidic cell array (Figure 44 and 43). The hotspot (300 W/cm^2), that fully covers the central microfluidic cell, is activated periodically (t_1) while the surrounding microfluidic cells are submitted to a base heat flux of 150 W/cm^2. When the hotspot is not activated, all the cells are submitted to the base heat flux of 150 W/cm^2 (t_2).

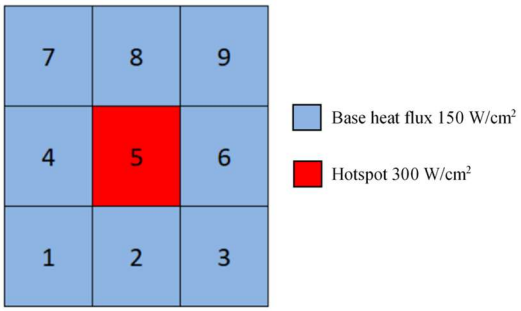

Figure 44: Heat flux distribution at t_1 on the 3x3 microfluidic cell array

Finally, in order to assess the global performance of the cooling device, the steady state results corresponding to the boundary conditions of t_1 and t_2 are integrated along a 5 minutes' time period.

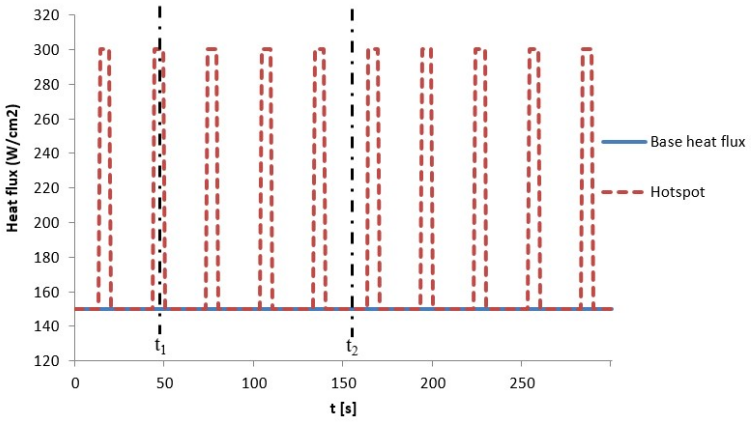

Figure 45: Time dependence of the heat loads

2.4.3.Results and discussion

Maximum flow rate assessment for a single microfluidic cell in extreme boundary conditions

The maximum flow rate (Q_{max}) needed to maintain the maximum temperature of the heated area below 100 ºC and assessed for a heat flux of 300 W/cm^2 and an inlet coolant temperature of 50 ºC (extreme boundary conditions), is 3.9 ml/min (Table 2). In these conditions, the thermal resistance coefficient of the cooling device, assessed through equation (9), is $1.6 \cdot 10^{-5}$ m^{2}ºC/W.

$$R = \frac{T_{chip} - T_{in}}{q''} \tag{9}$$

Table 2: Thermo-hydraulic performance of the cooling cell in worst conditions (300 W/cm^2 and inlet temperature 50 ºC)

T_{chip} [ºC]	$T_{chip,\,max}$ [ºC]	R [m^{2}ºC/W]	ΔT_{chip} [ºC]	ΔP [Pa]
98.3	100.0	$1.6 \cdot 10^{-5}$	5.1	1384

Compared to conventional microchannels or other internal geometries of the microfluidic cells [54], the tailored microchannels allow obtaining a relatively low maximum temperature difference across the microfluidic cell base (5.1 ºC). The maximum chip temperature is not located near the outlet, but in the center of the microfluidic cell, due to the effect on the tailored microchannel internal geometry (Figure 46).

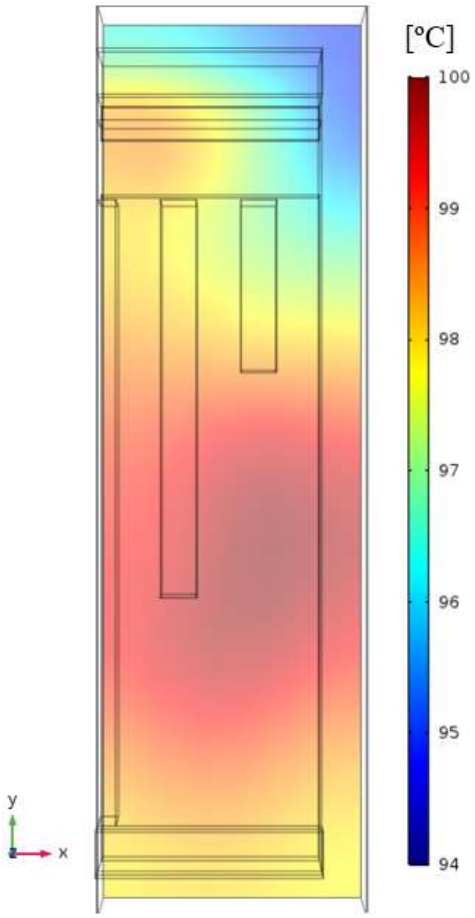

Figure 46: Chip temperature distribution for extreme boundary conditions and maximum flow rate

Performance of the microfluidic cell array for uniform and non-uniform heat loads

The flow rate of each of the microfluidic cells is now assessed considering the characteristic curve of the self-adaptive microvalves (V60, V75 and V90) and the thermal conduction across the entire computational domain. The thermal maps of the 3 x 3 microfluidic cells array, obtained for the 3 microvalve models at t_1 and t_2, show that their characteristic curves have an impact on both the average temperature and the temperature uniformity (Figure 47).

When the heat flux is uniform (t_2), the temperature distribution is similar for the 3 microvalve models, but the average temperature increases with the control temperature of the valve (Figure 48). For the non-uniform heat flux distribution (t_1), a similar trend is found, but a detailed analysis of the results (Table 3) shows a different behavior for the central microfluidic cells depending on the microvalve model V60, V75 and V90.

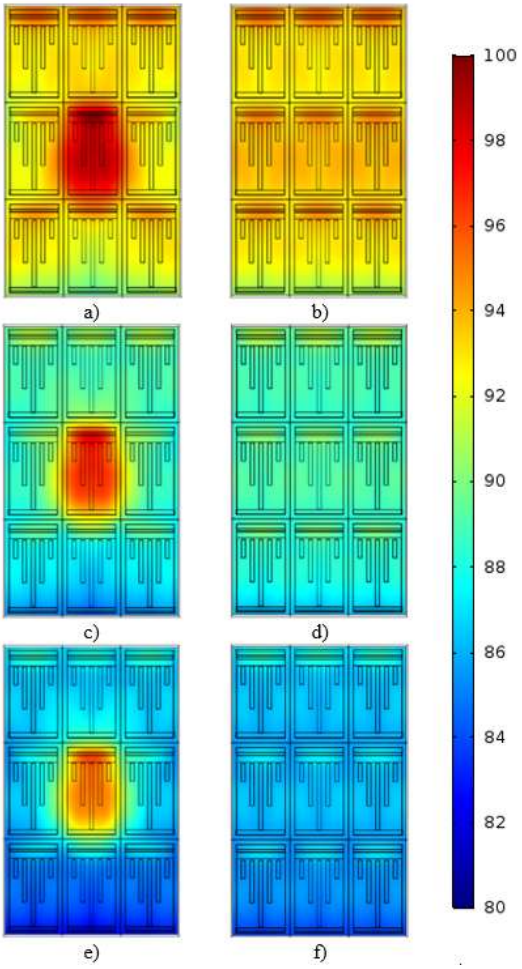

Figure 47: Thermal map of the chip surface for a) V90; t_1, b) V90; t_2, c) V75; t_1, d) V75; t_2, e) V60; t_1 and f) V60; t_2

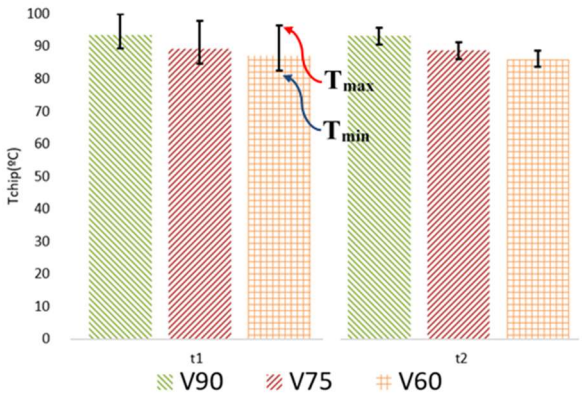

Figure 48: Average chip temperature and its variation across the entire chip surface for t_1 and t_2 for each valve

On the one hand, the global flow rate (sum of all the single microfluidic flow rates) is decreased by 19.3 % (Table 3) when microvalve V90 is used instead of V60 (at t_1). Furthermore, V90 valve brings the maximum temperature closer to the critical one (100 ºC) and improves the temperature uniformity by 25 %. These results show that the elevated slope of the V90 characteristic curve is adequate to limit the overcooling and improves the temperature uniformity.

Table 3: Thermo-hydraulic performance of the cooling 3 x 3 matrix cell

	Valve	T_{in} *[ºC]*	Q *[ml/min]*	T_{chip} *[ºC]*	$T_{chip,\ max}$ *[ºC]*	R *[m²ºC/W]*	ΔT_{chip} *[ºC]*	ΔP *[Pa]*	P_{pump} *[W]*
	V60	50.0	20.2	87.1	96.5	$2.2 \cdot 10^{-5}$	14.0	817	$2.75 \cdot 10^{-4}$
t_1	*V75*	50.0	18.6	89.3	97.9	$2.4 \cdot 10^{-5}$	13.3	818	$2.54 \cdot 10^{-4}$
	V90	50.0	16.3	93.4	99.8	$2.6 \cdot 10^{-5}$	10.5	908	$2.47 \cdot 10^{-4}$
	V60	50.0	18.3	86.0	88.6	$2.4 \cdot 10^{-5}$	5.0	559	$1.70 \cdot 10^{-4}$
t_2	*V75*	50.0	16.5	88.7	91.3	$2.6 \cdot 10^{-5}$	5.2	482	$1.32 \cdot 10^{-4}$
	V90	50.0	14.1	93.2	95.8	$2.9 \cdot 10^{-5}$	5.3	390	$9.18 \cdot 10^{-5}$

On the other hand, the flow rate of the central microfluidic cell (at t_1) is higher for V90 than for the other valves, causing a highest pressure drops in this cell and so, at the entire hydraulic circuit, as the cells are hydraulically connected in parallel. This result is due to the fact that the elevated slope of the V90 characteristic curve generates an improvement of the temperature uniformity of the array. As a consequence, the spreading effect decreases and the central cell (submitted to the highest heat flux) with V90 valve has to absorb nearly all the heat that is fed into it. Meanwhile, for the other valves (V60 and V75), the temperature non-uniformities generate thermal conduction heat fluxes from the central cell to the surrounding ones (Figure 49), and the flow rates needed to maintain the temperature below the critical one are lowers. Quantitatively, the central cell with the valve V60, V75 and V90 deliver by spreading to the other cells 28.14 %, 24.93 % and 15.97 % respectively.

So, for the non-uniform heat flux distribution (t_1), the impact of the lower global flow rate of V90 cell on the hydraulic pumping power (P_{pump}), with respect to V60 and V75, is partially counterbalanced by its higher pressure drop. On the contrary, for the uniform heat load (t_2), both the global flow rate and the pressure drops are lower for the V90 microfluidic cell, lowering the pumping power needed with respect to the other 2 valves.

In all the cases considered, the thermal resistance coefficient (R) of the 3 x 3 array of microfluidic cells increases slightly with respect to the single cell, as the flow rate per cell is lower.

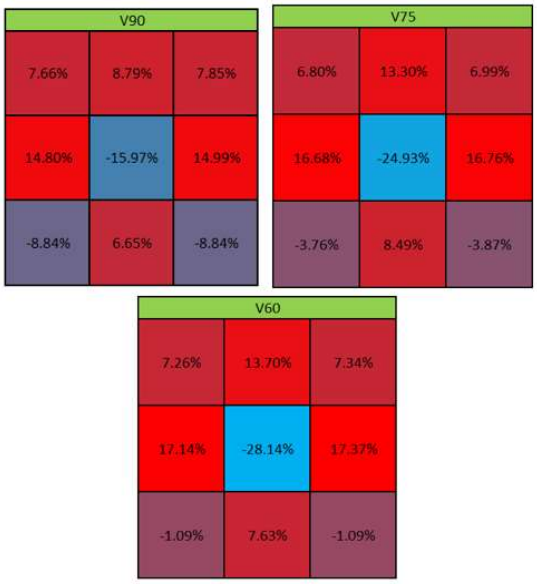

Figure 49: Power absorbed by each cell compared with the delivered power (%)

Performance of the microfluidic cell array in unsteady and non-uniform heat loads

The total flow rate of the 3 x 3 array of microfluidic cells varies depending on the heat load distribution at each moment, through the characteristic curve of the self-adaptive microvalve (Figure 50). As exposed in the previous chapter, for both the uniform and non-uniform heat loads, the flow rate needed to reach the temperature restriction, 100 ºC on the chip surface, decreases when the valve control temperature increases. The average flow rates of the 3 x 3 array of microfluidic cells, along the time considered, with V90 and V75 valves are, respectively, 77.9 % and 90.5 % of the one with V60 valve. This result indicates that, from the flow rate point of view, the design of the valve has to be focused to reach a quick aperture through a nearly discontinuous manner (perfect beam, [56]).

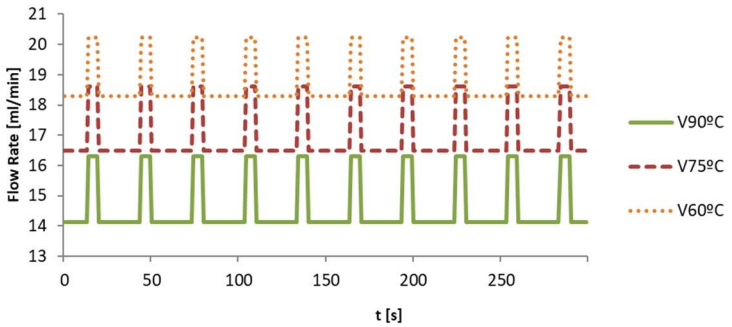

Figure 50: Total flow rate along the time period

The cooling device with V90 valve maintains the maximum temperature of the chip closer to the critical one than the other studied valves, indicating that it reduces the overcooling of the system (Figure 51). Furthermore, the variation of the maximum temperature of the chip surface, for both the uniform and the non-uniform heat load, is lower in the case of the cooling device with V90 valve (4.1 ºC) than for V60 (7.9 ºC) and V75 (6.6 ºC). This result indicates that V90 valve will induce less fatigue due to the thermal cycling than the other 2 studied valves.

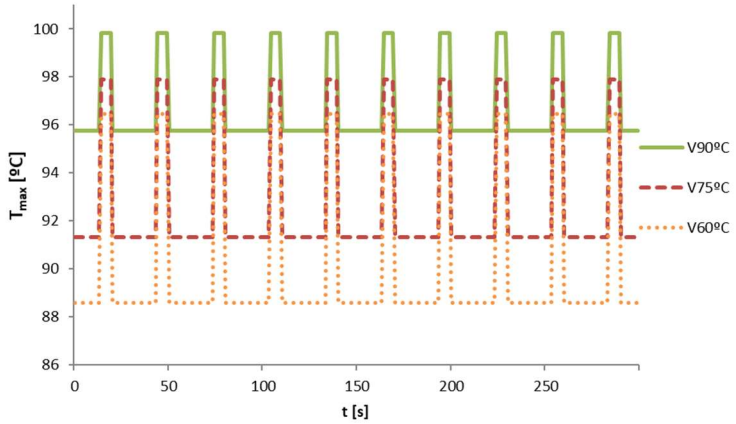

Figure 51: Maximum temperature of the chip surface along the time period

The valve opening range is an indicator of the efficiency of the cooling solution. If the opening value is far from the maximum temperature, it will produce overcooling so it will be less energy efficient. For this reason, the flow during all the integration time with the V60 valve is higher than with the other valves (Figure 50).

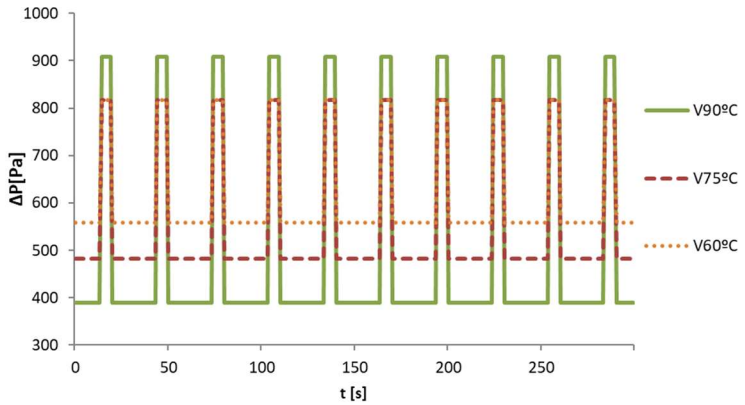

Figure 52: Pressure drop along the time period

For the non-uniform heat load (t_1), the flow rate of the central cell is respectively 91.21 %, 91.58 % and 98.08 % for V60, V75 and V90 of the maximum one (Q_{max}).

The higher flow rate in the central cell with V90 implies, for the non-uniform heat load, higher pressure drops.

The assessment of the time dependent total flow rate and pressure drops provides the hydraulic pumping power trend along the period considered (Figure 53), assessed through equation (10).

$$P_{pump} = \Delta P \cdot Q \tag{10}$$

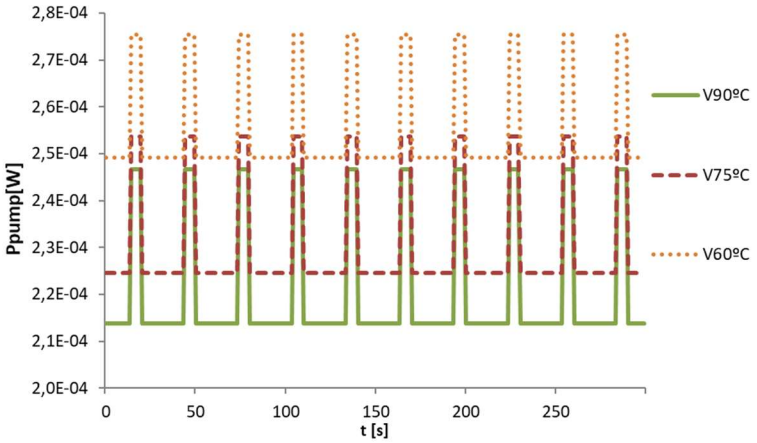

Figure 53: Pumping power of the whole cooling device along the time period

For the same temperature limitation, the average power consumption, assessed along the 5 minutes period, of the V75 and V60 are respectively 4.53 % and 15.49 % higher than the V90 power consumption. The V90 valve tailors better the local flow rates to the heat extraction needs, maintaining the chip temperature closer to the temperature limitation. Also, as explained previously, the pressure drop is increased at t_1 for V90 due to the lower spreading between the microfluidic cells, but this drawback is counterbalanced by the flow rate reduction.

The pumping energy for the studied cooling device with V90, V75 and V60 valves (E_{valve}) is, respectively, 27 %, 29 % and 32 % of the energy needed by the same cooling device but without the self-adaptive valves ($E_{no\text{-}valve}$), so without the capacity to tailor the flow rate distribution to unsteady and non-uniform heat load scenarios (Figure 54). Furthermore, V90 characteristic curve provides the highest temperature uniformity to the cooled surface (Figure 54), indicating that a sudden change of the double clamped beam actuating as the valve is more appropriate than a progressive one.

These results would vary as a function of the heat load scenario characteristics.

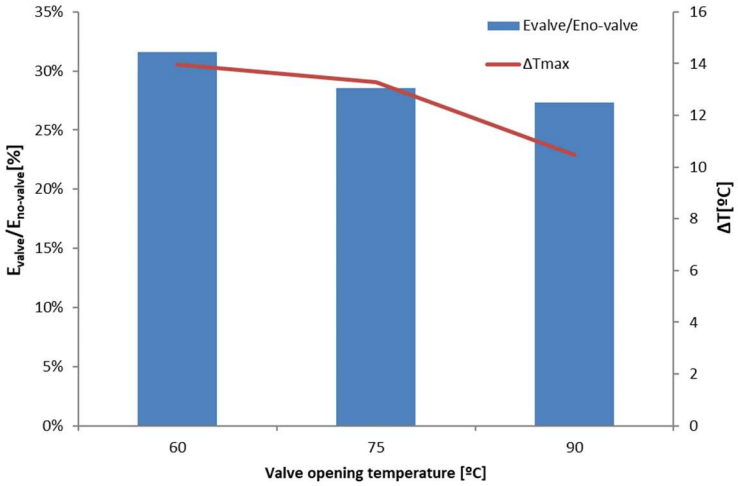

Figure 54: $E_{valve}/E_{no\text{-}valve}$ and temperature uniformity depending on microvalve control temperature.

2.4.4. Conclusion

The impact of the behavior of thermally dependent self-adaptive valves on the performance of a cooling scheme based on a matrix of microfluidic cells with individually variable coolant flow rate is assessed. The self-adaptive valves are doubly-clamped beams, made with a high thermal expansion material with respect to the base on which they are fixed, that buckle when their temperature increases and therefore let the coolant flow through a slot located below them. Previous studies show that the deflection of the beam, and therefore the variation of the flow rate through the valve, can present different behaviors (from discontinuous to continuous nonlinear) as a function of some design parameters.

After showing that the unidirectional heat flux hypothesis, assumed by some authors, is not verified due to the non-ideal behavior of the self-adaptive valves, a 3 x 3 array of microfluidic cells is proposed to assess the performance of the cooling device, taking into account the conduction between cells, for different valve characteristic curves. For a given unsteady and non-uniform heat load scenario, targeting the criteria of limiting the maximum temperature of the heated surface below 100 ºC, the time-dependent distribution of the microfluidic cell flow rates is assessed.

For the uniform heat flux distribution, both the flow rate and the pressure drop of the device using V90 valve, the one with the highest control temperature, are reduced with respect to V60 valve, by 23 % and 30 %, respectively.

However, for the non-uniform heat flux distribution, the flow rate of the cooling device with the V90 valve is still lower than the other studied ones, but its pressure drop is higher, counteracting partially the gains, in terms of pumping power, related

to the lower flow rate of V90 device. Indeed, while the central microfluidic cell, submitted to the highest heat flux, of the devices with V60 and V75 valves spreads a relatively large part of the received heat to the surrounding cells (25 and 28 %, respectively), V90 characteristic curve provides a distribution of the microfluidic cell flow rates that reduces the temperature variation across the heated surface and, therefore, the thermal conduction between cells (spreading of 15 % to the surrounding cells).

These behaviors imply that the energy needed for pumping along the time period considered is, for V90, V75 and V60, only 27.3 %, 28.6 % and 31.6 % respectively of the one needed by a similar cooling device without microfluidic valves. Apart from its benefits in terms of pumping power, the higher slope of the V90 characteristic curve provides a better temperature uniformity of the cooled surface, limits the overcooling and reduces the temperature variations along the heat load scenario.

Acknowledgements

The research leading to these results has been performed within the STREAMS project (www.project-streams.eu) and received funding from the European Community's Horizon 2020 program under Grant Agreement n° 688564.

3. Microfluidic cell cooling device for dense array CPV receivers

The cooling solution studied in this thesis is focused on microelectronic applications, but its performance in other fields where advanced and efficient cooling solutions are required is also studied.

3.1. Cooling challenges in CPV

Concentrator photovoltaics (CPV) is a promising technology to reduce the PV costs and to increase its efficiencies, which requires a cooling device that is able to provide a uniform temperature distribution with a low energy consumption [57,58].

Indeed, the power density is higher than in non-concentrated photovoltaics due to the sun concentration. The CPV cell's efficiency decreases with the temperature, so active cooling solutions are mandatory to keep the CPV cell's temperatures within an adequate range. Furthermore, cells at different temperatures will have their maximum power point (MPP) under different current and voltage, so the connection between them will produce a deviation from the MPP of each cell, known as the mismatch effect [59,60].

In order to cool the CPV cells, many different approaches, depending on the CPV type, have been tested.

Point-focus CPV devices which consist in concentrating the sun into a point can reach high concentrations in a relatively small space (2–14 mm). The high power densities that need to be dissipated can be extracted by natural convection by spreading the heat onto a large surface, with or without a passive heatsink [61,62]. However, this can be achieved only until a total dissipated power limit (around 40 W). For higher power, active cooling techniques should be considered [58].

Linear CPV, which consists in concentrating the sun into a row of CPV cells, is usually submitted to active cooling. Many research studies have been focused on cooling the linear CPV receiver with a channel under the cells [63–65]. Moreover, in some studies, the cells are placed inside the channel, taking advantage of dielectric fluids that are able to increase the cooling area by cooling the CPV cell using both the bottom and the top surface of the cell [66]. However, the use of a channel presents the same issues as microchannels, related to the heating of the fluid along the flow path, creating a temperature gradient in the same direction. This temperature gradient causes an efficiency drop in the module due to the mismatch effect [67].

Densely packed CPV receivers consist in concentrating the sun into an array of CPV cells, cooled by an active system. Due to their large area compared with the other CPV configurations, these receivers require a cooling system that is able to extract hundreds or thousands of Watts with a high compactness requirement. For this reason, researchers have been studying the use of advanced cooling systems in order to reach high heat transfer coefficients at reduced energy costs. As seen in

linear CPV, one cooling solution studied in densely packed CPV receivers is the immersion of the CPV module into a channel [68,69].

Another one, proposed by Royne and Dey [70], consists in the use of different configurations of jet impingement. However, this solution induces large differences in the heat transfer coefficient across the receiver, which can cause large temperature gradients. To improve the temperature uniformity, Barrau *et al.* [29] implement a hybrid system with jet impingement and tailored microchannels.

To sum up, CPV is a field where high temperatures reduce both the efficiency and the lifetime of the cells, while also large temperature gradients induce module efficiency losses due to the mismatch effect. Focusing on densely packed CPV receivers, where the cooling requirements are more challenging, the most commonly proposed solutions are based on microchannels, jet impingement or some combination of them. Microchannel devices have an inherent temperature gradient, due to the heating of the fluid along the path and the jet impingement presents an irregular heat transfer coefficient which evolves into irregular cooling. On the other hand, the combination of tailored microchannels and jet impingement can present a uniform temperature profile, but only in the heat flux conditions for which it has been designed. This system is not able to maintain the temperature uniformity along with all the operating conditions, which include time-dependent and non-uniform illumination profiles.

The self-adaptive cooling solution presented in this thesis meets all the requirements for its application in dense array CPV receivers. Indeed, it improves the CPV net efficiency by reducing the energy needed to cool the CPV system and reduces the mismatch effect by lowering the temperature non-uniformities across the module.

3.2. CPV modelling

In order to assess the impact of the microfluidic cell cooling device on the performance of a dense array CPV receiver, the results from the CFD models are used in combination with a model which represents the electrical behaviour of a CPV receiver under different irradiation and temperature boundary conditions. The CPV model is defined by the following equations:

$$I = I_L \frac{C}{C_0} - I_0 \cdot \left[e^{\frac{V}{V_T}} - 1 \right] \tag{11}$$

$$I_0 = I_0{}' \cdot T^3 \cdot e^{\left(\frac{-C_1}{K_B T}\right)} \tag{12}$$

$$V_T = \frac{K_B \cdot T \cdot \mathrm{n}}{e^-} \tag{13}$$

where

- I is the current [A]
- I_L is the short-circuit current [A]
- C is the sun concentration [suns]
- C_0 is the reference solar concentration [suns]
- I_0 the cell temperature dependence of the equivalent reverse diode current [A]
- V is the potential [V]
- V_T is the thermal voltage [V]
- $I_{0'}$ is the reverse current factor independent of the voltage [A/K^3]
- T is the cell temperature [K]
- C_1 is the equivalent band gap [J]
- K_B is the Boltzmann constant [J/K]
- n is the ideality reduced factor [-]

3.3. Distributed and self-adaptive microfluidic cell cooling for CPV dense array receivers

This chapter is the published conference paper "Distributed and self-adaptive microfluidic cell cooling for CPV dense array receivers" published on September 2017 at AIP Conference Proceedings.

The authors of this article are: Gerard Laguna[1], Jérôme Barrau[1], Luc Fréchette[2], Joan Rosell[1], Manel Ibañez[1], Montse Vilarrubí[1], Yina Betancourt[1], Hassan Azarkish[2], Louis-Michel Collin[2], Alvaro Fernandez[1] and Gonzalo Sisó[1]

[1]Dynamic Systems Applied to Solar Energy Research Group, University of Lleida, Lleida, Spain

[2]UMI-LN2, Institut Interdisciplinaire d'Innovation Technologique (3IT), Université de Sherbrooke, Sherbrooke, Canada

Abstract

Temperature non uniformities of the CPV receivers lead to mismatch losses. In order to deal with this issue, a cooling device, formed by a matrix of microfluidic cells with individually variable coolant flow rates, has been developed. This device tailors the distribution of the heat extraction capacity over the CPV receiver to the local cooling needs in order to reduce the temperature non-uniformities with respect to microchannel devices when submitted to uniform or non-uniform illumination profiles. At equal average temperature of the CPV receiver, power generation applying the matrix of microfluidic cells with individually variable coolant flow rate is 9.7 % higher than the one with conventional microchannel technology.

3.3.1.Introduction

Concentrating photovoltaics (CPV) is a promising technology to reduce the cost of PV power generation. The cooling of dense array CPV receivers must reach low thermal resistance coefficients below 10^{-4} m^2K/W [71], high compactness and relevant capacities to provide a high temperature uniformity of the PV receiver, both for reliability and efficiency issues [72,73]. Several works have assessed the impact of cooling schemes on the performance of the CPV devices when submitted to constant heat loads [28,53]. They showed than the optimum flow rate varies with the solar concentration. Some works [24] have shown the capacity of improved microchannel cooling schemes to obtain, through an adequate design, uniform temperature profiles when submitted to uniform and non-uniform heat flux distributions. Nevertheless, the heat flux distribution on a CPV receiver is non-uniform and time dependent [29]. As a consequence, cooling devices with constant and uniform flow rate distributions are overly conservatives and lead to non-uniform temperature distributions and oversized pumping powers. Temperature non uniformities increase the mismatch losses and mechanical stresses throughout the receiver, which causes reliability losses [74]. Furthermore, the pumping power needed to decrease the PV cell temperature and, therefore, to increase the PV efficiency, must be balanced with the PV output in order to find the optimum working point [29].

In this work, the impact of a cooling device, formed by a matrix of microfluidic cells with individually variable coolant flow rate, on the performance of a CPV receiver is assessed under non-uniform and time dependent heat load scenarios and compared to conventional microchannels.

3.3.2.Description of the cooling device

In the proposed configuration, the coolant (water) is distributed towards a matrix of microfluidic cells (Figure 55a). Each microfluidic cell has a temperature controlled microvalve [16] that self-adapts the cell flow rate to the local temperature. The microvalves adapt the coolant flow rate in each cell to the minimum required to maintain the desired temperature, allowing higher flow rates when the temperature rises due to increased local heat load. By adapting to the local heat extraction needs, the temperature is made more uniform across the cell array. The studied internal geometry of the microfluidic cell uses tailored fins (Figure 55b) to improve the temperature uniformity within a single cell and the flow path is short in order to reduce the pressure losses. The self-adaptive thermostatic microvalves (Figure 56) are located near the coolant outlet and on the hot side of each microfluidic cell and provides a coolant flow rate that increases significantly when the cell reaches a design operating temperature. The valve operates on a thermostatic principle, where the thermal expansion of the valve body with respect to the substrate will open an orifice allowing an increase in coolant

flow rate. This self-adaptive microvalve principle has been previously modeled and experimentally demonstrated for a single cell [16], but is applied in this study to a matrix of solar cells. This novel approach aims to increase the reliability of the CPV receiver by minimizing thermal cycling (time variations) and thermomechanical stresses (spatial variations), as well as minimize the time dependent pumping power.

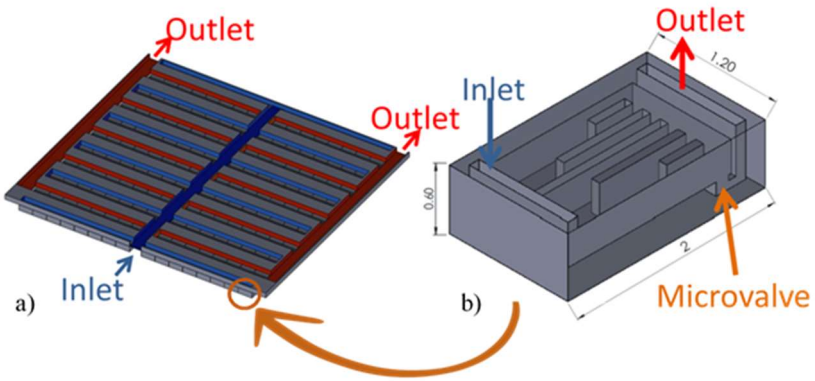

Figure 55: (a) Coolant distribution on the cell matrix (b) Microfluidic cell

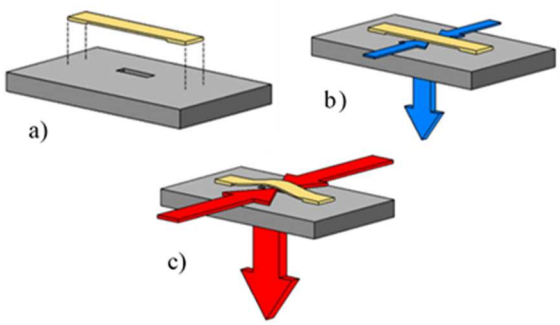

Figure 56: Microvalve (a) placement (b) cold position (c) hot position [16]

3.3.3.Impact of the cooling device on the CPV performance

To study the impact of this cooling approach, the performance of a CPV receiver composed by 6 strings of 8 PV cells in series [74] is predicted when submitted to an average solar concentration (C) of 600 suns and a non-uniform illumination profile (Figure 57; [29]). Two cooling configurations are compared: cooled by conventional microchannels versus cooled by the proposed matrix of microfluidic cells with individually variable coolant flow rate. The valve aperture has non-linear temperature dependence from its closed shape (until 323 K) up to its fully open shape (at 372 K, [16]).

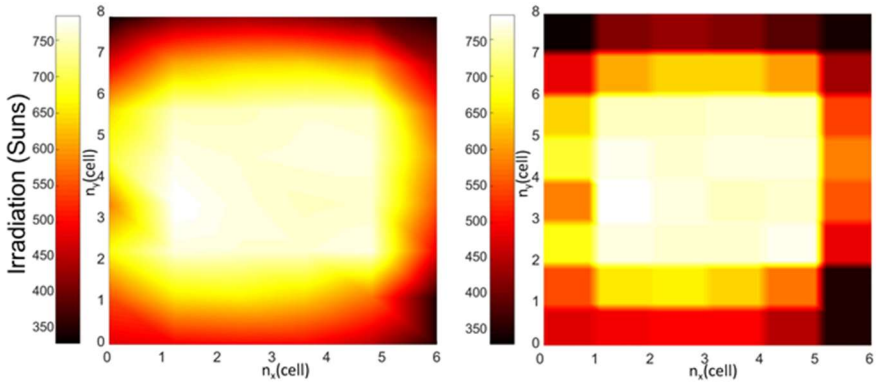

Figure 57: (a) Irradiation distribution (b) Irradiation distribution, averaged by PV cell

The characteristics (at 25 ºC) of the 1.0 x 1.0 cm^2 PV cells are described in Figure 58 and Table 4 [75].

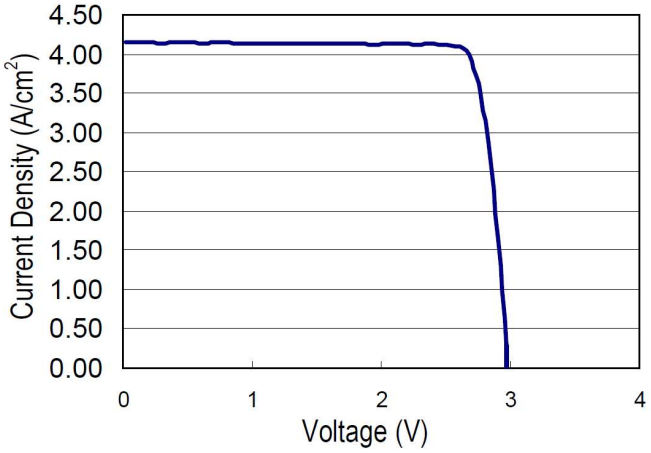

Figure 58: Nominal cell IV characteristic curve at 25 ºC and 350 suns [75]

Table 4: Typical cell electrical parameters at 25 ºC and 350 suns [75]

Parameter	*Value*
J_{sc}	4.14 A/cm^2
J_{mp}	4.05 A/cm^2
V_{OC}	2.97 V
V_{mp}	2.64 V
P_{mp}	10.68 W/cm^2
FF	86.9 %
Efficiency	30.5 %

To assess the temperature profile given by the microchannel cooling device an equivalent thermal resistance model is used, with two nodes by PV cell: one relative to the cell temperature and the other to the coolant temperature [76]. A thermal resistance coefficient of the microchannel device of $5 \cdot 10^{-5}$ Km^2/W [24] is used.

Since convection to the coolant fluid is the dominant heat transfer path and the temperature differences between cells are low (10 K in the whole CPV receiver), lateral conduction between cells is neglected in this study. The non-uniform distribution of the coolant flow rate of the matrix of microfluidic cells is represented in Figure 59. In the case of the proposed cooling device, the thermal behavior of each microfluidic cell is assessed by resolving both the heat transfer obtained by the cooling device (correlation extracted from a CFD numerical model) and the flow rate given by the temperature of the self-adaptive microvalve [16].

The total flow rates of both cooling devices have been determined in order to reach an identical average temperature (67 ºC) of the CPV receiver and to assess the effect of the temperature non uniformity on the PV output.

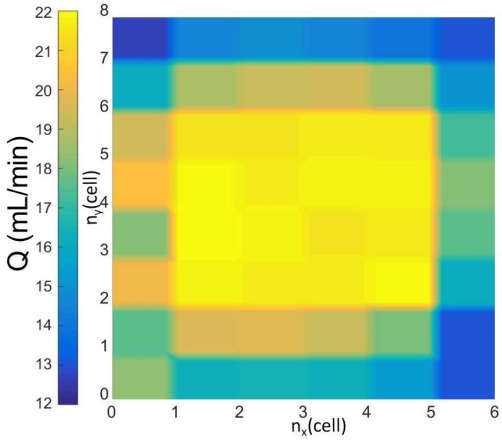

Figure 59: Flow distribution for microfluidic cell system

The maximum temperature difference of the CPV receiver is 34 K and 10 K for conventional microchannel and the matrix of microfluidic cells, respectively (Figure 60a and Figure 60b). For the microchannel device, heating of the coolant along the flow path implies a displacement of the maximum temperature with respect to the irradiation pattern. The PV cell characteristic IV curve has been used to calibrate the reduced model used for the assessment of the PV cell power output under different irradiation and temperature conditions. The model can be defined by the following equations (14):

$$I = I_L \frac{C}{C_0} - I_0 \cdot \left[e^{\frac{V}{V_T}} - 1 \right] \tag{14}$$

Where V and I are the potential and the current of the PV cell, respectively. C_0 is the reference solar concentration (350 suns) and I_0 is the cell temperature (T) dependence of the equivalent reverse diode current:

$$I_0 = I_0' \cdot T^3 \cdot e^{\left(\frac{-C_1}{K_B T}\right)} \tag{15}$$

Where the I_0' is the reverse current factor, independent of the temperature and the thermal voltage V_T, defined as:

$$V_T = \frac{K_B \cdot T \cdot n}{e^-} \tag{16}$$

The obtained values are presented in Table 5:

Table 5: Parameters obtained from the reduced model

Description	*Symbol*	*Value*
Short-circuit current	I_L	4.14 A
Reverse current factor	I_0'	0.30419 A/K^3
Equivalent bandgap	C_1	3.1918 J
Ideality reduced factor	n	1.613

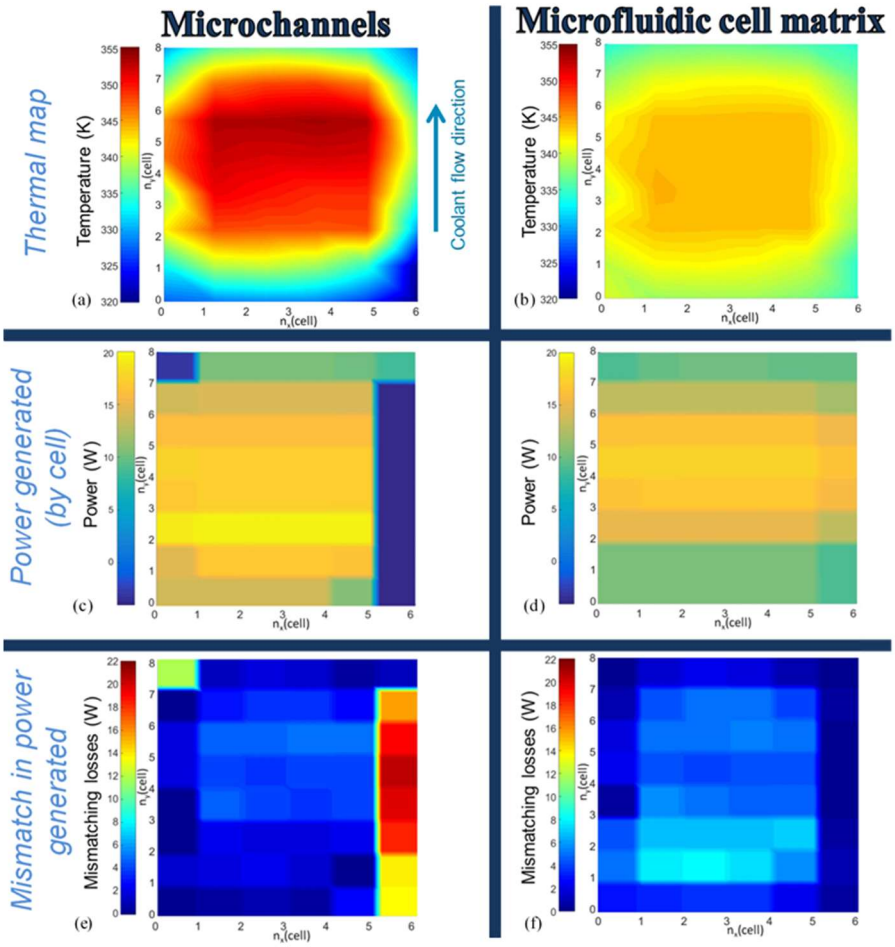

Figure 60: a) CPV thermal map cooled by microchannels (average 340.5 K) b) CPV thermal map cooled by microfluidic cell matrix (average 340.5 K) c) CPV power generated for each PV cell cooled by microchannels (average 12.5 W) d) CPV power generated for each PV cell cooled by microfluidic cell matrix (average 13.7 W) e) CPV mismatch generated for each PV cell cooled by microchannels (average 4.7 W) f) CPV mismatch generated for each PV cell cooled by microfluidic cell matrix (average 3.6 W).

The I-V curve of the CPV receiver is assessed and used to determine the maximum power point. The power generated by each cell in these conditions is represented in Figure 60c and Figure 60d. The CPV power generated by the PV receiver cooled by microfluidic cell matrix is 9.6 % higher than the one generated by the PV receiver cooled by microchannels.

The power generated by each cell in the studied series/parallel configuration is compared to the one that could be produced, in the same illumination and temperature conditions, when the PV cells are electrically isolated. The mismatch losses (Figure 60e and Figure 60f) are 27.4 and 20.3 % for the microchannel cooling device and the matrix of microfluidic cells, respectively.

3.3.4. Conclusions

The advances in Concentration PV cell technology imply the increase of the Fill Factor and, therefore, lead to higher impacts of the mismatch losses associated with the CPV receiver's temperature non uniformities. The matrix of microfluidic cells with individually variable coolant flow rate is able to provide high temperature uniformities under time dependent and non-uniform heat loads.

Global power generations of the CPV receiver cooled by microchannels and microfluidic cells are, respectively, 72.6 % and 79.7 % with respect to the sum of the electrically isolated cells production at the same illumination and temperature conditions. At equal average temperature of the CPV receiver power generation using the matrix of microfluidic cells with individually variable coolant flow rate is 9.7 % higher than the one with conventional microchannel technology.

Acknowledgments

The research leading to these results has been performed within the STREAMS project and received funding from the European Community's Horizon 2020 program under Grant Agreement n° 688564.

3.4. Dense array CPV receivers: Impact of the cooling device on the net PV output for different illumination profiles

This chapter is the published conference paper "Dense array CPV receivers: Impact of the cooling device on the net PV output for different illumination profiles" published in September 2018 at AIP Conference Proceedings.

The authors of this article are: Gerard Laguna[1], Montse Vilarrubí[1], Alvaro Fernàndez[1], Gonzalo Sisó[1], Joan Rosell[1], Manel Ibañez[1], Josep Illa[1], Ferran Badia[1], Luc Fréchette[2], Maxime Darnon[2], Louis Michel Collin[2], Alain Dollet[3], and Jérôme Barrau[1].

[1]Dynamic Systems Applied to Solar Energy Research Group, University of Lleida, Lleida, Spain

[2]UMI-LN2, Institut Interdisciplinaire d'Innovation Technologique (3IT), Université de Sherbrooke, Sherbrooke, Canada

[3]PROMES CNRS, rambla de la thermodynamique, Tecnosud, 66100 Perpignan, France.

Abstract

Illumination and temperature non uniformities lead to mismatch losses in dense array CPV receivers. A cooling device, formed by a matrix of microfluidic cells with individually variable coolant flow rates, has been implemented in order to smooth the temperature profile with respect to the illumination one. In this study, once the temperature issue has been reduced thanks to the self-adaptive cooling device, the impact of the illumination non uniformity magnitude on the receiver performance is assessed. For a given electrical configuration, the receiver output losses increase linearly with the illumination non-uniformity.

3.4.1.Introduction

The cooling of dense array CPV receivers must reach thermal resistance coefficients below 10^{-4} m^2K/W [71], high compactness and relevant capacities to provide a high temperature uniformity of the PV receiver, both for reliability and efficiency issues [72,73]. Previous studies have been focused on reducing the temperature non uniformities through cooling devices with stepwise varying width internal geometries [24,28,29]. Improved temperature uniformities and reduced pumping powers, with respect to microchannels, have been reported. However, the optics used for dense array CPV receivers provide a wide range of illumination profiles and, therefore, it becomes mandatory to tailor, at the design stage, the internal geometry of the cooling device to a given heat load distribution.

A cooling device, formed by a matrix of 34 x 75 microfluidic cells with individually variable coolant flow rate, has been implemented to reach the previously listed requirements without needing the characterization of the illumination profile [54,77]. Indeed, the temperature regulated self-adaptive valves [16] tailor the coolant distribution to the heat load map at each instant. This cooling device provides both improved temperature uniformity of the receivers and reduced pumping power. Laguna *et al.* [78] showed, for a given non uniform illumination profile and electrical configuration, that the electrical output of the CPV receiver cooled by an array of microfluidic cells with self-adaptive flow rate regulation was increased by 9.7 % with respect to conventional microchannels. Furthermore, the pumping power of the array of microfluidic cells, for a given heat load scenario and a given thermal resistance, is only 10.8 % of the one of conventional microchannels [54].

In this study, the impact of the illumination profile on the output of the dense array CPV receiver, when cooled by an array of microfluidic cells, is assessed.

3.4.2.Modelling

For this study, a CPV dense array of 6x8 cells (Total area: 6.7 x 8.9 cm^2) has been selected, formed by 8 modules in series, each module with 6 CPV cells in parallel (Figure 61). This electrical configuration is the one reported by several authors as the best production output under non uniform radiation [79].

The electrical output of the CPV receiver is assessed through the model described in Laguna *et al.* [78], in which the experimental PV cell characteristic IV curve has been used to calibrate the reduced standard Schottky diode model [80], utilized for the assessment of the PV cell power output under different irradiation and temperature conditions.

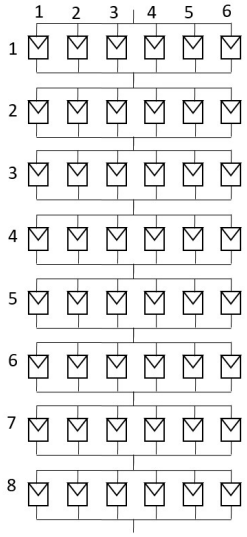

Figure 61: Electrical configuration

The matrix of microfluidic cells (cell dimensions: 1.2 x 2.0 mm^2) is located underneath the CPV receiver and receives the coolant from a distribution layer, designed to generate an equilibrated circuit and a low pressure drop (Figure 62).

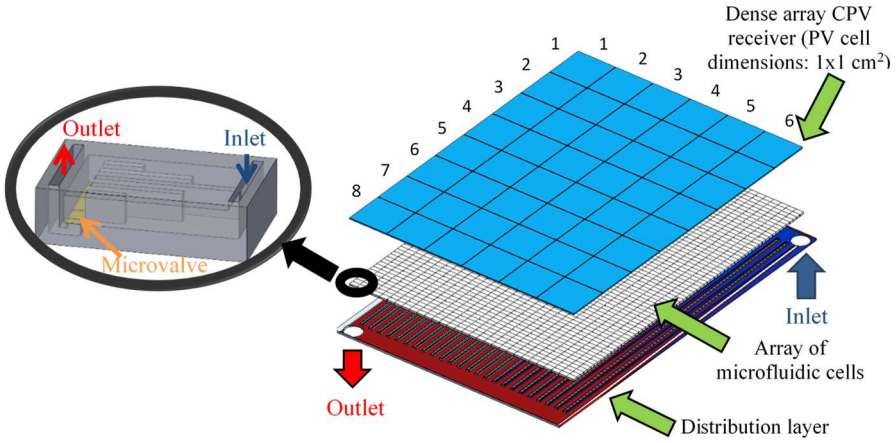

Figure 62: Exploded view of the dense array CPV receiver and the cooling device formed by an array of 34x75 microfluidic cells

In order to isolate the effect of the temperature distribution on the electrical power, the water flow rate has been adjusted for the different irradiation profiles so the average temperatures of the CPV dense array are identical, equal to 86 ºC, and the coolant inlet temperature (water) is fixed at 30 ºC. For all the illumination profiles the CPV temperature ranges are from 70 to 93 ºC. The thermal analysis is carried out with a finite element solver (COMSOL) [54].

3.4.3.Results

Several illumination profiles (Figure 63), all with an average irradiance of 800 suns, are compared to the ideal uniform pattern in order to assess their impact on the electrical output when the receiver is cooled by the matrix of microfluidic cells. Six different types of illumination profiles have been selected. These profiles cover the majority of situations found in the normal operation of the CPV receivers from uniform illumination to the out-of-axis profile. The uniform pattern is used as a reference (Figure 63a), since, in this case, all cells work under the same conditions and there are no mismatch losses. Once the work conditions of one PV cell differ from the others, its Maximum Power Point doesn't coincide with the neighboring cells and, therefore, mismatch losses appear. In line with results obtained in a different application [54], Figure 63 shows that the temperature profile generated by this cooling device is smoothed with respect to the illumination one. Furthermore, the matrix of microfluidic cells decouples the CPV cell temperatures from their location on the receiver [78]. These behaviors allow reducing the mismatch effect with respect to microchannel cooling. Indeed, the non-uniformity inherent to its cooling scheme (related to the coolant temperature increase along the microchannel flow path) is superposed to the illumination profile, boosting the temperature non uniformities.

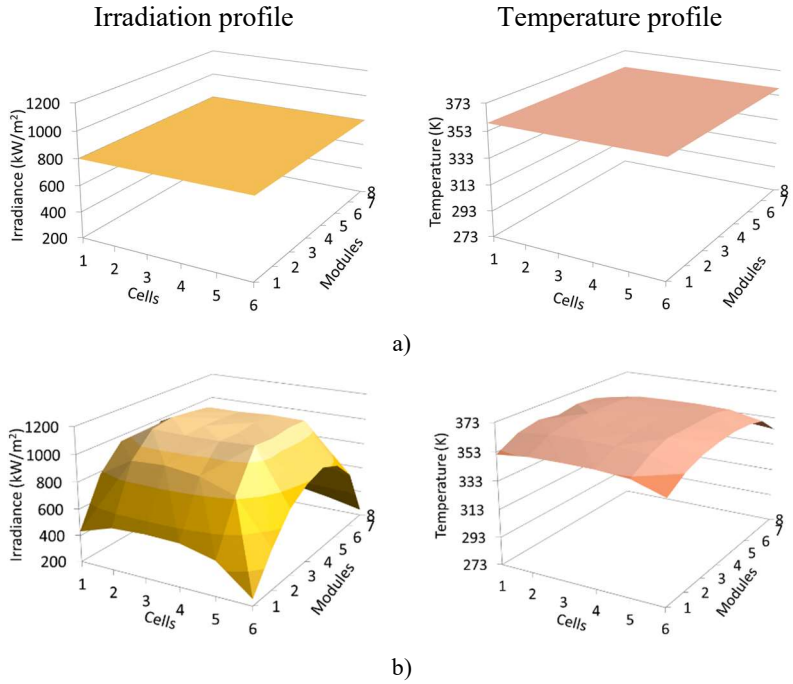

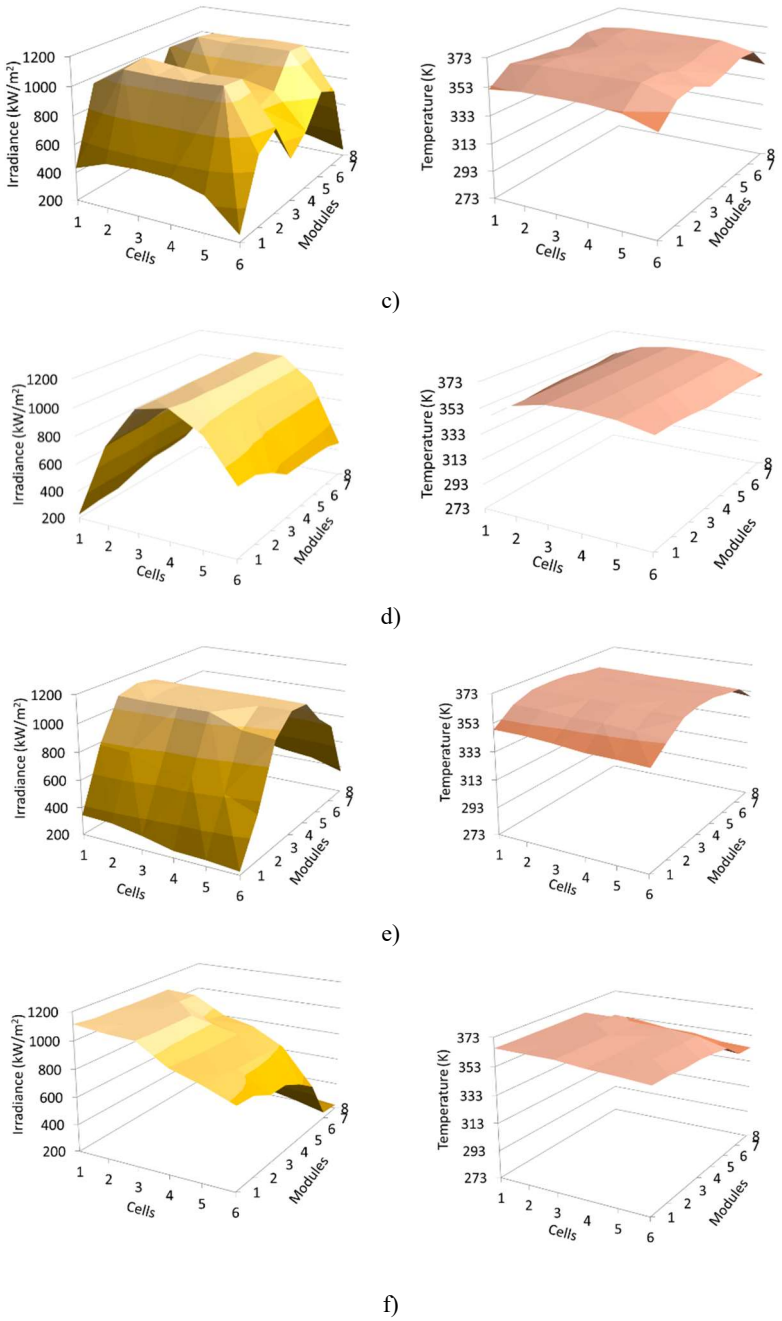

Figure 63: Illumination and temperature profiles. a) P0: Uniform, b) P1: 1 central maximum, c) P2: 2 maximums, d) P3: dispersion within modules e) P4: large dispersion between modules, f) P5: off-axis illumination

The output from the CPV receiver is assessed under the irradiance and temperature conditions defined previously (Figure 64). When the irradiation between modules is non-uniform (P1, P2, P4, P5), the modules with less irradiation have the short

circuit current lower than the one of the modules submitted to the maximum illumination. As the current increases, the modules with the worst conditions work in negative potential, activating the bypass diodes associated with each of the modules and generating one peak by module in the P-V graphs.

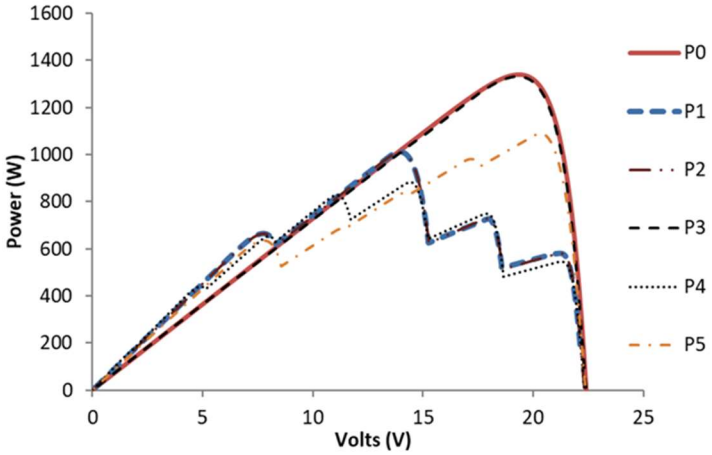

Figure 64: P-V curves of the CPV receiver for several illumination profiles. P0: Uniform, P1: 1 central maximum, P2: 2 maximums, P3: dispersion within modules, P4: large dispersion between modules, P5: off-axis illumination

This figure highlights the asymmetrical effect of the distribution of non-uniformity in the output of the system: if non-uniformity is along the cells of the same module (P3), there are almost no power losses with respect to the uniform illumination profile but if the non-uniformity is between the different modules (P1, P2, P4 and P5), the mismatch losses increase. The impact of non-uniformities between different modules, expressed through the standard deviation of the mean irradiation of the modules (σ_m, Equation 17), on the mismatch losses is represented in Figure 65.

$$\sigma_m = \sqrt{\frac{\sum_{i=1}^{n_m}\left(R_{Si} - \overline{R_S}\right)^2}{(n_m - 1)}} \tag{17}$$

R_{Si} is the mean solar irradiation of the module i, n_m the number of modules (8) and $\overline{R_S}$ the mean irradiation on the entire CPV receiver (800 suns). The mismatch losses percentages are assessed as the power reduction with respect to P0 illumination profile.

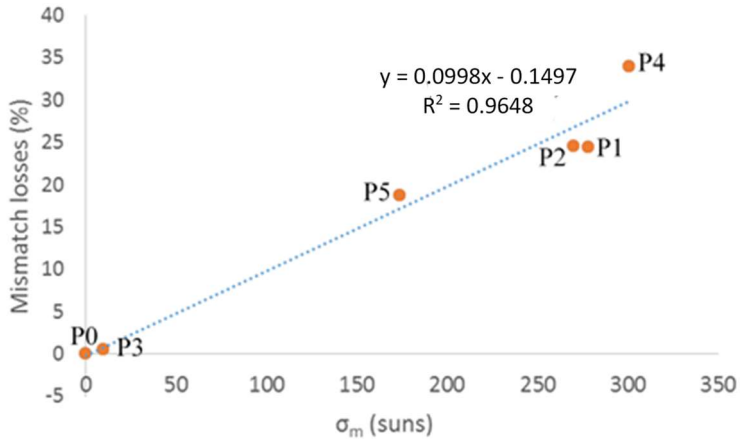

Figure 65: Mismatch losses for different illumination profiles as a function of the standard deviation of the mean irradiation of the modules

On the other hand, the statistical significance of the standard deviation of irradiance within the modules has been studied, determining that this parameter does not affect the CPV receiver output. It can be observed that the non-uniformities of the illumination profiles within a single module (P3) do not affect significantly the electrical output.

The mismatch losses increase linearly from 0 % for a uniform illumination profile ($\sigma_m = 0$ suns) to 34 % for strongly non-uniform radiation ($\sigma_m = 300$ suns).

3.4.4. Conclusions

The self-adaptive cooling device presented in this work, formed by a matrix of microfluidic cells with individually variable coolant flow rate, is able to smooth the temperature profile with respect to the illumination one. Depending on the illumination profile, and for the studied electrical configuration, the by-pass diodes generate peaks in the PV curve of the CPV receiver that represent power losses with respect to the uniform illumination case. These losses increase linearly, from 0 % to 34 %, with the illumination non-uniformity between modules. But this impact is asymmetric, as the illumination non uniformities within the modules have nearly no incidence on the CPV output. This asymmetry comes from the asymmetry in the electrical connections in the configuration studied. In order to reduce the gap between the high CPV cells efficiency and the system one, the mismatch losses, originated mainly by temperature and irradiance non uniformities, should be reduced.

Acknowledgments

The research leading to these results has been performed, in part, within the STREAMS project and received funding from the European Community's Horizon 2020 program under Grant Agreement N° 688564.

3.5. Assessment of the impact of non-uniform illumination and temperature profiles on a dense array CPV receiver performance

This chapter is the published paper "Assessment of the impact of non-uniform illumination and temperature profiles on a dense array CPV receiver performance" published in July 2018 at Solar Energy.

The authors of this article are: Álvaro Fernández[1], Gerard Laguna[1], Joan Rosell[1], Montse Vilarrubí[1], Manel Ibañez[1], Gonzalo Sisó[1], Josep Illa[1] and Jérôme Barrau[1].

[1]Dynamic Systems Applied to Solar Energy Research Group, University of Lleida, Lleida, Spain

Abstract

The performance of dense array Concentrating PhotoVoltaics (CPV) receivers is reduced by the increase of average temperature and temperature non-uniformities which arise from illumination profiles and the characteristics of the cooling mechanism used. The magnitude of the impact of both illumination and temperature non uniformities depend on the electrical configuration of the CPV cell array. In this study, the impact of a cooling device, formed by a matrix of microfluidic cells with individually variable coolant flow rate, on the performance of a CPV receiver submitted to a non-uniform irradiance scenario is assessed and compared with microchannel cooling for three electrical configurations. The proposed cooling scheme tailors the flow rate distribution, and therefore the local heat extraction capacity, to the illumination profile, allowing the reduction of the temperature difference across the CPV receiver up to one third of the one obtained through microchannel cooling. This characteristic of the microfluidic cells cooling device, combined to its low pumping power, generates an improvement of the Net PV power of 3.83 % for one of the configurations, the 6x8 matrix one.

3.5.1.Introduction

Concentrating PhotoVoltaics (CPV) is one of the most promising ways to reduce the levelized cost of energy (LCOE) of solar energy technologies [81]. To reach this objective, apart from the system cost reduction, global efficiency improvement is identified as a key factor [82]. To reach this goal, the constant improvement of the CPV cells efficiency should be accompanied by the reduction of the gap between the efficiencies of cells and systems [82]. CPV dense array receivers have a great potential for the system optimization as all the main components are mounted in a single receiver. However, this technology presents the drawback of requiring active cooling devices that must be efficient and maintain low and uniform receiver temperature [83].

Indeed, the non-uniformities of the temperature [80] negatively affect the production of energy of PV cells. Some authors [29,84–86] have focused their effort to generate uniform temperature profiles of the receiver by tailoring the distribution heat extraction capacity of the cooling device to the illumination profile and the coolant flow rate [87]. They showed that this kind of cooling device is able to generate a temperature uniformity, expressed as the standard deviation of the temperature, of 0.7 K across the entire CPV receiver, improving both the system reliability and the PV production.

For a complete dense array CPV receiver, the usual concentrators, even with secondary optics, create non-uniform irradiance distributions which generate, among other drawbacks, mismatch losses between the PV cells in the array. The electrical connections between the PV cells play a relevant role in the reduction of these energy losses [88]. Vivar *et al.* [89] demonstrated that the use of PV cells of different shapes and sizes in the receiver array, combined to the optimisation of the electric configuration, allows reducing drastically the mismatch losses. Other authors [74,79,90] proposed an algorithm to determine in each case and for each concentrator, the best cell array electrical configuration. Working with 1 cm^2 metamorphic multi-junction high efficiency cells, they identified, for several illumination profiles, the optimized electric configuration and demonstrated that this configuration can affect the global efficiency of the CPV receiver by more than 5 %.

These works have the major drawback that they are done supposing the CPV array working under uniform temperature and constant illumination profiles, assumptions that are not exact in the field operation conditions. In this study, a cooling device [50,54], formed by a matrix of microfluidic cells with individually variable coolant flow rate, is presented as an alternative for dense array CPV receivers. This device tailors the distribution of the heat extraction capacity to the illumination and temperature conditions while minimizing the pumping power needed. The impact of this cooling device on the performance of a CPV receiver

submitted to a non-uniform irradiance scenario is assessed and compared with microchannel cooling for several electric configurations.

3.5.2.Modelling

Global layout

For this study a CPV dense array of 6x8 cells has been selected (Figure 66):

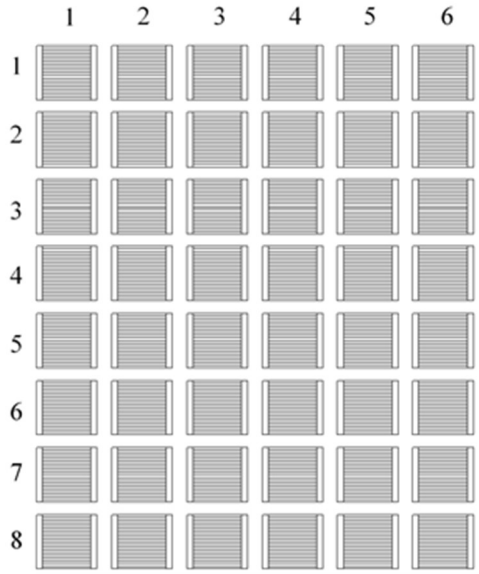

Figure 66: Schematics of the placement distribution of the 48 PV cells [82]. *Total area: 6.7 x 8.9 cm²*

The PV cell used in this study is the triple-junction cell "C4MJ Metamorphic Fourth Generation CPV Technology" from Spectrolab [91] (I-V curve in Figure 67).

The 48 PV cells are connected in 3 different ways to observe the effect of non-uniform irradiance and temperature (Figure 68).

As the main objective of this work is to assess the impact of the cooling device in the CPV receiver performance, a matrix configuration is compared to series and parallel configurations. The serial configuration was selected so that it produces the minimum currents of all possible configurations.

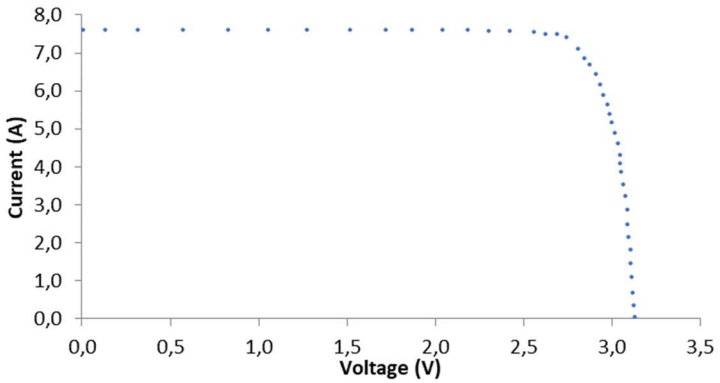

Figure 67: SPECTROLAB triple-junction cell I-V curve. [87]

The 6 x 8 matrix is the configuration reported by several authors as the best production output under non uniform radiation [74]. The 8 x 6 electrical configuration was also assessed and the power output was slightly lower than for the 6x8 one (difference lower than 0.6 %). Finally, the parallel one is by the moment the least practical connection due to its high current output but serves as a reference model.

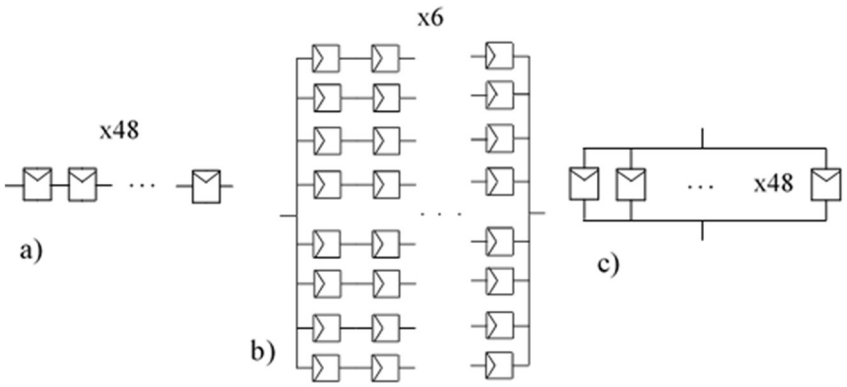

Figure 68: Example of the electrical configurations for the 48 PV cells. a) Series, b) 6x8 Matrix and c) Parallel configurations

Cooling devices

In order to cool down the CPV dense array, two devices are studied. On the one hand, a conventional microchannels cooling system [32], which consists of parallel channels with a hydraulic diameter below 1 mm, is applied. This cooling scheme is actually one of the most used for high heat flux applications due to its relatively low thermal resistance - lower than 10^{-4} K.m^2/W - [71,72]. However, this technology generates large temperature gradients along the coolant flow path and high pressure drops, that implies high pumping power. The global layout of this cooling solution applied to the CPV receiver is shown in Figure 69.

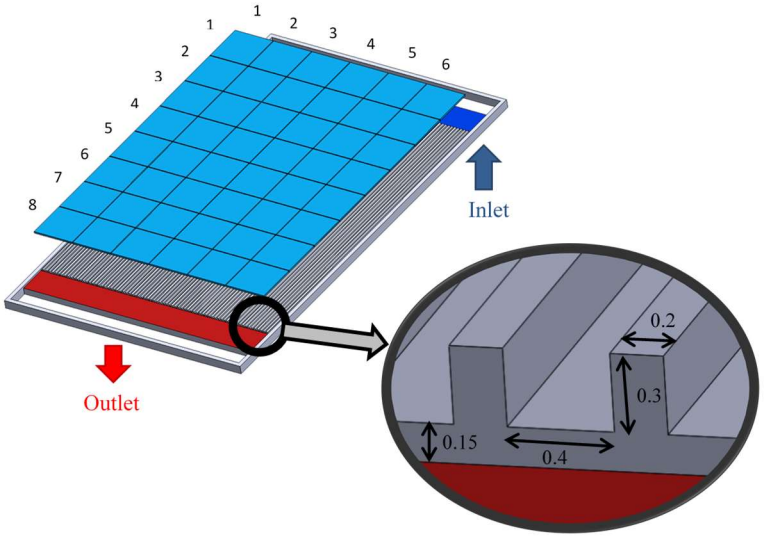

Figure 69: Exploded view of the dense array CPV receiver and the microchannels cooling device. dimensions in mm.

The coolant flows through the microchannels in the direction of the longest side of the receiver (8.9 cm, the dimensions of 8 PV cells including the space between each other). Each microchannel is 0.4 mm wide and 0.3 mm deep.

On the other hand, the impact of using a microfluidic cells cooling system was investigated [50,54]. The cooling scheme (Figure 70) consists in a matrix of microfluidic cells (dimensions 1.2 x 2.0 mm^2) with thermally activated microvalves [16], which tailor the local coolant flow rate to the local need of heat extraction capacity, avoiding overcooling and improving the temperature uniformity [54].

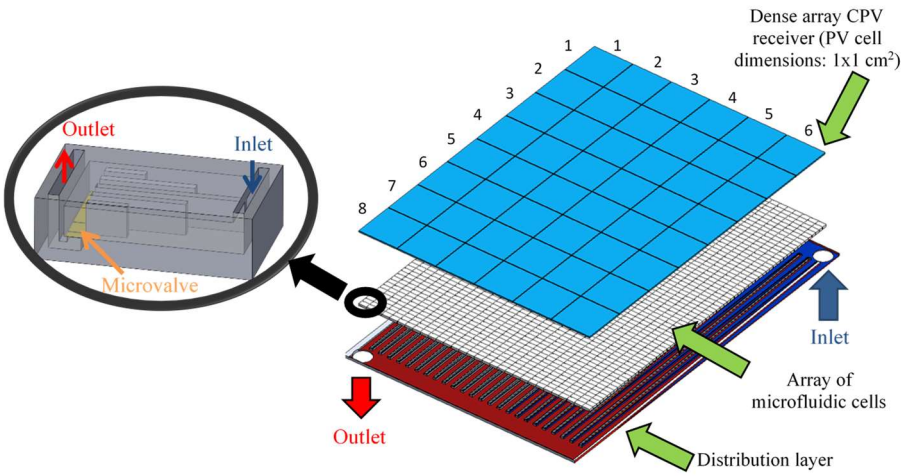

Figure 70: Exploded view of the dense array CPV receiver and the cooling device formed by an array of microfluidic cells and zoom view of one microfluidic cell

A distribution layer provides coolant to the microfluidic cells. When the local heat flux augments, the temperature of the microvalve increases. The relatively high thermal expansion coefficient of the microvalves, with respect to the support, implies their buckling and, therefore, allows increasing the local coolant flow rate. Once the heat flux decreases, the microvalve turns back to its closed shape. This behaviour allows to increase the temperature uniformity and to reduce the pumping power [54].

Thermal modelling

The main objective of the thermal modelling is to obtain the temperature distributions provided by microchannels and microfluidic cell cooling systems for a given irradiance profile. These data are used to assess the electrical performance of the CPV receiver as a function of the connection configuration.

An irradiance distribution, similar to measured illumination profiles used in previous studies [79], has been adjusted to reach a mean irradiance of 800 suns (Figure 71), varying from 225 to 1115 suns, with a standard deviation of 288 suns.

In order to isolate the effect of the temperature distribution on the electrical power, the water flow rate has been adjusted for the cooling devices so the mean temperatures of the CPV dense array are identical, equal to 86.1 ºC, and the coolant inlet temperature (water) is fixed at 30 ºC. The thermal analysis is carried out with a commercial finite element solver (COMSOL). For the microchannel cooling device, the longitudinal symmetries of the geometry have been used to simplify the model. In the case of the array of microfluidic cells, spatial integration of steady-state results has been implemented, as explained in detail in [54].

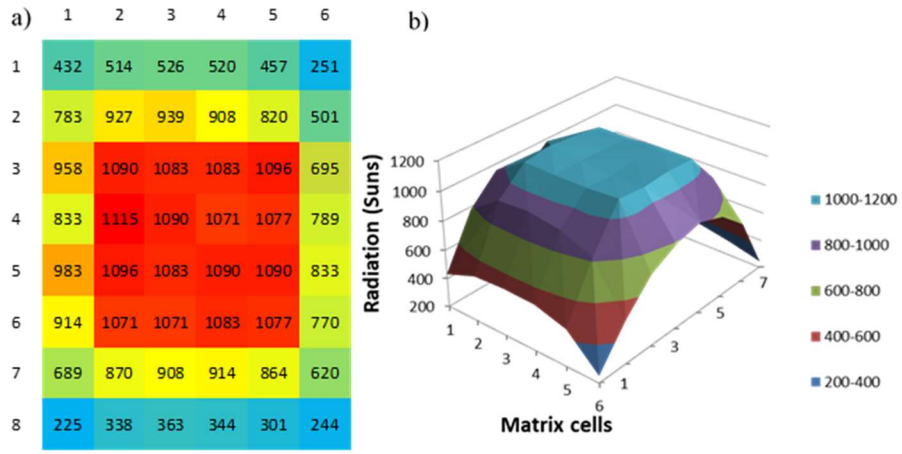

Figure 71: Non-uniform irradiance distribution (suns) a) numerical data; b) shape of the illumination profile

The microfluidic cell cooling device creates a more uniform temperature distribution than the microchannel one (Figure 72). Indeed, the maximum

temperature difference across the CPV receiver is reduced up to 1/3 of the one generated by the microchannel cooling device. Furthermore, while the microfluidic cells cooling device produces a temperature distribution pattern similar to the one of the irradiance distribution, the coolant temperature increase along the flow path of the microchannels which implies a displacement of the maximum temperatures with respect to the maximum irradiance area.

a)

	1	2	3	4	5	6
1	325.6	328.0	328.5	327.8	324.9	318.7
2	339.9	343.8	344.5	343.1	339.1	329.9
3	352.5	356.7	357.2	356.4	353.7	342.2
4	358.9	366.2	366.7	365.5	362.6	352.4
5	369.7	374.4	375.1	374.3	371.1	361.1
6	375.0	380.7	381.9	381.2	377.5	366.2
7	374.1	380.5	382.5	381.6	377.0	366.8
8	365.8	371.0	372.9	371.5	367.0	360.4

b)

	1	2	3	4	5	6
1	351.4	353.7	354.1	353.9	352.1	344.7
2	359.9	362.5	362.7	362.2	360.6	353.4
3	363.1	365.2	365.1	365.1	365.3	358.1
4	360.8	365.6	365.2	364.9	365.0	360.0
5	363.5	365.3	365.1	365.2	365.2	360.8
6	362.3	364.9	364.9	365.1	365.0	359.6
7	357.9	361.5	362.2	362.3	361.4	356.4
8	343.6	348.3	349.2	348.5	346.9	344.5

Figure 72: Temperature distribution (K) when the 48 PV cells are being cooled by the microchannels (a) and the microfluidic cells (b) cooling device. For the microchannels, the maximum temperature difference is 63.8 K (Standard deviation: 18.2 K). For the microfluidic cells, the maximum temperature difference is 22 K (Standard deviation: 6.6 K). The average temperature for the cooling devices is 359.6 K (86.1 ºC).

As the main objective of the work is to compare the performance of the CPV receiver when cooled by the new cooling device and by microchannels, the illumination and temperatures over a single CPV cell are considered uniform. This hypothesis is conservative as the array of microfluidic cells provides higher temperature uniformity (also within a single CPV cell) than microchannels.

Even if the flow rate needed to cool down the CPV receiver is similar for both cooling devices (Table 6), the lower pressure drops of the microfluidic cell cooling device and its capacity to tailor the flow rate to the heat load imply that the pumping power is 0.042 W, only 17.5 % of the one consumed by the microchannel cooling device.

Table 6: Comparison between the two cooling devices of the main parameters.

Global thermal performance	*Microchannels*	*Microfluidic cells*
Pumping power [W]	0.24	0.042
Water flow rate [l/min]	0.495	0.499
Pressure drop [Pa]	29069	5046
Maximum temperature difference [K]	63.8	22
Saved pumping power [%]	-	83

Electrical modelling

The experimental PV cell characteristic IV curve has been used to calibrate the reduced standard Schottky diode model [80,92], utilized for the assessment of the PV cell power output under different irradiation and temperature conditions. The reduced standard model is used for a simple PV cell but has already been used for triple-junction PV cells [93]. In this study, the model will be fitted for a triple-junction cell so what was known as the band gap is called effective energy gap [93]. Assuming a constant light spectrum, the model can be defined by the following equation:

$$I = I_L \cdot \frac{C}{C_0} - I_0 \cdot \left[e^{\frac{V}{V_T}} - 1 \right] \tag{18}$$

and its inverse equation:

$$\mathrm{V} = \mathrm{V_T} \cdot \ln\left(\frac{I_L}{I_0} - \frac{I}{I_0} + 1 \right) \tag{19}$$

Where V and I are the potential and the current of the PV cell, respectively, I_L is the light generated current, C_0 is the reference solar concentration (500 suns), C is the solar concentration on the PV cell, V_T is the thermal voltage and I_0 is the reverse diode current:

$$I_0 = I_0' \cdot T^3 \cdot e^{\frac{-E_g \cdot e^-}{k_B \cdot T}} \tag{20}$$

Where k_B is the Bolztman constant, T is the cell temperature (K), I_0' is the coefficient independent from the temperature of the reverse diode current, E_g is the effective energy gap. The thermal voltage V_T is defined as:

$$V_T = \frac{k_B \cdot T \cdot n}{e^-} \tag{21}$$

Where n is the effective ideality factor and e^- is the electron charge.

I-V curve calibration

The reduced model has been fitted by least square error changing 4 parameters: The short circuit current I_L, the reverse current coefficient I_0', the effective ideality factor n and the effective energy gap E_g. This calibration has been carried out simultaneously with the direct and inverse model equations in order to reduce the

errors that would appear when shifting from one calibrated model (the direct one) to the other (the inverse one). To do this, the effective ideality factor and reverse current coefficient were modified by using an error reduction algorithm (Table 7).

Table 7: Results after the I-V calibration.

Description	*Symbol*	*Value*	*Units*
Short-circuit current	I_L	7.533	A
Reverse current coefficient	I_0'	0.11104	A/K^3
Effective ideality factor	n	4.123	-
Effective energy gap	E_g	1.1397	eV

The current, voltage (Figure 73) and I-V curves (Figure 74) obtained through the reduced model reproduce the experimental values given in the cell datasheet, validating the calibration procedure.

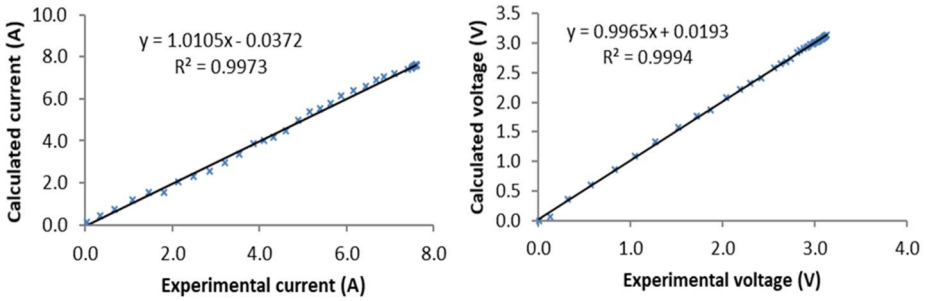

Figure 73: a) Model equation correlation. b) Inverse equation correlation

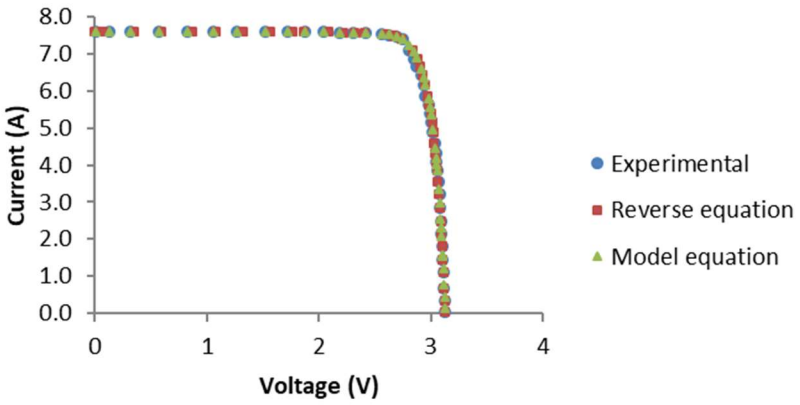

Figure 74: Comparison between the experimental values, the ones obtained from the model equation and the ones obtained from the inverse model equation for 25 ºC and 500 suns

Temperature calibration of the I-V curve

The temperature calibration allows the reduced model to adapt to different cell temperatures (Figure 75). It has been done by changing the equivalent band gap. The parameters that change with temperature are: the short circuit current by 8.2 µA/(cm^2·ºC), the open circuit voltage by -6.4 mV/ºC and the maximum power voltage point by -6.7 mV/ºC [16,71,75,78,92–95]. Using a conjugated gradient error reduction algorithm, the effective energy gap obtained is: *Eg = 1.1397 eV*. The short circuit current is nearly independent to the temperature variation (slope of $8.2 \cdot 10^{-6} \frac{A}{ºC}$).

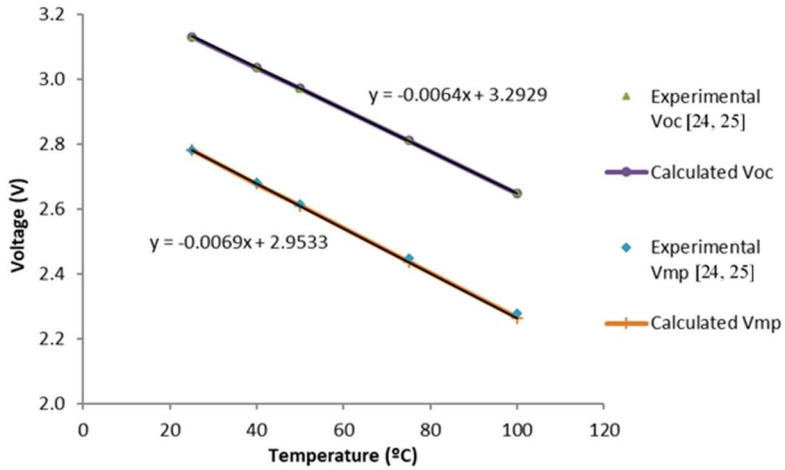

Figure 75: Comparison between the experimental [94] *and the calculated with the model (Equation 19) after the temperature calibration.*

3.5.3. Results and discussion

The PV power, produced by the CPV receiver, is assessed for each of the electrical configurations applying both microfluidic cell and microchannel cooling devices under the irradiance and temperature conditions defined previously (Table 8). As the main objective of this work is to compare the impact of the cooling solutions in similar conditions, the spread in the cell performances, which ranges from 1 % to 3 % [75], has not been taken into account. Indeed, the additional non-uniformities of the CPV receiver conditions due to this effect are much lower than the irradiation ones.

Table 8: Power [W] comparison for the studied electrical configurations being cooled with microchannels and microfluidic cells [W].

Electrical configuration	*Microchannels*	*Microfluidic cells*	*Increment*
Series	857.8	861.0	0.37 %
6x8 matrix	1036.3	1075.8	3.81 %
Parallel	1309.9	1333.04	1.77 %

Series configuration

For the calculations, a bypass diode (voltage drop of 0.5 V) is placed in parallel with every single cell connected in series.

In the series configuration, the highest temperature uniformity generated by the microfluidic cell cooling device implies a PV power increase, with respect to the microchannel cooling device, of 0.37 %.

It has been observed that for the maximum power point of the system, some cells are consuming energy through the bypass diode. This happens when the string current is higher than the short circuit current of a cell. The short circuit current of each cell depends on the irradiance profile. In a PV dense array connected in series, the temperature distributions don't affect the power generation when the cells are producing energy and the average temperature remains the same [96]. The increment in power generation produced by the microfluidic cells cooling device resides in the fact that this system reduces the average temperature of the cells that produce energy to the detriment of the ones that consume.

The irregularities in the I-V and P-V curve in the series configuration (Figure 76) exist due to the current passing through the bypass diode in some cells. The non-uniform irradiance distribution affects the current that is being produced in each cell. As all the cells must have the same current due to the series configuration, the maximum power of the system involves a current that generates a negative voltage in some cells.

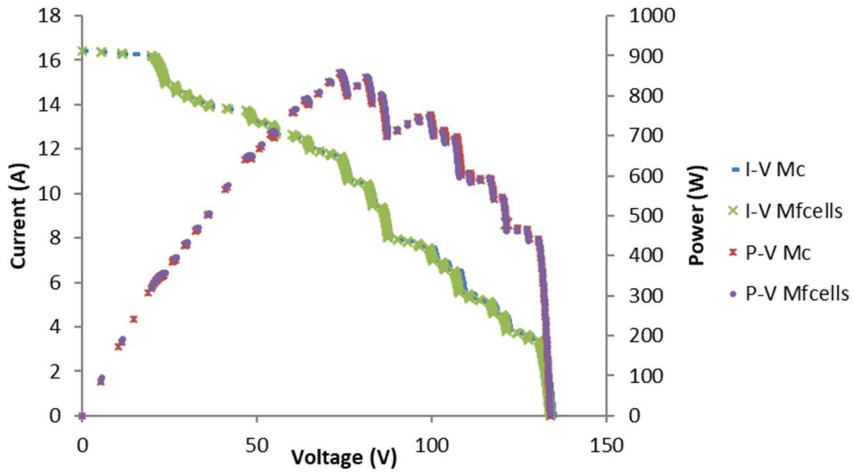

Figure 76: I-V and P-V curves for the temperature distributions obtained from the microchannels and microfluidic cells cooling device under the specified irradiance distribution when the PV cells are connected in series.

In the series configuration and under the non-uniform irradiance distribution, the increment in the PV power obtained when using microfluidic cells instead of

microchannels is relatively low. Even though the temperature distribution is more uniform -maintaining the same average temperature across the entire CPV receiver, the average temperature of the cells that are producing energy is only 1 K cooler for the microfluidic cells cooling than for microchannels. It has been mentioned previously that, in the series configuration, the group of cells that are producing energy are only affected by their average temperature, and not by their temperature non uniformity.

6x8 matrix configuration

Like in the series configuration, a bypass diode is considered for the cells connected in series.

In the matrix configuration, the highest temperature uniformity generated by the microfluidic cell cooling device implies a PV power increase, with respect to the microchannel cooling device, of 3.81 %.

In a PV dense array connected in matrix the series that has the lowest open circuit voltage is the series that causes the highest power losses [96]. In this scenario, this series is the less irradiated one (Figure 71). It is assumed that all the series share the same voltage.

The microchannels cooling system produces a temperature distribution that causes the last series to be one of the hottest while being the less irradiated. This lowers the open circuit voltage of the series and reduces the electrical power of the CPV dense array, compared with the one obtained with microfluidic cells. Microfluidic cells allow the less irradiated series to have the lowest temperatures which increase the open circuit voltage and the electrical power.

Also in this matrix configuration, the irregularities of the I-V and P-V curves occur due to the current passing through bypass diodes in some cells (Figure 77).

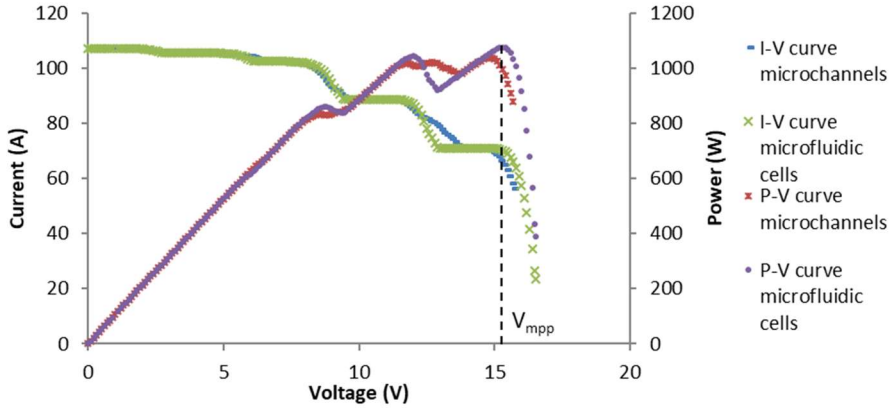

Figure 77: I-V and P-V curves for the temperature distributions obtained from the microchannels and microfluidic cells cooling device under the specified irradiance distribution when the PV cells are connected in 6x8 matrix configuration.

The maximum power point for the microfluidic cells scenario corresponds to a voltage of 15.3 V (*Vmpp*). The voltages of the CPV cells in this matrix configuration and the current of each branch in parallel are presented (Figure 78), at the maximum power point, for the microchannel and microfluidic cell cooling device.

Current differences of almost 2 A are observed in series 6, 7 and 8 between the 2 cooling solutions studied. Those series are the hottest ones in the microchannels scenario and series 8 is the less irradiated one.

a)

	1	2	3	4	5	6	I(A)
1	2.84	2.87	2.87	2.87	2.86	1.00	3.8
2	2.79	2.82	2.82	2.82	2.82	1.23	7.6
3	2.70	2.72	2.72	2.72	2.75	1.68	10.6
4	2.46	2.64	2.63	2.63	2.65	2.30	11.8
5	2.55	2.58	2.57	2.58	2.60	2.43	11.9
6	2.54	2.57	2.56	2.57	2.59	2.48	10.2
7	2.52	2.56	2.56	2.57	2.58	2.51	7.5
8	2.50	2.56	2.56	2.56	2.56	2.56	1.7

b)

	1	2	3	4	5	6	I(A)
1	2.66	2.69	2.70	2.70	2.67	1.88	3.8
2	2.66	2.70	2.70	2.69	2.67	1.88	7.6
3	2.63	2.67	2.67	2.67	2.67	1.99	10.5
4	2.45	2.65	2.64	2.63	2.64	2.29	11.7
5	2.57	2.62	2.62	2.62	2.62	2.26	12.5
6	2.56	2.64	2.64	2.64	2.64	2.18	11.6
7	2.51	2.64	2.65	2.65	2.64	2.21	9.3
8	2.31	2.63	2.65	2.64	2.60	2.47	3.3

Figure 78: Voltage [V] of the array cells when producing 15.3 V per series. Current per series on the right side. a) Microchannels.Current output: 65.1 A b) Microfluidic cells. Current output: 70.3 A The colour indicates the voltage level of each cell.

Parallel configuration

In this scenario, bypass diodes are not needed because all the PV cells are polarized by the work voltage.

In a PV dense array connected in parallel, the non-uniform irradiance distribution does not affect the electrical production and the less irradiated cells produce the highest power losses [96]. It is assumed that all the cells have the same voltage and the maximum voltage of the system corresponds to the lowest open circuit voltage of the cells in the array (Figure 79).

For the parallel configuration, there are no irregularities in the I-V and P-V curves (Figure 79) because of the absence of bypass diodes. The difference in the electrical power is related to the temperature distribution obtained with the two cooling devices. Microchannels make the less irradiated cells become hotter than in microfluidic cells and, therefore, these cells produce less energy. Even though the parallel configuration produces more energy than the others, it is unrealizable due to the huge amounts of current that are produced in high solar concentration applications.

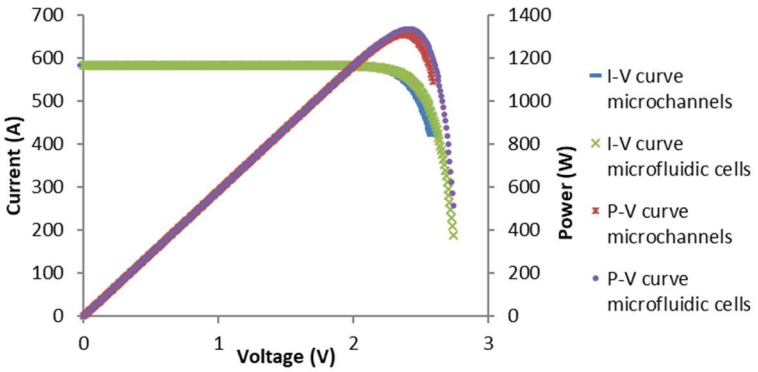

Figure 79: I-V and P-V curves for the temperature distributions obtained from the microchannels and microfluidic cells cooling device under the specified irradiance distribution when the PV cells are connected in parallel

Comparison of the 3 electrical configurations

To reach the identical average temperature of the CPV receiver, the microfluidic cell cooling device needs only 17.5 % of the pumping power consumed by the microchannel. This characteristic implies that the difference of the Net PV power (PV Power – Pumping Power) produced by the CPV receiver, when cooled by the microfluidic cells and the by the microchannels, is higher than when we consider the PV power.

Figure 80 shows that the parallel configuration produces the maximum Net PV power of the 3 configurations considered (1333 W) when cooled by the microfluidic cells. This means that, theoretically, it is the configuration less affected by the non-uniformity of radiation and temperature. However, the currents of almost 600 amperes are unrealizable due to the Joule effect and the size of the cables needed.

Matrix configuration produces 1075.8 W when cooled by microfluidic cells, the second highest power of the studied configurations. In this configuration, the improvement of the temperature uniformity generated by the microfluidic cells has the major impact of the 3 studied configurations: 3.83 % of the Net PV power with respect to microchannel cooling.

Finally, the series configuration produces only 861 W with microfluidic cells. Indeed, this configuration is the most affected by the mismatch effect. The clear advantage of this configuration among the others is the low current produced compared to the others. It has been seen that higher increments in power can be achieved if heat extraction could be controlled.

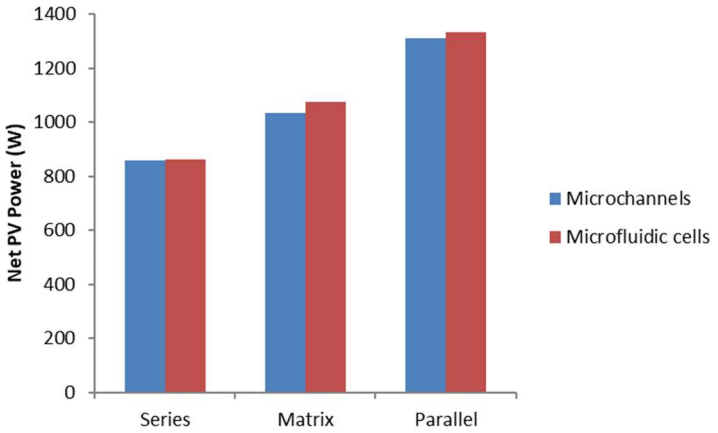

Figure 80: Net PV power comparison between the series, matrix and parallel configurations when being cooled by microchannels and microfluidic cells cooling devices.

3.5.4. Conclusion

In this study, the impact of the cooling device characteristics on the performance of a CPV dense array receiver has been studied, under a non-uniform irradiance distribution, for three different electrical configurations. A new cooling scheme, based on the use of an array of microfluidic cells with thermally activated microvalves that tailor the local flow rate to the local heat load is presented and compared to conventional microchannels. To assess the effect of the temperature non uniformities generated by microfluidic cells and microchannel cooling devices, the flow rates have been settled in order to ensure that the average temperature of the CPV receiver is identical in both cases. The main conclusions are the following:

- Independently of the applied cooling device, the series configuration is the most affected by the non-uniform irradiance distribution, obtaining the lowest electrical power. The parallel configuration is not affected by the non-uniform irradiance so produces the highest electrical power. However, the low voltages and high currents obtained make this solution unreliable. The matrix one has been found to be a practical compromise between advantages and inconvenient of series and parallel configurations.
- In the matrix configuration, the worse irradiated branches are the ones that limit the overall power of the receiver. This drawback is enhanced if their temperatures, with respect to the average one of the receiver, are high. The capacity of the microfluidic cells cooling device to generate a relatively high temperature uniformity, with respect to the microchannel device, reduce these power losses.
- In the series configuration, the increment in power generation produced by the microfluidic cells cooling device resides in the fact that this system reduces the average temperature of the cells that produce energy to the

detriment, for a fixed average temperature of the receiver, of the ones that consume. In this configuration, the non-uniform temperature distribution does not affect the power generation of the cells that have a positive voltage.

- The Net PV power obtained while using the microfluidic cells cooling device is incremented, with respect to microchannel cooling, in all the configuration scenarios. This improvement, due to both the best temperature uniformity and the lowest pumping power associated to the use of this new cooling scheme, ranges from 0.39 % for the series configuration up to 3.83 % for the 6x8 matrix one.
- These results open a new way for the LCOE reduction of dense array CPV receivers, by increasing their receiver efficiency through the use of cooling devices adapted to the illumination profile and the electrical configuration. This study demonstrates that the microfluidic cell cooling devices, with microvalves that tailor the local flow rate to the local heat load, have a great potential for their use in dense array CPV receivers.

Acknowledgements

The research leading to these results has been performed within the STREAMS project and received funding from the European Community's Horizon 2020 program under Grant Agreement N° 688564.

4. Experimental study

4.1. Experimental setup

The last part of the thesis is focused on the experimental test developed to achieve the Proof of Concept of the STREAMS cooling solutions and compare it with microchannels.

To realise the experimental study, a test bench has been designed to control all the boundary conditions and characterise the cooling solution behaviour. In the test bench (Figure 81), the purified and deionised water circulates in a clockwise direction. First of all, the filter captures all the particles in the fluid and is used as a water tank. Following the coolant path through the circuit, the membrane pump and the flowmeter are used to control and measure the flow rate. A membrane pump has been chosen for its capacity to deliver small flow rates (10–50 ml/min) and a damper is used to reduce the pump oscillations. Next, the heat exchanger allows control of the inlet temperature of the cooling fluid by means of the heat exchange with the water from the thermostatic bath. Finally, on each side of the cooling device, water columns are placed, together with pressure sensors and thermocouples. An air purge is placed at the inlet in order to avoid air bubbles in the device.

The hydraulic circuit has three bypasses. The first one, bypassing the filter, prevents contact of the fluid with the air when the filter is not completely full of water. The second one, bypassing the pump, serves to deliver flow rates lower than those provided by the pump. Finally, the third one, bypassing the test device and its surrounding sensors, permits the recirculation of the water in the entire circuit to reach stationary fluid temperatures.

Water columns are placed, as a security element, at the inlet and outlet of the test device in order to make sure that the pressure ranges of the device, at both the inlet and the outlet, are adequate for the microfluidic valves. Once the pressure limitations are verified, the water columns are closed in order to avoid their actuation as a flow rate damper.

Apart from the hydraulic circuit, an infrared camera is connected to monitor the thermal map of the device, acting also as a security element. A data acquisition system is used to collect all the analogical data from the test bench and measure the power delivered from the controlled power sources and the resistance temperature detectors (RTD) fabricated on top of the device. The whole experimental setup is connected to a computer where a LabVIEW interface collects and stores all the data, while also controlling the pump and the power sources (Figure 81).

4.1.1. Elements of the experimental setup

Filter

The filter used has the function of keeping any residue from the circuit in order to protect the test device. In addition, it is used as a water tank to ensure that the circuit

is always full of water, so avoiding the entry of air. This is a 5-micron propylene sediment filter, which is suitable to prevent corrosion problems.

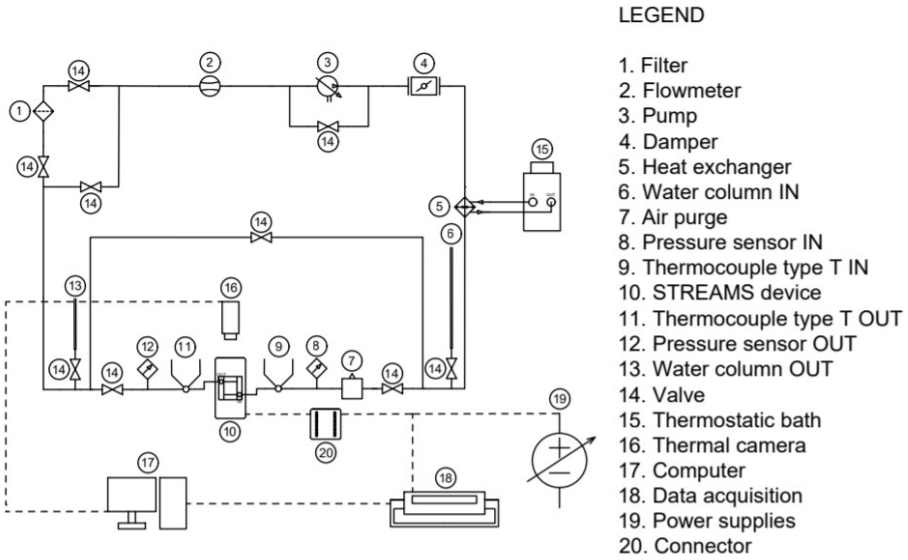

Figure 81: Test bench scheme

Flow meter

A flow meter is required to continuously monitor the coolant flow rate through the cooling device. The M15 Bronkhorst CORI-TEACH flowmeter is chosen because of its measurement ranges, precision, and for its compatibility with LabVIEW.

This flow meter has three ranges of measurements that the user can change; the small range from 3.3 to 83 ml/min, the normal range from 16 to 1660 ml/min and the high range from 50 to 5000 ml/min. The normal interval is set as the range of operation. The precision of this device is greater than ± 1% of the measurement when it is greater than 10 ml/min working in the normal range.

Pump

The NF 5 KPDCB-4 pump from KNF is a membrane pump with a power of 0.9 W and with a control voltage from 0 to 5 V. The flow pumped by the pump is conditioned by the control voltage, which, through the power supply, can be controlled manually or through LabVIEW.

Damper

A hydraulic shock absorber is needed due to the use of a membrane pump. With the hydraulic shock absorber FPD06KPZ from KNF, the same brand as the pump, it is possible to smooth the variation of flow rate and pressure between the pulses of the pump.

Heat exchanger

The plate heat exchanger IDS 14-20H from IDROGAS is used for exchanging heat between the fluid from the thermostatic bath and the fluid in the circuit. The maximum working temperature of the heat exchanger is 200 ºC.

Water column

Two columns of water have been installed, one before the entry of the device and the other after the exit, in order to avoid exceeding the maximum pressure difference that the valves can handle before experiencing plastic deformation. If the maximum pressure difference were exceeded, the fluid of the circuit would fill the columns to the point of overflow, to prevent the pressure inside the device exceeding its maximum. The columns are useful to show the difference of pressure on the test device and as a security element.

Air purge

This component prevents the entry of air bubbles into the test device. This element was specially constructed in the laboratory for this function, consisting of a syringe, 2 rigid nozzles with a diameter of 3.2 to 4 mm, a flexible tube of 3.2 mm diameter, a binder clip and Silicoset 158 acc silicone resin. All the bubbles that are trapped can exit by pressure with the opening of the clip (Figure 82).

Figure 82: Air purge

Pressure sensor

In order to know the differential pressure between the inlet and outlet of the test device, a pair of pressure sensors 8285701 from RS PRO are used. One is located just before the inlet and the other just after the outlet. The pressure sensors have a measurement range of 0 to 250 mbar. The precision of this device is ± 0.25 % of the measurement range.

Thermocouples

The thermocouples measure the water temperature at the inlet and the outlet of the device in order to measure the temperature increase of the flow in the device. Thermocouples TJC100-CPSS-IM050 from OMEGA are thermocouples type T with an accuracy of ± 0.5 ºC from -40 to 125 ºC or ± 0.4 % of the measurement of 125 to 350 ºC. In their location, measuring the water temperature, they should not exceed 100 ºC, so a precision of ±0.5 ºC is considered.

Thermostatic bath

In order to control the temperature of the fluid at the inlet of the test device, the use of a thermostatic bath is required. The PD07R-20-A12E from PolyScience is compatible with LabVIEW and is able to give a constant temperature in the range

of -20 to 200 ºC, which includes the operating range of the project, from 20 to 50 ºC. This device provides stability of ±0.005 ºC.

Data acquisition

The data acquisition system is required to receive all the data from the thermocouples, the pressure sensors and for reading the voltage and current of each RTD. The data acquisition system Keysight 34972A can be controlled using LabVIEW with an accuracy of ±0.004 % of the measured value. This device was purchased with three reading modules, two 34901A multiplexers and one 34907A.

The module 34901A has 20 input channels to read voltage differences and thermocouples temperatures so it is used to read the voltage from the pressure sensors, the voltage applied to the RTD and the voltage from shunt resistors in order to measure the current through each heater. The current is measured by shunt resistors because each module 34901A has only 2 channels to read the current while 16 RTDs are located on each device.

The 34907A is a multi-function module chosen for the functionality of the totaliser, which can read the pulses from the membrane pump as feedback to know the rotation velocity of the motor.

Power sources

Controlled power sources are used to control the power applied to the heaters that simulate the microchip. The test bench is equipped with two types of power supplies. The Metrix AX 1360-P, which has two programmable channels controlled by LabVIEW, can deliver 30 V and 3 A in each channel. Additionally, there is a third channel with a fixed output of 2.5 V / 3.3 V / 5 V with a maximum intensity of 3 A. This power supply provides an accuracy of the output voltage of ±0.5 % of the reading plus 2 digits. The test bench is equipped with three of these power supplies, which send power to the heaters and give the pump control voltage.

The second type of power supply is the PSI 9200-04T from Elektro-Automatik, a programmable power supply with one channel that is also controlled by LabVIEW. This device is used to power the most demanding heaters and is able to provide 200 V and 4 A, with an accuracy of 0.1 % of the nominal value.

Infrared camera

An IR camera is used to assess the temperature distribution of the chip and, therefore and indirectly, characterise the behaviour of the self-adaptive cooling device. The FLIR A655sc has the ability to record up to 200 Hz, and is compatible with LabVIEW. This characteristic allows this component to be used as a complementary security element. The camera has its own software to process the images and can be used with a macro lens in order to be able to view objects at a micrometric scale, with a 50 μm spatial resolution. This device has an accuracy of

±2 °C or ±2.00 % of the reading; however, the emissivity of the devices is irregular due to the residues of the device gluing process and the data from the IR camera has only been used as a qualitative indicator.

4.2. Fabrication of the cooling devices

Once the design stage was concluded, different masks were created to start the microfabrication process of the selected geometries. In order to characterise the microfluidic cooling solution, the microfluidic cell cooling system with valve, without valve and a microchannel device has been fabricated. Three layers of wafers are needed to fabricate the microfluidic cell:

- the top one where the heaters are placed and the microfluidic cell geometry is etched.
- the second one which has inlets, outlets and the flow path elbow where the valve is located
- the third layer which closes the elbow and has the inlet/outlet holes for the hydraulic connections with the distributor (Figure 83).

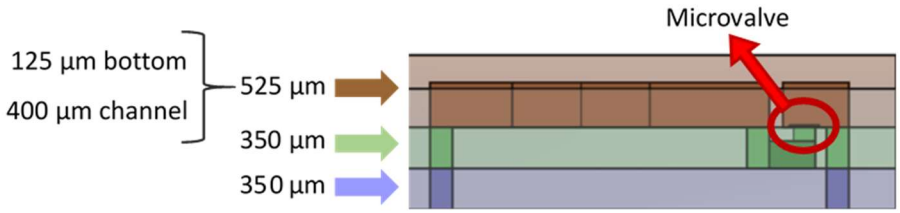

Figure 83: Cell layers

The masks were designed in order to use as much of the surface of the wafer as possible, using a wafer of 10 cm diameter, so the masks are designed in order to fabricate 9 devices, 3 of each type (Figure 84).

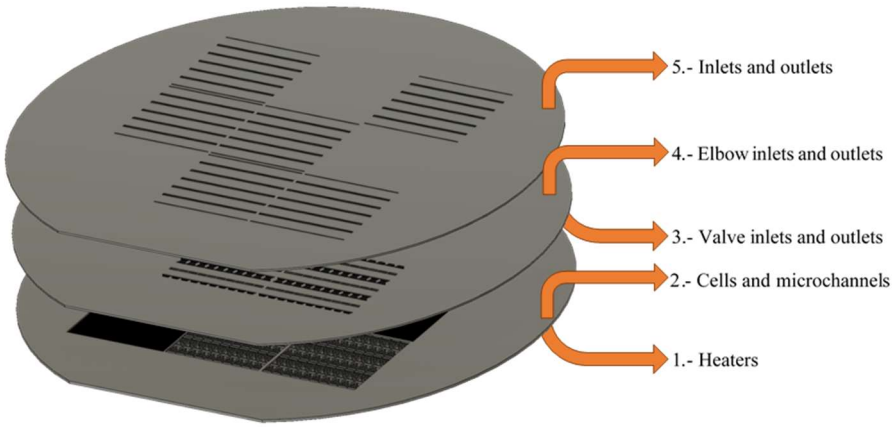

Figure 84: The three wafers to fabricate 9 cooling devices indicating the elements of each wafer face

On the top of the device, the first wafer includes the heaters which are made through the deposition of 200 nm of gold and 900 nm of nickel which are isolated with a 3 μm layer of SiO_2 (Figure 85).

The geometries of the microfluidic cells and the microchannels are etched 400 μm deep into the other side of the first wafer, leaving a distance of 125 μm from the heaters placed on the other side of the wafer (Figure 86).

The second wafer (350 μm thick) is the one where the microfluidic valve, made of silver, is placed. To microfabricate them, the shape of the valve is etched into sacrificial material (SiO_2) on which the silver forming the valves is deposited (Figure 87). After depositing the valves, the cells' inlets, outlets and the cavities which form the flow path elbow are etched (Figure 88).

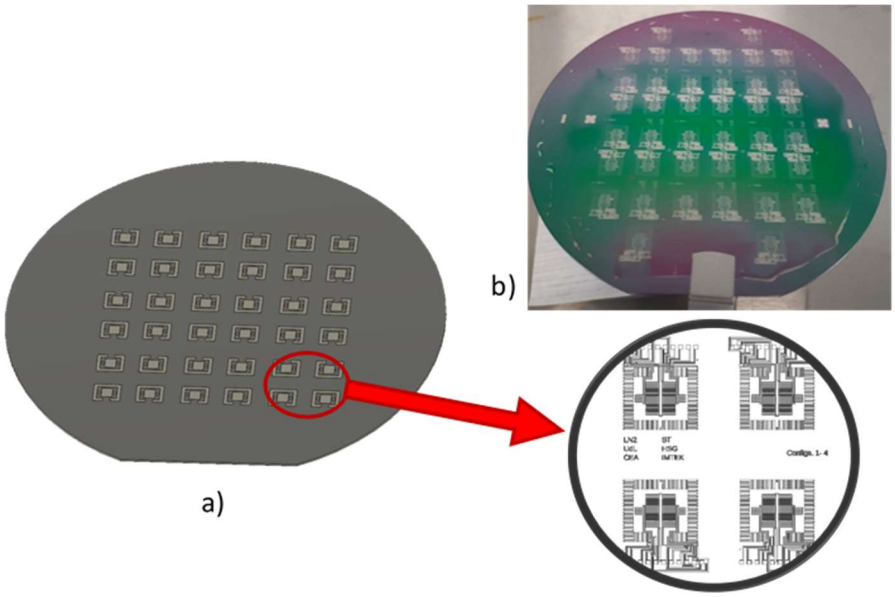

Figure 85: a) 3D model of the first wafer on the heater's side, b) photo of the first wafer from the heater side

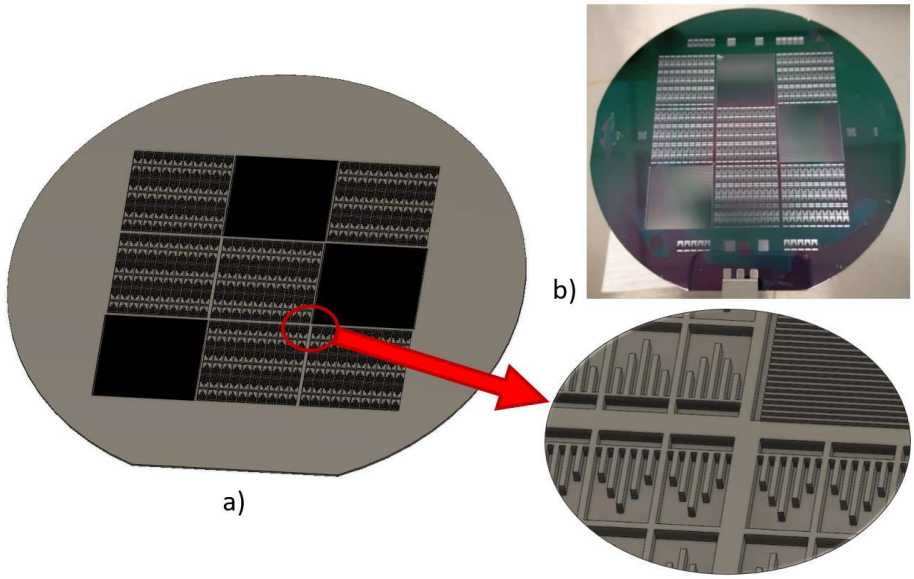

Figure 86: a) 3D model of the first wafer on the cooling geometries side, b) photo of the first wafer from the cooling geometries side

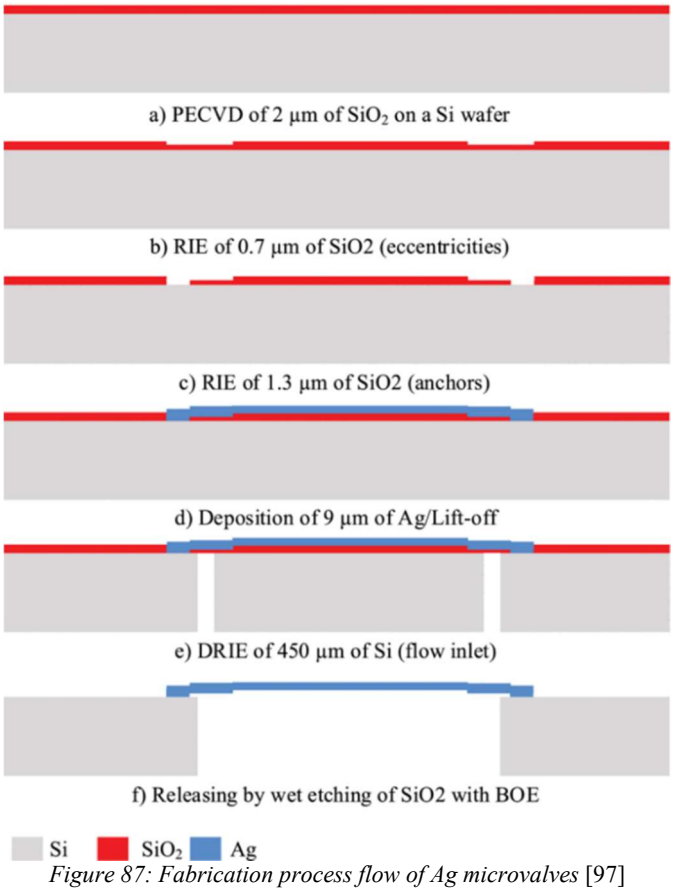

Figure 87: Fabrication process flow of Ag microvalves [97]

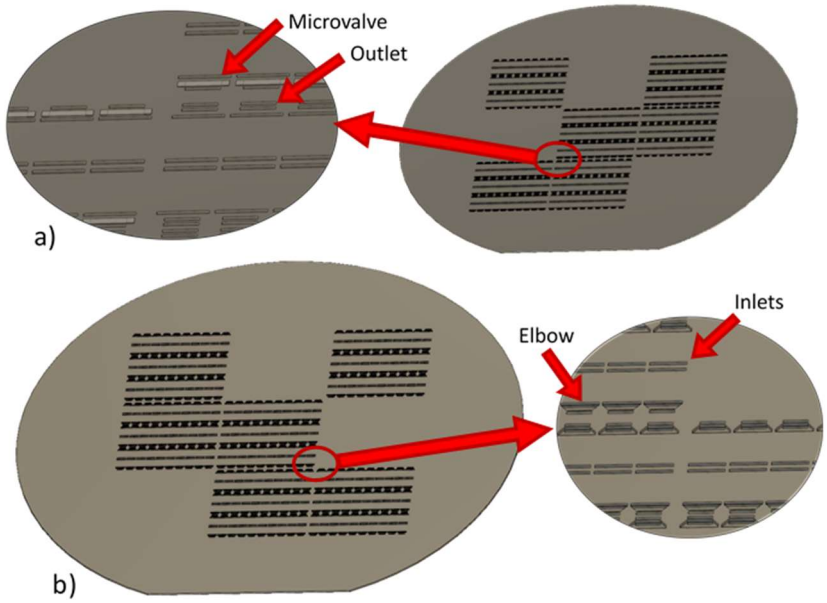

Figure 88: Second wafer: a) microvalves side, b) elbow side

The third wafer is needed to close the microfluidic cell, closing the elbow, and allowing the flow path only through the etched slots corresponding to the inlets and outlets (Figure 89).

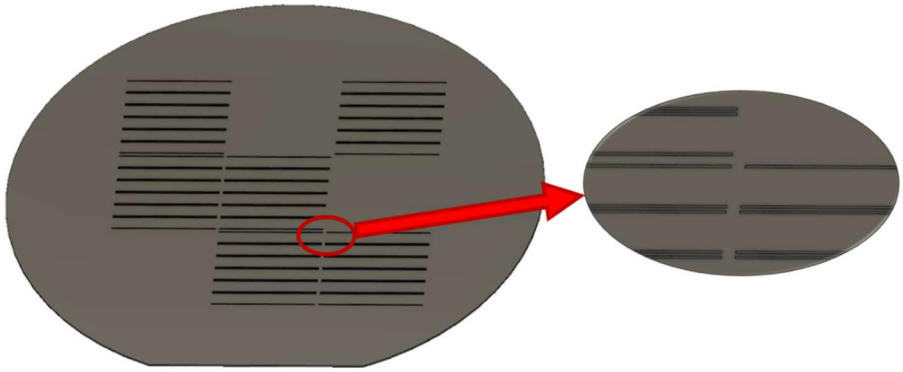

Figure 89: Third wafer with inlets and outlets trenches

Once the wafers are made, they are attached by gold eutectic bonding. Then each wafer is cut into dies having the 9 separated devices. At this point, the microfluidic cell cooling devices and the microchannel devices are assembled each on their respective distributor. The assembly process for the microfluidic cell devices consists of applying epoxy glue to all the walls which separate the inlet and the outlet of the device, placing the device and sealing all the joints. On the microchannels device, it is only necessary to apply epoxy glue on the joints because the device is fed from the side (Figure 90). The epoxy applied on the microchannels

device must be a glue which cures rapidly to avoid leakages and closure of the microchannel paths. A UV epoxy, which cures in 10 seconds when exposed to UV light, has been used.

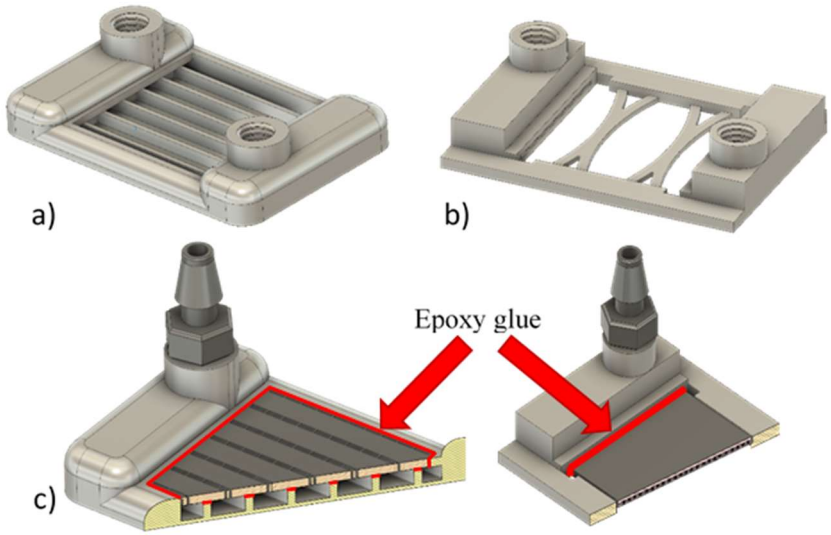

Figure 90: a) Microfluidic cell distributor, b) microchannels distributor, c) microfluidic cells and microchannels gluing process

Finally, the device is glued on a PCB board and the wire bonding process is done in order to connect all the heaters of each device. Additionally, a cover was designed and glued to the PCB board in order to protect the device during transport of the devices (Figure 91).

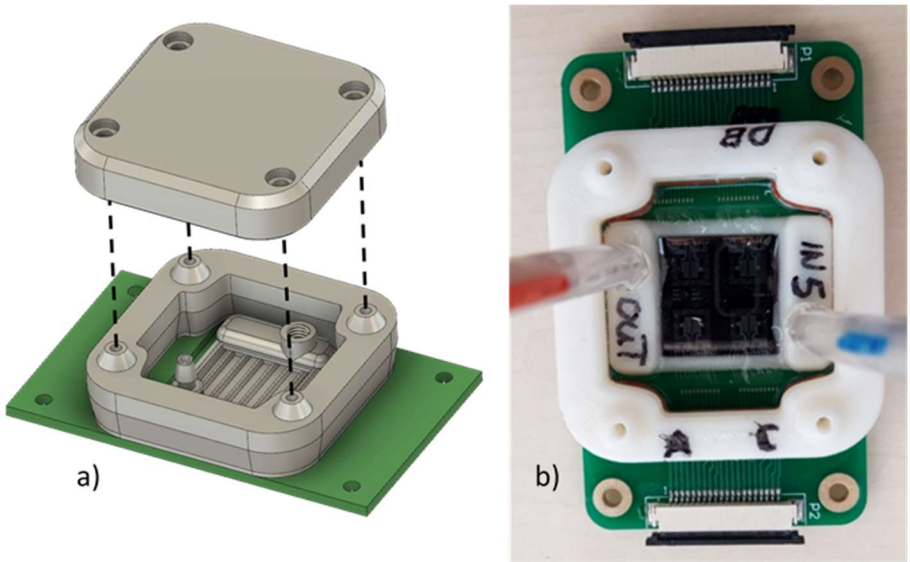

Figure 91: a) Representation of the device assembled, b) one of the devices fabricated

4.3. Experimental study of a microfluidic cell cooling for microelectronics

This chapter is the un-published paper "Experimental study of a microfluidic cell cooling for microelectronics".

The authors of this article are: Gerard Laguna[1], Desideri Regany[1], Gemma Antoni[1], Rajesh Pandiyan[2], Amrid Amnache[2], Manel Ibañez[1], Luc Fréchette[2] and Jérôme Barrau[1]

[1]Dynamic Systems Applied to Solar Energy Research Group, University of Lleida, Lleida, Spain

[2]UMI-LN2, Institut Interdisciplinaire d'Innovation Technologique (3IT), Université de Sherbrooke, Sherbrooke, Canada

Abstract

A novel microfluidic cooling solution, based on a microfluidic cell array, has been developed with the aim of facing the mid-term microelectronics cooling needs. The thermo-hydraulic performance of two configurations of the cooling scheme, with and without self-adaptive valves, are experimentally assessed and compared to conventional microchannels. Under non-uniform and time-dependent heat load scenarios, when applying variable flow rate as a function of the maximum temperature of the chip, the proposed solutions are able to tailor the distribution of the local heat extraction capacity to the application needs. The benefits are basically an improvement of the temperature uniformity of the chip, with an impact on the reliability of the device, and the reduction of the pumping power needs. The energy savings for the microfluidic cell array are 83.7 % and 74.7 %, without and with valves, respectively, compared to conventional microchannels.

4.3.1.Introduction

Microelectronics, as predicted by Moore's Law, was increasing its components by chip and complexity in an exponential way [2]. In the evolution of microelectronics, the chip power density was constant by the increase of the component's efficiency so the thermal management problem was having no change over time [5] since around 2004 [3,6]. The number of components by chip was increasing but the increase in efficiency was slowing down. This new paradigm becomes to a microelectronics power density increase which promotes the multicore chips and also limits its velocity in order to maintain the electronics between the operation temperature [3].

For many years, microelectronics thermal management has been based, basically, on continuous air cooling depending on the power level, using passive approach by natural convection or active air cooling with a fan and heat sink. However, the increase of the power extraction needs and the space limitations make liquid cooling an appropriate compact cooling solution due to its capabilities. For this, many authors have been studying liquid cooling, focusing on microchannels heat sinks [33], manifold microchannel heat sinks [35,98] and spray and jet cooling [99]. Most of the studies were carried out under uniform and non-variant heat flux conditions, focusing on the reduction of the maximum temperature. These devices, which are prepared to cool down the most demanding conditions on the most demanding chip zone, overcool the less demanding parts of the chip in this worst-case scenario, and the entire device when the heat extraction needs vary along a given work cycle. Also, these cooling devices generate large temperature gradients, increasing the thermal stresses and reducing the reliability of the electronic devices. Furthermore, temperature non-uniformities generate imbalances in CMOS devices [37]. Some research has been focused on reducing this temperature gradient by using variable microchannel width in the streamwise direction [24,41,42], double-layer microchannel structures [43] and hybrid jet impingement/microchannel cooling schemes [25]. In all the cases, the proposed solutions are optimized for the most challenging operation case, so they don't adapt to the time-dependent conditions leaving room for improvement.

In order to develop a cooling system able to tailor its distribution of the heat extraction capacity to the time-dependent and non-uniform heat flux, aiming to reduce both the temperature gradients and the pumping power, some studies introduce a self-adaptive microfluidic system [17,77]. This smart device is formed by an array of microfluidic cells. Each cell has a microfluidic valve [16] which opens and closes by thermal expansion so it increases or reduces the local flow rate in function of the local temperature. Stated another way, this system tailors spatially and timely the cooling capacity on each cell, increasing the cooling energy efficiency. The impact of this solution has also been studied for other cooling applications, such as dense array CPV receivers [100].

In this work, the impact of the array of microfluidic cells, with and without self-adaptive valves, is assessed experimentally and compared to conventional microchannels. In a first stage, constant non-uniform heat flux distributions are applied in order to characterize the thermo-hydraulic performance of the tested solutions. Finally, the performance of the devices is assessed under a non-uniform and time-dependent heat load scenario.

4.3.2. Description of the cooling device

The cooling device is formed by an array of microfluidic cells carved into a silicon wafer (dimensions: 3250 µm long, 1950 µm wide and 1125 µm high). After the inlet, the fluid passes through a central chamber configured by 6 tailored microchannels of 160 µm wide (Figure 92a). This microfluidic geometry increases the heat transfer coefficient along the flow path counteracting the increase of the coolant temperature with the aim of providing a better temperature uniformity. At the outlet, the flow is collected in an elbow closed by a microvalve made of silver. When the local temperature increases, the valve opens and the flow reaches the outlet chamber to exit the cell [16]. The device is composed of an array of 6 x 10 cells, achieving a chip surface of 20 x 20 mm^2. A distributor allows to feed the coolant at an identical temperature in all the cells, which are all hydraulically connected in parallel. The cell rows are flipped between each other, in order to make easier the design of the distributor and to avoid thermal spreading between cell inlets and outlets (Figure 92b). This microfluidic cell cooling system (MC6T) is experimentally compared to a standard microchannel cooling solution (MC) of identical external dimensions and depth than the proposed solutions, formed by channels of 100µm width (Figure 92c).

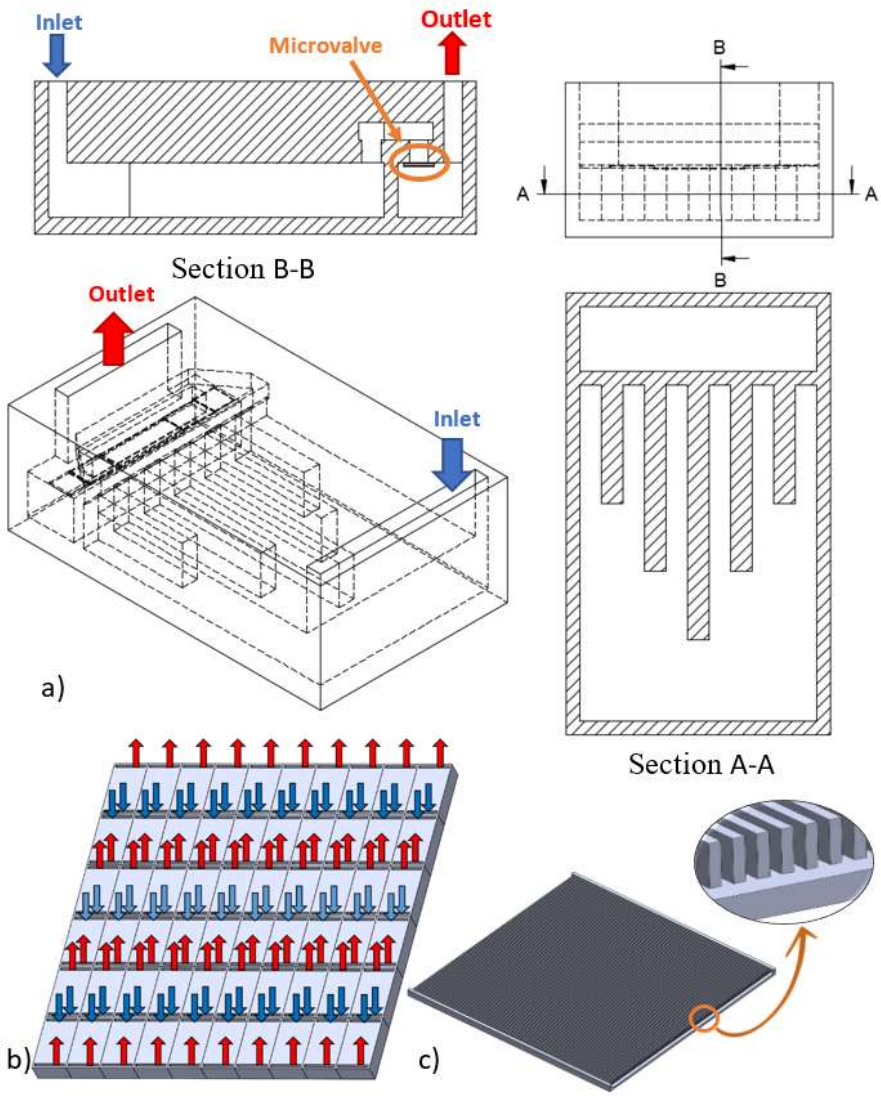

Figure 92: a) Microfluidic cell plans b) Microfluidic cell array c) Microchannels device

The distributor, designed to feed the coolant in all the cells and collect the flow from them has been 3D printed with ABS. It consists of an inlet cavity (in blue on Figure 93) connected to the microfluidic cells entry and an outlet cavity (in red on Figure 93) to collect the flow from the cells.

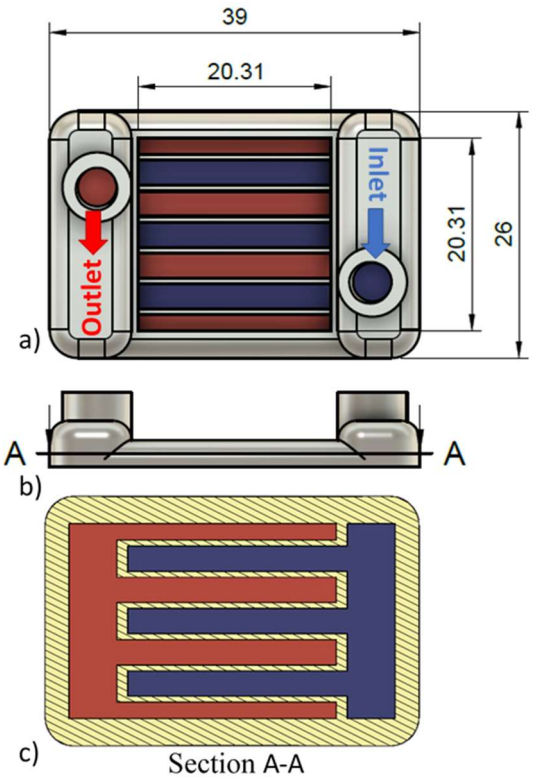

Figure 93: a) Microfluidic cell distributor, in blue the inlet cavity and in red the exit cavity b) Front view c) Section A-A

In order to simulate the non-uniform high heat flux densities, like the ones generated in multimedia processors composed of CPU, GPU, Graphic accelerators and memories, a thermal test chip (Figure 94b) is designed and integrated on top of the cooling devices (Figure 94c). The device chip representation is composed by 4 TTC in order to simulate the non-uniformities caused by the use of the multicore structures (Figure 94a). Each TTC is composed by 4 resistance temperature detections (RTD). These resistances can dissipate heat on the device and, by the measurement of their resistance, their temperature can be read, thus providing a thermal map of the device. Each TTC is composed by a central resistance, two hotspots (located on the right and left of the central resistance) and a peripheral one (Figure 94b).

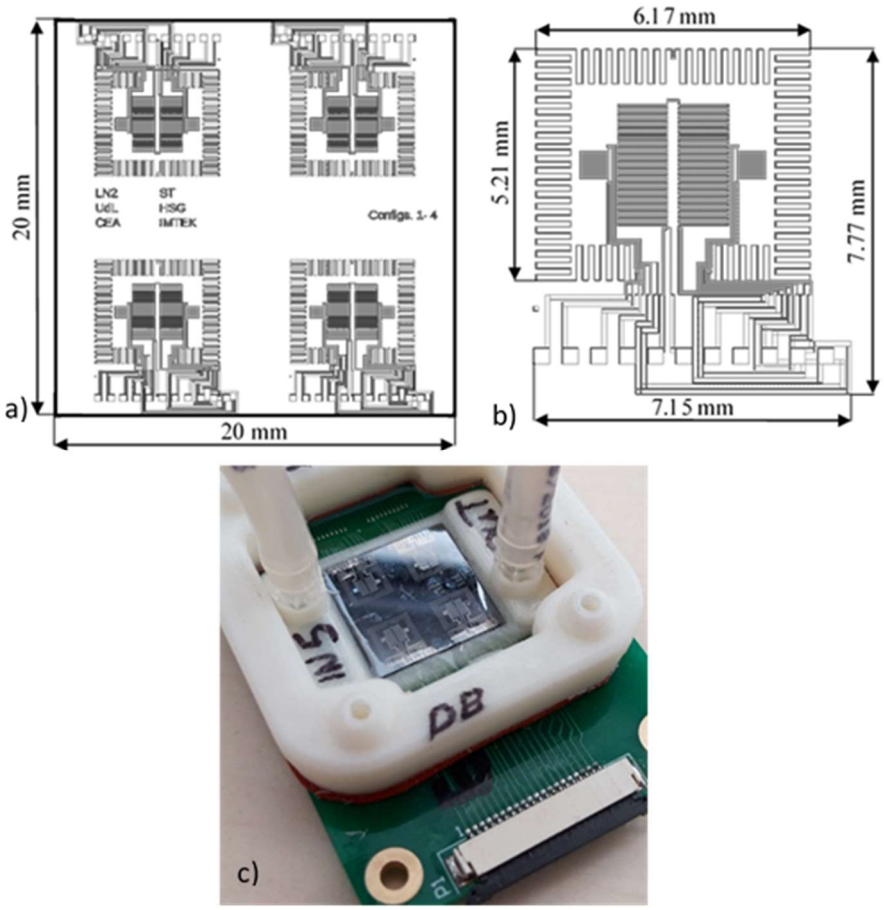

Figure 94: a) Placement of the 4 TTC on the device b) Thermal Test Chip (TTC) c) Microfluidic cell cooling device

4.3.3. Experimental setup

The schematic design of the experimental setup used for this study is shown in Figure 95. The test bench is equipped with a filter to clean the fluid in the circuit, a membrane pump to deliver flow rates up to 60 ml/min, a damper to stabilize the fluctuation of the flow rate due to the oscillation of the pump membrane and a heat exchanger to control the fluid temperature. Thermocouples (type T) and pressure sensors are located at the inlet and outlet of the device in order to measure the temperature increase of the fluid and the pressure drop. Additionally, an air purge is placed at the inlet side and an infrared camera is installed in order to monitor the thermal map of the device.

A LabVIEW interface collects all the data from the devices directly or through the data acquisition and also command the controlled power sources connected to the RTDs of the device.

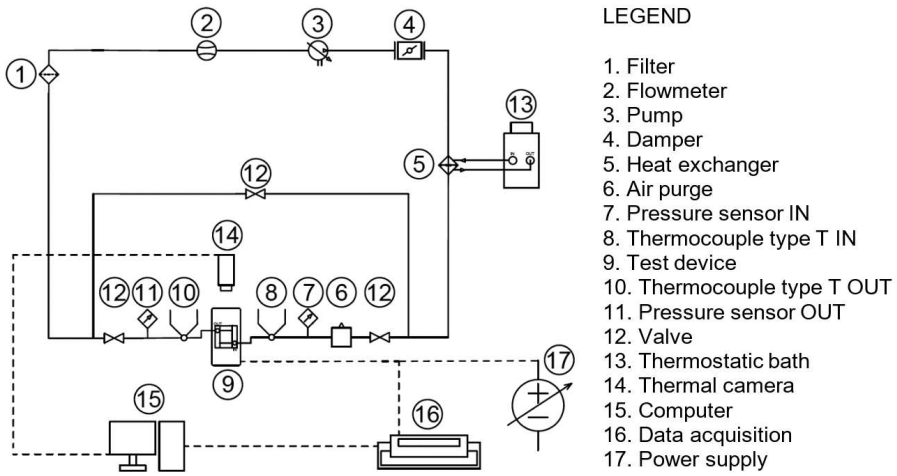

Figure 95: Experimental setup scheme

4.3.4.Steady-state heat load scenario results

The testing boundary conditions applied in steady-state are an inlet temperature of 28 ºC, constant flow rates of 16, 30 and 50 ml/min and a reference heat load of 10.78 W, 6.86 W on a peripheral and 3.91 W on the central heater of the same TTC.

The pressure drop of the array of microfluidic cells (MC6T) presents a reduction of 81.5 % with respect to the microchannel device (MC) at low flow rate (Q = 16 ml/min). This proportion is similar for higher flow rates (Figure 96).

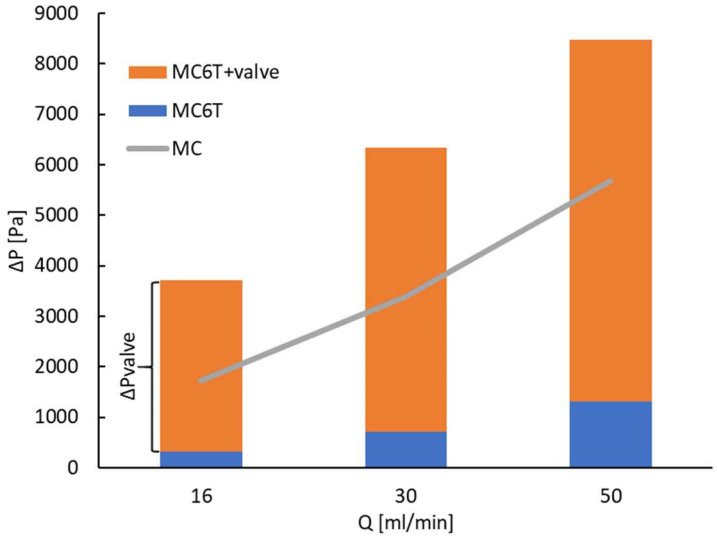

Figure 96: Pressure drop (±62.5 Pa, ±0.12 ml/min).

This result demonstrates that the microfluidic cells cooling scheme allow to reduce drastically large pressure drops, one of the major drawbacks of microchannel cooling devices. For constant flow rate, this implies a reduction in the Hydraulic Pumping Power (HPP) of MC6T with respect to MC, between 75 and 82 % (Figure 97).

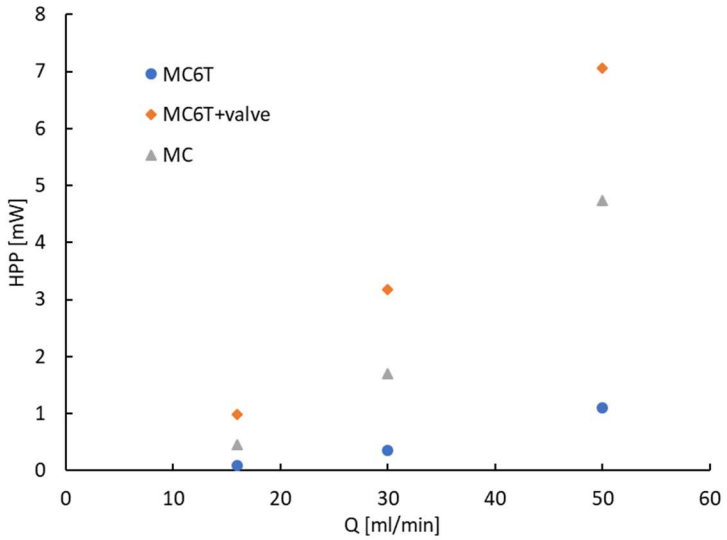

Figure 97: Hydraulic Pumping Power (HPP) variation with the flow rate (±0.07 mW, ±0.12 ml/min).

For the array of microfluidic cells with self-adaptive valves controlling the flow rate distribution (MC6T+valve), the additional pressure drop generated by the valves (much higher than the pressure drop generated by the flow path within the microfluidic cell) implies that the pressure drop is higher than for the other tested devices. This characteristic is mandatory to allow the temperature dependent self-adaptive valves to act as a passive control of the coolant distribution. Note that fixed flow rate is considered in this test and few self-adaptive valves are open due to small heat load. In real operating conditions (non-uniform and time-dependent heat load scenarios), this behavior does not cause a major impact on the Hydraulic Pumping Power (HPP), as the flow rate is reduced (related to the PID control of the total flow rate) until there's need of higher heat extraction capacity.

The total thermal resistance of the microchannel cooling device is lower (but in the same order of magnitude) than for the array of microfluidic cells (Figure 98). This is due to the fact that the array of microfluidic cells geometry (MC6T) generates a flow rate, inside the tailored channels that is 3.6 times lower than in any one of the microchannels by the division of the flow into more channels. In addition, for MC6T, these tailored channels represent only 1/3 of the flow length in the microfluidic cells. Furthermore, the hydraulic diameter is higher in MC6T than in MC, being a flow path of 160 µm for the MC6T and 100 µm for the MC, so the

Reynolds number inside the tailored channels is 5,8 times lower in the array of microfluidic cells than in microchannels.

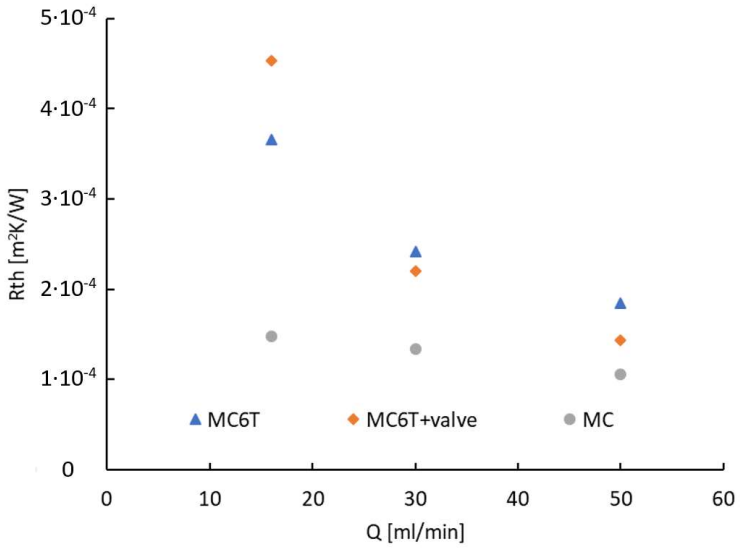

Figure 98:Thermal resistance coefficient (±1.1·10^{-4} m^{2}K/W, ±0.12 ml/min).

The difference of thermal resistance between the microchannel device and the array of microfluidic cells with self-adaptive valves decreases when the flow rate increases. This behavior, also observable for the maximum and average temperatures of the chip surface (Figure 99), indicates that, locally, the tailored distribution of coolant allows to feed more coolant flow rate where the heat extraction capacity needs to be augmented, leading to a decrease of the local thermal resistance for the microfluidic cells with the major heat flux.

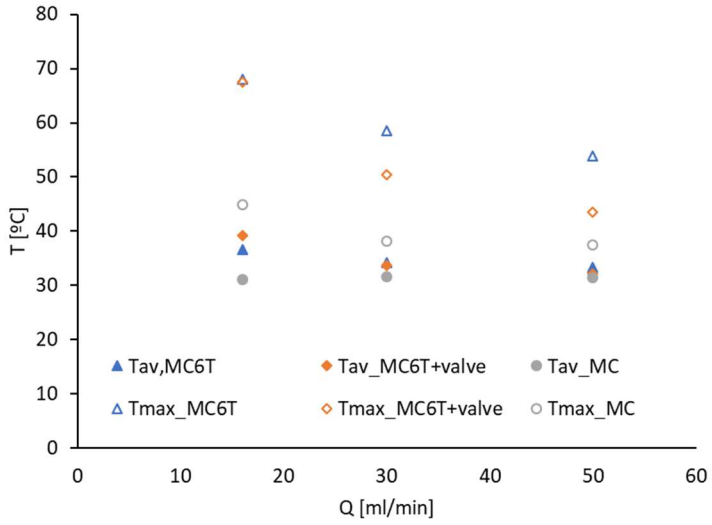

Figure 99:Variation of temperatures; Tav refers to the average surface temperature and Tmax to the maximum surface temperature (±2.5 ºC, ±0.12 ml/min).

The temperature pattern of MC6T depends only on the heat flux distribution (Figure 100), as the geometry generates a uniform heat extraction capacity with a similar inlet temperature of the coolant for each microfluidic cell. This demonstrates a key feature of the cell array configuration.

For the array of microfluidic cells with self-adaptive valves (MC6T+valve), the temperature distribution pattern corresponds to the geometry of the microfluidic cells. This result confirms the capacity of the cooling solution to tailor the distribution of the heat extraction capacity for transient and non-uniform heat load scenarios. In conclusion, in the microfluidic cells array, local heat extraction is achieved and heat load time and space heterogeneity are managed adequately.

On the contrary, for the microchannel device, the temperature distribution depends both on the heat flux distribution and on the geometry of the device. An example is observed in Figure 100c, where heat flux is located at the beginning of the flow path and thermal energy is transported in the direction of the flow (from right to left).

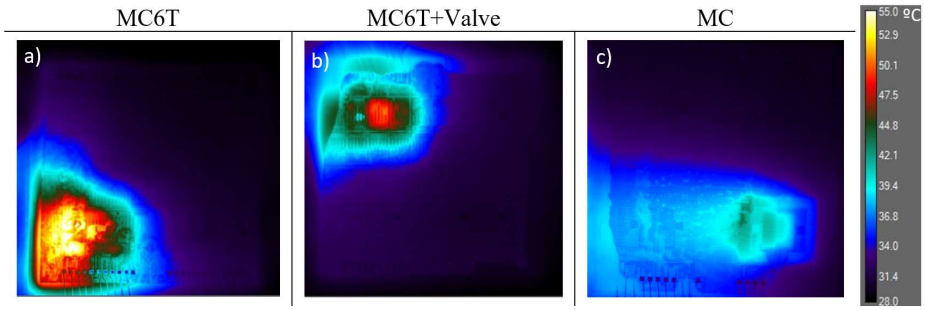

Figure 100: Devices temperature distribution for one Peripheral and one Central heater powered, and 30 ml/min of flow rate a) MC6T cell b) MC6T cell with valve c) Microchannels (±2.1 ºC).

4.3.5. Time-dependent heat load scenario results

The boundary conditions applied in the non-uniform and time-dependent scenario are a constant inlet temperature of 49 ºC and a time-dependent heat load scenario (Figure 101). Maximum heat load values of 80 W/cm^2 and 60 W/cm^2 are applied for the central heater and the peripheral heater, respectively, of two TTCs. The minimum heat load applied to all the heaters is 1 W/cm^2 in order to deliver a background heat flux and to read the temperatures from the RTDs.

In order to tailor the heat extraction capacity to the cooling needs, a flow rate control algorithm, depending on the maximum chip temperature, is defined. When non-uniform and time-dependent heat loads scenarios are applied, flow rate control avoids overcooling in periods when background heat loads are applied.

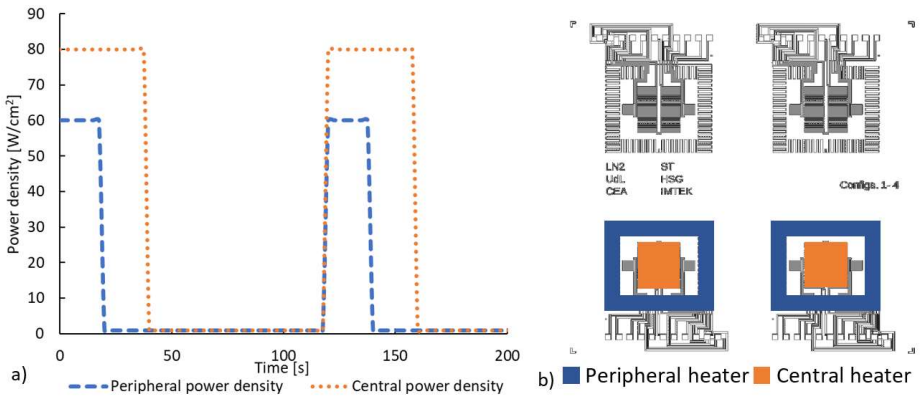

Figure 101: a) Heat load temporal variation b) Central and peripheral heat loads applied

When applying the flow control algorithm overcooling occurs when the heaters are in background heat flux conditions (Figure 102). This is for the pump 4 ml/min minimum flow rate limitation. Also, a temperature peak is registered when heaters turn on. This is explained by the slow response of the control system so this peak can be avoided by decreasing the time step of the measurement system (now set to 2.5 s).

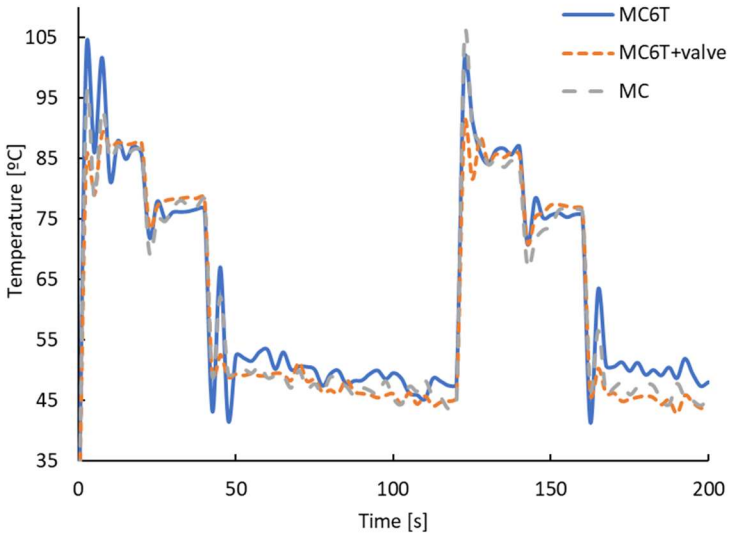

Figure 102: Device maximum temperature over time (±2.1ºC). Microfluidic cell cooling device without valve (MC6T), microfluidic cell cooling device with valve (MC6T+valve) and microchannel cooling solution (MC).

The maximum temperatures of the three studied devices are similar along the 200 s time period (Figure 102). The flow rate needed to cool the MC6T device is higher than the microchannels one due to its higher thermal resistance (Figure 98). However, the flow rate needed to cool down the MC6T with valve when heat flux

is applied is similar to the microchannels device (Figure 103a). This effect demonstrates the capacity of the microfluidic valve to tailor locally the flow rate, achieving low thermal resistances where it is needed. Despite this, due to the pump minimum flow rate, the coolant applied to the devices in the low heat flux period is identical.

The intrinsic low pressure drop of the cells geometry, due to the short length of the microfluidic cell reducing the water path, makes the MC6T geometry the one with less pressure drop in all the time period, pointing the main drawback of the microchannels. However, the MC6T with valve presents a similar pressure drop than microchannels when low heat flux is applied but when heat extraction needs are high the pressure drop is lower than in microchannels. This result is obtained even when the valves induce high pressure drops in the circuit (Figure 103b), as observed with fixed coolant flow rate.

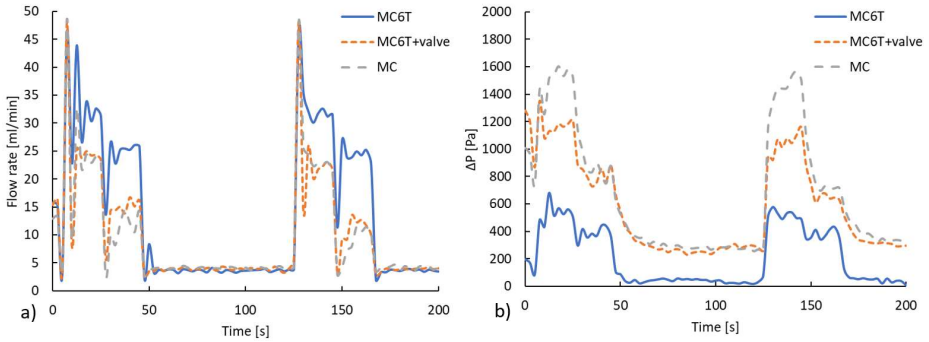

Figure 103: a) Flow rate applied to the different geometries (±0.12 ml/min) b) Pressure drop from the different geometries (±62.5 Pa)

Consequently, the devices MC6T with and without valves enhance the pumping power savings with respect to conventional microchannels with tailored flow rate (Figure 104). This comparison is made with an equal flow rate control algorithm and, therefore, depends only on the geometry of the tested cooling solutions. When comparing with microchannels applying constant flow rate, (current state of the art) huge pumping power savings are observed.

The larger average flow rate and pressure drop are obtained for the microchannels in the fixed flow rate configuration (Figure 105a). On the opposite side, the devices with lower flow rate are the microchannels with tailored flow rate and the MC6T with valves, presenting an average flow rate of 9.64 and 9.92 ml/min respectively. Due to its geometry, the MC6T device reduces by 86.3 % the pressure drop with respect to microchannels with fixed flow rate (Figure 105a). However, this geometry needs 13.78 ml/min, higher average flow rate than both the microchannels and the array of microfluidic cells with valves submitted to a tailored flow rate.

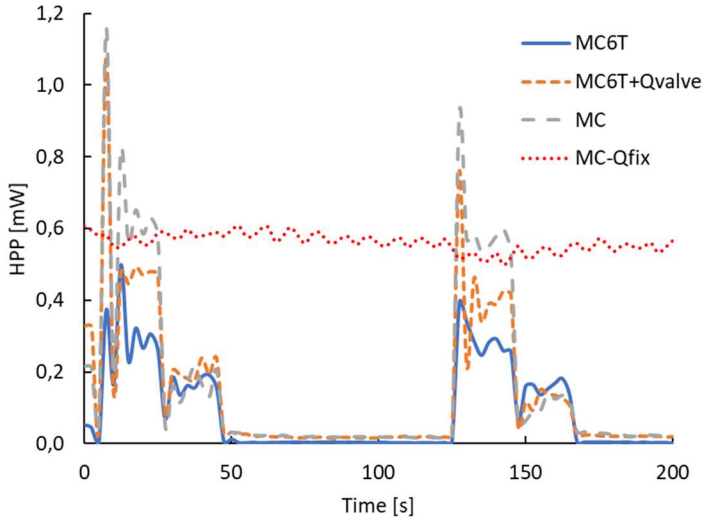

Figure 104: Hydraulic Pumping Power consumed by the studied geometries (±0.5 μW)

Along the time period considered, the savings of pumping energy of the MC6T cooling device, with and without valves, with respect to microchannels, are 15.5 % and 45.6 %, respectively (Figure 105b). Moreover, when the MC6T cooling devices are compared to conventional microchannels without tailored flow rates, the hydraulic pumping power savings become of 74.7 % and 83.7 %, for the array of microfluidic cells with and without valves, respectively. On the other hand, the device MC6T with valves produces the lowest temperature non-uniformity when high heat flux is applied (second 130 of the time period; 33.4 ºC). This result illustrates the main advantage of using self-adaptive valves, the ability to tailor the flow rate distribution across the entire device to the local heat extraction needs. Also, the temperature non-uniformity of the MC6T and the microchannels with tailored flow rate are close (43.6 ºC and 43.9 ºC respectively), achieving with the MC6T a similar temperature non-uniformity with lower energy needs compared with microchannels (Figure 105b).

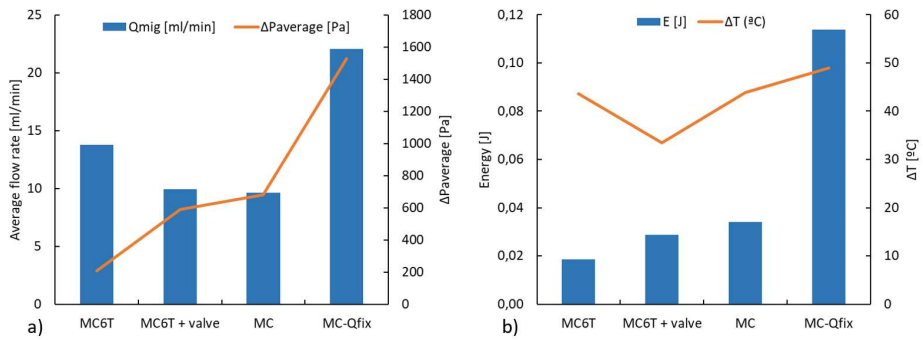

Figure 105: a) Comparison of average flow rate (±0.12 ml/min) and average pressure drop for each studied geometry (±62.5 Pa) b) Comparison of the energy needed to refrigerate the devices the 200 s time period (±0.00025 J) and the temperature non-uniformity at t = 130 s (±2.1 ºC)

4.3.6. Conclusions

The pressure drop of the array of microfluidic cells without self-adaptive valves is one fifth of the microchannels one, when submitted to the same total flow rate, confirming the high impact of this novel cooling scheme on one of the main drawbacks of microchannels. For the microfluidic cell cooling solution with valves, the large pressure drop, compared with other studied solutions, induced by the self-adaptive valves has been observed. This behaviour is necessary to allow the system to tailor the distribution of the coolant to the non-uniform needs of local heat extraction capacity.

Indeed, when applying a non-uniform and time-dependent heat load scenario together with a flow rate tailored to the maximum temperature of the chip, the capacity of the MC6T cooling device to reduce with flow rate regulation, in comparison to existing solutions, both the temperature non-uniformities and the pumping power is experimentally validated. This device presents the lowest hydraulic power consumption reducing 45 % with similar temperature uniformity the energy needs compared with microchannels with flow rate regulation.

On the other side, the MC6T cooling solution with self-adaptive valves manages to reduce the energy needs by 15.45 % meanwhile reducing the temperature non-uniformity by 24 % with respect to microchannels with an identical tailored flow rate algorithm.

These results validate the self-adaptive cooling scheme actuation and open new perspectives for the development of smart and compact cooling solutions in a wide range of applications with non-uniform and time-dependent heat load scenarios (microelectronics, Concentration PhotoVoltaics…), where high temperature uniformities and efficient cooling have a high impact on the reliability and performance.

5. Discussion and conclusions

5.1. Discussion

In this thesis, a novel and self-adaptive cooling device is designed, numerically assessed and experimentally tested. The main objective of this work is to validate this concept for microelectronics applications. However, the impact of this system on the performance of a dense array CPV receiver is also studied.

Microfluidic cell numerical studies

As a first stage, three configurations of microfluidic cells are numerically assessed, both as single cells and within an array, in order to characterise and compare their behaviour.

In these studies, the microfluidic cell array demonstrates its capacity to overcome the drawbacks of microchannels, reducing the pressure drop by having a short flow path length and increasing the temperature uniformity by the use of microfluidic valves. However, the internal geometry of the cell has a huge impact on system performance. For cells without internal elements (MC0), the heat transfer is low and a large flow rate is required to keep an acceptable maximum chip temperature. These drawbacks are addressed by implementing six microchannels into the cell (MC6), but these microchannels will induce overcooling in the inlet of the cell, due to the combination of the low temperature of the fluid, the jet impact at the cell inlet and the low thermal resistance of the microchannels. Therefore, with the aim of both improving the temperature uniformity and reducing the pressure drop, tailored microchannels (MC6T) are implemented, in order to balance the increase of the fluid temperature along the flow path with the distribution of the local heat extraction. When submitted to a non-uniform and time-dependent heat load scenario, the array of microfluidic cells with the MC6T geometry reduces, with respect to the microchannels, the flow rate and the pressure drop by 42.5 % and 81.0 %, respectively. These results lead to an average pumping power reduction of 89.1 %, while the temperature uniformity is improved by the use of the microfluidic valves.

Based on a previous study by Sharma *et al.* [30], these numerical studies do not consider heat spreading among cells. However, the valve has a progressive opening, so the temperatures of the cell array depend on the local equilibrium point between the local flow rate, which depends on the valve opening, and the heat flux applied to the cell. A 3 x 3 array of microfluidic cells is implemented to assess the heat spreading with three different valves in a non-uniform heat load scenario: the central cell is submitted to a high heat flux (300 W/cm^2), while the surrounding ones are submitted to half of this value (150 W/cm^2). The three studied valves V60, V75 and V90 start to open at 60 ºC, 75 ºC and 90 ºC, respectively, to be completely open at 100 ºC. When a steeper slope valve is implemented (V90), the temperatures of the cell are closer to the setpoint, reducing the temperature non-uniformity (by 48 % with respect to the V60 valve), so with less spreading between cells and less

overcooling due to the increase of temperature uniformity. Furthermore, the total flow rate with the V90 valve is 27 % lower than with the V60 valve, leading to a reduction by 15 % of the energy consumption.

In the previous study, a thermal gradient along the cells surface, a consequence of the configuration of the microfluidic cell array, is observed. Indeed, the coldest part of one cell (inlet) is close to the hottest zone of another cell (outlet). This implies a spreading effect which causes an increase of the inlet temperature and, therefore, of the temperature of the entire cell. In order to avoid this thermal spreading, a flip configuration is implemented where the contact between inlets and outlets is avoided. For an array of 10 microfluidic cells submitted to 20 W/cm^2 and with the same flow rate, the thermal gradient with the previous configuration is 11 ºC and with the flipped configuration is 4 ºC.

For the device fabrication, the flip cell configuration is used in order to avoid, or limit in the case of non-uniform heat loads, this effect. With the application of the flip cell distribution, the initial assumption of no thermal spreading is valid when no hotspots are considered.

This part of the study allowed to numerically assess the cooling performance of the array of microfluidic cells with self-adaptive valves. At this stage, it has been impossible to validate experimentally the numerical model as no previous studies on this type of cooling solution has been previously developed. Due to microfabrication requirements, some modifications of the geometry have been implemented from the numerical model to the fabricated ones. However, the main characteristics have been conserved and the Proof of Concept demonstrated that the results obtained in this numerical assessment are aligned with the experimental ones.

Impact of microfluidic cells in a dense array CPV receivers

The first studies are focused on the characterisation of the behaviour of the self-adaptive microfluidic cell array, when submitted to heat loads representative of microelectronic applications. The impact of this cooling scheme on the performance of a dense array CPV receiver, where the non-uniformity of the heat flux distribution presents a different pattern, is also the object of study.

In a first study, the performance of a dense array CPV receiver under a non-uniform irradiation profile cooled by the array of self-adaptive microfluidic cells is compared with the same device cooled by microchannels. The flow rates are tailored in order to reach the same average temperature. Under average irradiation of 600 suns, the net PV power of the CPV receiver cooled by microchannels and microfluidic cells are, respectively, 72.6 % and 79.7 % with respect to the sum of the electrically isolated cells production at the same illumination and temperature

conditions, leading to an increase of 9.7 % of the power generation when using the array of microfluidic cells instead of conventional microchannel technology.

In a second analysis, the performance of a CPV dense array receiver composed of 6 x 8 cells (8 modules in series, each module with 6 CPV cells in parallel) has been assessed for 6 different illumination profiles when submitted to an average irradiance of 800 suns and an average temperature of 86 ºC. The mismatch losses depend linearly on the standard deviation of the mean irradiation applied to each of the 8 modules, from 0 % of mismatch effect from the uniform illumination profile to 34 % for a large irradiation dispersion between modules.

In order to assess the impact of the cooling solution applied to mitigate the mismatch losses, the behaviour of the CPV system with three different electrical configurations for an 8 x 6 cell array with microfluidic cell cooling and microchannels is assessed. The three configurations are: 48 CPV cells connected in series, 8 modules in parallel of 6 CPV cells in series each module, and 48 cells connected in parallel.

In the first configuration, the 48 CPV cells in series, the microfluidic cell system increases, with respect to the microchannel cooling device, the maximum power point by 0.37 %. It is observed that, for the maximum power point of the system, some cells are consuming energy through the bypass diode. This happens when the string current is higher than the short-circuit current of a cell, which depends on the irradiance profile. In a CPV dense array connected in series, the temperature distributions do not affect the power generation when the cells are producing energy and the average temperature remains the same. The increment in power generation produced by the microfluidic cells cooling device arises from the fact that this system reduces the average temperature of the cells that produce energy to the detriment of the ones that consume.

In the second case, 8 modules in parallel of 6 CPV connected in series, the microfluidic cell system increases, with respect to the microchannel cooling device, the maximum power point by 3.81 %. The microchannels cooling system produces a temperature distribution that causes the last module of 6 cells in series to be one of the hottest and in the studied case also corresponds to the least irradiated. This lowers the open circuit voltage of the series and reduces the electrical power of the CPV dense array, compared with the one obtained with microfluidic cells. Microfluidic cells allow the least irradiated series to have the lowest temperatures, increasing the open circuit voltage and the electrical power output.

In the 48 CPV cells in parallel configuration, the microfluidic cell system increases, with respect to the microchannel cooling device, the maximum power by 1.77 %. The difference in electrical power is related to the temperature distribution obtained with the two cooling devices. Microchannels make the least irradiated cells become hotter than in microfluidic cells and, therefore, these cells produce less energy.

Even though the parallel configuration produces more energy than the others, the currents of almost 600 A are unrealizable due to the Joule effect and the size of the cables needed.

The study shows that the power generation depends more on the electrical connexion than on the cooling device. For the three analyzed configurations, the major impact obtained by cooling with microfluidic cells device, in comparison with microchannels, is an increase of 3.81 % of the power generation. Meanwhile, the power generation increases more than 50 % for the parallel configuration when compared to the series configuration. However, in this analysis reliability aspects are not taken into consideration. The increase of temperature uniformity with microfluidic cells decreases the thermo-mechanical stress of the CPV receiver, reducing its degradation and, thereby, increasing its lifetime.

Also, the illumination profile on a dense array CPV receiver is more predictable than in microelectronics. This consideration makes possible, at the design stage, to tailor the distribution of the coolant flow rate across the geometry, improving the performance with respect to the microchannels. However, this fixed configuration is not able to adapt to changes like having part of the heliostats shadowed by some clouds or maintenance activities in the heliostats. In comparison with cooling devices designed specifically for a given illumination profile, the array of microfluidic cells with self-adaptive valves is capable to tailor the heat extraction capacity for all the transitory illumination profiles and the steady-state operation without the need of a specific characterization of the illumination profile. Therefore, both the associated cost and the time needed for the design of the cooling device are reduced.

These results open a new way to increase the efficiency and reliability of dense array CPV receivers by using cooling devices which tailor the distribution of the heat extraction capacity, through microvalves that tailor the local flow rate to the local temperature, to the illumination profile and the electrical configuration.

Experimental study of microfluidic cell cooling system

Once the concept is numerically validated, the proposed geometry is designed, fabricated and tested. The characterisation of several self-adaptive valve geometries, implemented by a partner, led to an enlargement of the valve used in the microfluidic cell and a reallocation of the valve in order to open in the flow direction. These changes imply a microfluidic cell growth and an outlet chamber placement.

A specific test bench is developed in order to characterise the behaviour of the cooling devices under non-uniform and time-dependent heat load scenarios. With this test bench, the STREAMS objectives in terms of cooling performance are validated.

The microfluidic cell cooling system with and without microfluidic valves is compared to a microchannels device. On the one hand, applying a steady-state analysis with a constant flow rate, the pressure drop of the microfluidic cell without valves is only 20 % of the microchannels one, confirming the high impact of this novel cooling scheme on one of the main drawbacks of microchannels. On the other hand, the self-adaptive valves induce a large pressure drop compared with other studied solutions. This behaviour is mandatory to allow the system to tailor the distribution of the coolant to the non-uniform needs of the heat extraction capacity. It should be noted that the steady-state analysis is done with a few self-adaptive valves opened due to the low heat load. In real operation (non-uniform and time-dependent heat load), this effect does not have a major impact on the hydraulic pumping power as the flow rate in the time-dependent scenario is reduced by the use of a control algorithm in order to tailor the flow rate to the heat extraction demand.

With non-uniform and time-dependent heat load, the microfluidic cell without self-adaptive valves and with flow rate regulation reduces the pumping power needs along the studied period by 83.7 % and improves the temperature uniformity by 10.8 % compared with constant flow rate microchannels. Compared with the microchannels with the same flow rate regulation, the pumping power needs are reduced by 45.6 % and there are similar temperature non-uniformities. This improvement of the pumping energy needs is mostly caused by the 69 % reduction of the pressure drop with respect to microchannels.

The microfluidic cell system with self-adaptive valves reduces the energy needs in the studied heat load scenario by 74.7 % and 15.5 %, compared with non-regulated (conventional) and regulated microchannels, respectively. The microfluidic cell cooling device with valves presents higher pressure drops than without, but needs a lower flow rate due to the adequate distribution of the coolant through the device. This tailored distribution of the heat extraction capacity leads to an increase of the temperature uniformity by 23 % with respect to the cells without valves, but also an increase of 50 % in the energy needs.

This experimental comparison has been done between the microfluidic cell geometry with 160 µm tailored microchannels and 100 µm width microchannels. Ideally, for comparison proposes, the microfluidic cell tailored microchannels width and the width of the microchannels should have been the same but due to an error in the dimensioning the two cooling systems end up with different flow path width. This difference increases the thermal resistance of the microfluidic cell in comparison with the microchannels device. Despite this drawback, the microfluidic cell cooling system improves the temperature uniformity and the pumping power requirements.

The comparison between the microfluidic cell system and the microchannels technology could be done with different microchannels approach, reducing, even

more, the width of the channels and therefore increasing the cooling area. However, for comparison proposes, the cell internal geometry should be changed to internal microchannels of the same characteristic.

5.2. Conclusions

The objectives proposed at the beginning of this thesis have been achieved:

1. A novel cooling device for microelectronic applications, based on an array of microfluidic cells, has been designed and validated. The experimental results have shown that, without valves and a regulated flow rate, the proposed geometry, in a non-uniform and time-dependent heat load scenario, reduces the average pressure drop by 86.3 % with respect to microchannels with a fixed flow rate. Comparing both geometries with pump regulation in order to tailor the total flow rate to the heat extraction needs, the average pumping power in the microfluidic cell system is reduced by 69.2 % compared to the microchannels. In both cases, the 25 % pressure drop reduction target is achieved.
2. The proposed array of microfluidic cells with self-adaptive valves tailors the coolant flow rate distribution to the local heat extraction capacity needs. A 38.9 % coolant flow rate reduction, comparing the microfluidic cell system with valves with the same geometry without valves, has been experimentally measured. Apart from the flow rate reduction, the temperature uniformity of the device with valves is improved by 23.4 % compared with the device without valves. Compared with microchannels with a fixed flow rate, the temperature uniformity is improved by 31.7 %.
3. When a pump flow rate control algorithm is applied to the studied cooling solutions, the energy savings of the array of microfluidic cells with and without valves are 15.5 % and 45.6 % respectively, compared with the microchannels. This energy reduction is less than the target of 50 % reduction. However, when compared to the current state of the art (microchannels with constant flow rate), the energy savings are 74.7 % and 83.7 % for the microfluidic cells with and without valves, respectively.
4. A test bench has been designed and built in order to test the cooling devices. The test bench is controlled by LabVIEW for its capability to connect with several devices. The code developed to control the whole setup measures the temperatures from the 16 RTDs on the device, the device inlet and outlet temperatures, the pressure drop, the flow rate and the power delivered to each resistance. Also controlled is the heat flux applied to each resistance, and the pump flow rate can be fixed or tailored to the device's maximum temperature.

5. Finally, the microfluidic cooling numerical results are used to assess the cooling technology in the CPV. The improvement in temperature uniformity from the array of microfluidic cells cooling system allows the mismatch losses in the dense array CPV receiver to be reduced by 23.4 % for an average 600 suns non-uniform irradiation distribution at an average temperature of 67 ºC compared with the CPV cooled by microchannels. This achievement, combined with the lower pumping power required by this system to reach a given heat extraction capacity, in comparison with microchannels, with an average radiation of 800 suns, leads to an increase of the net PV power produced by the receiver of between 0.37 % and 3.81 %, depending on the electrical configuration.

6. Future work

In the course of this thesis, a novel cooling concept based on an array of microfluidic cells with self-adaptive valves has been designed and experimentally validated. However, in order to become a consolidated technology more effort is required.

Part of this effort must focus on the experimental assessment of the microfluidic cell under more non-uniform and time-dependent heat loads in order to assess the behaviour of the system under different real microelectronics conditions to fully characterise the microfluidic cell behaviour. Moreover, it should be considered the modification of the internal geometry to different types of microchannels in order to improve not only the pumping power requirements but also taking into account system level requirements like the exergetic efficiency.

The other key point is related to the study of the self-adaptive valves by themselves, in order to reach, with respect to their own temperature, a more non-linear behaviour, which has been proven to boost the reduction of the temperature non-uniformities. Also, reliability tests are required in order to assess the lifetime and the fatigue of the microfluidic valves. These tests are planned within the project *Experimental Validation and Commercial Viability of an Energy Efficient Universal Cooling Scheme*, financed by the *Generalitat de Catalunya* through the Grant *Indústria del Coneixement 2018– modalitat Producte*, whose main aim is to reach TRL6 (technology demonstrated in relevant environment).

As the results obtained with the numerical study of the microfluidic cell cooling system applied to dense array CPV receivers are encouraging, one of the next steps is to experimentally assess the gains relative to the implementation of this cooling system in a real CPV system. For this kind of application, the possibility of implementing the proposed cooling solution in the mesoscale will lead to the exploration of other self-adaptive technologies, like Shape Memory Alloys (SMA). Moreover, the possibility of implementing a biphasic cooling flow rate should be considered in order to boost the temperature uniformity.

7. References

[1] Moore G. Cramming more components onto circuits integrate. Electronics 1965;38.

[2] Moore G. Progress In Digital Integrated Electronics. IEEE Text Speech 1975;1:11–3.

[3] Shalf JM, Leland R. Computing beyond moore's law. Computer (Long Beach Calif) 2015;48:14–23. https://doi.org/10.1109/MC.2015.374.

[4] Kogge P. Reading the Entrails: How Architecture Has Evolved at the High End. IPDPS Keynote 2014. https://doi.org/10.1109/IPDPS.2014.60.

[5] Dennard RH, Rideout VL. Design of Ion-Implanted MOSFET's with Very Small Physical Dimensions. Solid-State Circuits 1974;9:256–68. https://doi.org/10.1016/S0925-9635(99)00161-2.

[6] Johnsson L, Netzer G. The impact of Moore's Law and loss of Dennard scaling: Are DSP SoCs an energy efficient alternative to x86 SoCs? J Phys Conf Ser 2016;762. https://doi.org/10.1088/1742-6596/762/1/012022.

[7] Borkar S, Chien AA. The future of microprocessors. Commun ACM 2011;54:67–77. https://doi.org/10.1145/1941487.

[8] Esmaeilzadeh H, Blem E, St. Amant R, Sankaralingam K, Burger D. Dark silicon and the end of multicore scaling. IEEE Micro 2012;32:122–34. https://doi.org/10.1109/MM.2012.17.

[9] Sharma CS, Tiwari MK, Zimmermann S, Brunschwiler T, Schlottig G, Michel B, et al. Energy efficient hotspot-targeted embedded liquid cooling of electronics. Appl Energy 2015;138:414–22. https://doi.org/10.1016/j.apenergy.2014.10.068.

[10] Yang S, Xiang D, Bryant A, Mawby P, Ran L, Tavner P. Condition Monitoring for Device Reliability in Power Electronic Converters: A Review. IEEE Trans Power Electron 2010;25:2734–52. https://doi.org/10.1109/tpel.2010.2049377.

[11] Cho J, Kim Y. Improving energy efficiency of dedicated cooling system and its contribution towards meeting an energy-optimized data center. Appl Energy 2016;165:967–82. https://doi.org/10.1016/j.apenergy.2015.12.099.

[12] Miranskyy A V., Al-zanbouri Z, Godwin D, Bener AB. Database engines: Evolution of greenness. J Softw Evol Process 2018;30:1–25. https://doi.org/10.1002/smr.1915.

[13] Meijer GI. Cooling Energy-Hungry Data Centers 2010;328:318–20.

[14] Project STREAMS. Streams Project – Electronic Cooling n.d. http://project-streams.eu/ (accessed August 16, 2019).

[15] Héder M. From NASA to EU: The evolution of the TRL scale in Public Sector Innovation. Innov J 2017;22:1–23.

[16] McCarthy M, Tiliakos N, Modi V, Fréchette LG. Temperature-regulated nonlinear microvalves for self-adaptive MEMS cooling. J Microelectromechanical Syst 2008;17:998–1009. https://doi.org/10.1109/JMEMS.2008.927742.

[17] Laguna G, Vilarrubí M, Ibañez M, Betancourt Y, Illa J, Azarkish H, et al. Numerical parametric study of a hotspot-targeted microfluidic cooling array for microelectronics. Appl Therm Eng 2018;144:71–80. https://doi.org/10.1016/j.applthermaleng.2018.08.030.

[18] Laguna G, Vilarrubí M, Ibañez M, Rosell J, Badia F, Azarkish H, et al. Impact of the self-adaptive valve behavior on an array of microfluidic cells under unsteady and non-uniform heat load distributions. J Appl Fluid Mech 2019;12:29–36.

[19] COMSOL Multiphysics. Heat Transfer Module - User's Guide. Comsol Multiphysics Manual, version 5.4, 2018, p. 1–702.

[20] COMSOL Multiphysics. CFD Module - User's Guide. Comsol Multiphysics Manual, version 5.4, 2018, p. 1–710.

[21] Naphon P, Wiriyasart S, Wongwises S. Thermal cooling enhancement techniques for electronic components. Int Commun Heat Mass Transf 2015;61:140–5. https://doi.org/10.1016/j.icheatmasstransfer.2014.12.005.

[22] Khan MG, Fartaj A. A review on microchannel heat exchangers and potential applications. Int J Energy Res 2011;35:553–82. https://doi.org/10.1002/er.1720.

[23] Dede EM, Liu Y. Experimental and numerical investigation of a multi-pass branching microchannel heat sink. Appl Therm Eng 2013;55:51–60. https://doi.org/10.1016/j.applthermaleng.2013.02.038.

[24] Riera S, Barrau J, Omri M, Fréchette LG, Rosell JI. Stepwise varying width microchannel cooling device for uniform wall temperature: Experimental and numerical study. Appl Therm Eng 2015;78:30–8. https://doi.org/10.1016/j.applthermaleng.2014.12.012.

[25] Barrau J, Chemisana D, Rosell J, Tadrist L, Ibañez M. An experimental study of a new hybrid jet impingement/micro-channel cooling scheme. Appl Therm Eng 2010;30. https://doi.org/10.1016/j.applthermaleng.2010.05.013.

[26] Barrau J, Omri M, Chemisana D, Rosell J, Ibañez M, Tadrist L. Numerical study of a hybrid jet impingement/micro-channel cooling scheme. Appl Therm Eng 2012;33–34:237–45. https://doi.org/10.1016/j.applthermaleng.2011.10.001.

[27] Sung MK, Mudawar I. Experimental and numerical investigation of single-phase heat transfer using a hybrid jet-impingement/micro-channel cooling scheme. Int J Heat Mass Transf 2006;49:682–94. https://doi.org/10.1016/j.ijheatmasstransfer.2005.08.021.

[28] Barrau J, Rosell J, Chemisana D, Tadrist L, Ibañez M. Effect of a hybrid jet impingement/micro-channel cooling device on the performance of densely packed PV cells under high concentration. Sol Energy 2011;85:2655–65. https://doi.org/10.1016/j.solener.2011.08.004.

[29] Barrau J, Perona A, Dollet A, Rosell J. Outdoor test of a hybrid jet impingement/micro-channel cooling device for densely packed concentrated photovoltaic cells. Sol Energy 2014;107:113–21. https://doi.org/10.1016/j.solener.2014.05.040.

[30] Sharma CS, Tiwari MK, Poulikakos D. A simplified approach to hotspot alleviation in microprocessors. Appl Therm Eng 2016;93:1314–23. https://doi.org/10.1016/j.applthermaleng.2015.08.086.

[31] Graef E, Huizing B, Mahnkopf R, Hidemi Ishiuchi J, Hayashi Y, Ikumi N, et al. International technology roadmap for semiconductors 2.0: 2015 2015:79.

[32] Tuckerman DB, Pease RFW. High-performance heat sinking for VLSI. IEEE Electron Device Lett 1981;2:126–9. https://doi.org/10.1109/EDL.1981.25367.

[33] Lee PS, Garimella S V., Liu D. Investigation of heat transfer in rectangular microchannels. Int J Heat Mass Transf 2005;48:1688–704. https://doi.org/10.1016/j.ijheatmasstransfer.2004.11.019.

[34] Sharma CS, Tiwari MK, Michel B, Poulikakos D. Thermofluidics and energetics of a manifold microchannel heat sink for electronics with recovered hot water as working fluid. Int J Heat Mass Transf 2013;58:135–51. https://doi.org/10.1016/j.ijheatmasstransfer.2012.11.012.

[35] Escher W, Michel B, Poulikakos D. A novel high performance, ultra thin heat sink for electronics. Int J Heat Fluid Flow 2010;31:586–98. https://doi.org/10.1016/J.IJHEATFLUIDFLOW.2010.03.001.

[36] Kandlikar SG, Bapat A V. Evaluation of jet impingement, spray and microchannel chip cooling options for high heat flux removal. Heat Transf Eng 2007;28:911–23. https://doi.org/10.1080/01457630701421703.

[37] Sharma CS, Zimmermann S, Tiwari MK, Michel B, Poulikakos D. Optimal thermal operation of liquid-cooled electronic chips. Int J Heat Mass Transf 2012;55:1957–69. https://doi.org/10.1016/j.ijheatmasstransfer.2011.11.052.

[38] Hetsroni G, Mosyak A, Segal Z, Ziskind G. A uniform temperature heat sink for cooling of electronic devices. Int J Heat Mass Transf 2002;45:3275–86. https://doi.org/10.1016/S0017-9310(02)00048-0.

[39] Rubio-Jimenez CA, Kandlikar SG, Hernandez-Guerrero A. Numerical analysis of novel micro pin fin heat sink with variable fin density. IEEE Trans Components, Packag Manuf Technol 2012;2:825–33. https://doi.org/10.1109/TCPMT.2012.2189925.

[40] Sharma CS, Tiwari MK, Zimmermann S, Brunschwiler T, Schlottig G, Michel B, et al. Energy efficient hotspot-targeted embedded liquid cooling of electronics. Int J Heat Mass Transf 2015;88:684–94. https://doi.org/10.1016/j.apenergy.2014.10.068.

[41] Xie G, Zhang F, Sundén B, Zhang W. Constructal design and thermal analysis of microchannel heat sinks with multistage bifurcations in single-phase liquid flow. Appl Therm Eng 2014;62:791–802. https://doi.org/10.1016/j.applthermaleng.2013.10.042.

[42] Riera S, Barrau J, Rosell JI, Fréchette LG, Omri M, Vilarrubí M, et al. Smoothing effect of the thermal interface material on the temperature distribution in a stepwise varying width microchannel cooling device. Heat Mass Transf Und Stoffuebertragung 2017;53. https://doi.org/10.1007/s00231-017-2045-0.

[43] Lin L, Chen Y-Y, Zhang X-X, Wang X-D. Optimization of geometry and flow rate distribution for double-layer microchannel heat sink. Int J Therm Sci 2014;78:158–68. https://doi.org/10.1016/j.ijthermalsci.2013.12.009.

[44] Dang B, S. Bakir M, Meindl JD. Integrated thermal-fluidic I/O interconnects for an on-chip microchannel heat sink. Electron Device Lett IEEE 2006;27:117–9.

[45] Kandlikar SG, Grande WJ. Evaluation of Single Phase Flow in Microchannels for High Heat Flux Chip Cooling — Thermohydraulic Performance Enhancement and Fabrication Technology. Heat Transf Eng 2004;25:5–16. https://doi.org/10.1080/01457630490519772.

[46] Brunschwiler T, Rothuizen H, Paredes S, Michel B, Colgan E, Bezama P. Hotspot - adapted Cold Plates to Maximize System Efficiency. Conf Pap THERMINIC 2009 2009.

[47] Collin L-M, Colonna J-P, Coudrain P, Shirazy MRS, Cheramy S, Souifi A, et al. Hot spot aware microchannel cooling add-on for microelectronic chips in mobile devices. 2017 16th IEEE Intersoc Conf Therm Thermomechanical Phenom Electron Syst 2017:460–4. https://doi.org/10.1109/ITHERM.2017.7992523.

[48] Green C, Fedorov AG, Joshi YK. Fluid-to-Fluid Spot-to-Spreader (F2/S2) Hybrid Heat Sink for Integrated Chip-Level and Hot Spot-Level Thermal Management. J Electron Packag 2009;131:025002. https://doi.org/10.1115/1.3104029.

[49] Sharma CS, Schlottig G, Brunschwiler T, Tiwari MK, Michel B, Poulikakos D. A novel method of energy efficient hotspot-targeted embedded liquid cooling for electronics: An experimental study. Int J Heat Mass Transf 2015;88:684–94. https://doi.org/10.1016/j.ijheatmasstransfer.2015.04.047.

[50] Azarkish H, Barrau J, Coudrain P, Savelli G, Collin L-M, Frechette LG. Self-adaptive microvalve array for energy efficient fluidic cooling in microelectronic systems. 2017 16th IEEE Intersoc Conf Therm Thermomechanical Phenom Electron Syst 2017:522–9. https://doi.org/10.1109/ITHERM.2017.7992531.

[51] Sharma CS, Tiwari MK, Poulikakos D. A simplified approach to hotspot alleviation in microprocessors. Appl Therm Eng 2016;93:1314–23. https://doi.org/10.1016/j.applthermaleng.2015.08.086.

[52] Naphon P, Wiriyasart S, Wongwises S. Thermal cooling enhancement techniques for electronic components. Int Commun Heat Mass Transf 2015;61. https://doi.org/10.1016/j.icheatmasstransfer.2014.12.005.

[53] Riera S, Barrau J, Perona A, Dollet A, Rosell JI, Fréchette L. Uniform temperature profile for a dense array CPV receiver under non uniform illumination profile. AIP Conf Proc 2014;1616:207–10. https://doi.org/10.1063/1.4897062.

[54] Laguna G, Azarkish H, Vilarrubí M, Ibañez M, Rosell J, Betancourt Y, et al. Microfluidic Cell Cooling System for Electronics. Therm Investig ICs Syst 2017:1–4.

[55] Sharma CS, Tiwari MK, Poulikakos D. A simplified approach to hotspot alleviation in microprocessors. Appl Therm Eng 2016;93:1314–23. https://doi.org/10.1016/j.applthermaleng.2015.08.086.

[56] McCarthy M, Tiliakos N, Modi V, Fr??chette LG. Thermal buckling of eccentric microfabricated nickel beams as temperature regulated nonlinear actuators for flow control. Sensors Actuators, A Phys 2007;134:37–46. https://doi.org/10.1016/j.sna.2006.05.027.

[57] M.A.Farahat. Improvement the thermal electric performance of a photovoltaic cells by cooling and concentration techniques. 39th Int Univ Power Eng Conf 2004;2:623–8.

[58] Lee S. Thermal challenges and opportunities in concentrated photovoltaics. 2010 12th Electron Packag Technol Conf EPTC 2010 2010:608–13. https://doi.org/10.1109/EPTC.2010.5702711.

[59] Mittelman G, Kribus A, Dayan A. Solar cooling with concentrating photovoltaic/thermal (CPVT) systems. Energy Convers Manag 2007;48:2481–90. https://doi.org/10.1016/j.enconman.2007.04.004.

[60] Antón I, Silva D, Sala G, Bett AW, Siefer G, Luque-Heredia I, et al. The PV-FIBRE Concentrator: A System for Indoor Operation of 1000X MJ Solar Cells 2007:431–47. https://doi.org/10.1002/pip.

[61] Micheli L, Reddy KS, Mallick TK. Plate micro-fins in natural convection: An opportunity for passive concentrating photovoltaic cooling. Energy Procedia 2015;82:301–8. https://doi.org/10.1016/j.egypro.2015.12.037.

[62] Gualdi F, Arenas O, Vossier A, Dollet A, Aimez V, Arès R. Determining passive cooling limits in CPV using an analytical thermal model. AIP Conf Proc 2013;1556:10–3. https://doi.org/10.1063/1.4822187.

[63] Kerzmann TL, Schaefer LA. An energy analysis of a linear concentrating photovoltaic system with an active cooling system. High Low Conc Syst Sol Electr Appl V 2010;7769:1–8. https://doi.org/10.1117/12.863908.

[64] Du B, Hu E, Kolhe M. Performance analysis of water cooled concentrated photovoltaic (CPV) system. Renew Sustain Energy Rev 2012;16:6732–6. https://doi.org/10.1016/j.rser.2012.09.007.

[65] Xu Z, Kleinstreuer C. Concentration photovoltaic-thermal energy co-generation system using nanofluids for cooling and heating. Energy Convers Manag 2014;87:504–12. https://doi.org/10.1016/j.enconman.2014.07.047.

[66] Han X, Wang Y, Zhu L. Electrical and thermal performance of silicon concentrator solar cells immersed in dielectric liquids. Appl Energy 2011;88:4481–9. https://doi.org/10.1016/j.apenergy.2011.05.037.

[67] Xu X, Meyers MM, Sammakia BG, Murray BT. Thermal modeling and life prediction of water-cooled hybrid concentrating photovoltaic/thermal collectors. J Sol Energy Eng Trans ASME 2013;135:1–8. https://doi.org/10.1115/1.4006965.

[68] Zhu L, Boehm RF, Wang Y, Halford C, Sun Y. Water immersion cooling of PV cells in a high concentration system. Sol Energy Mater Sol Cells 2011;95:538–45. https://doi.org/10.1016/j.solmat.2010.08.037.

[69] Zhu L, Wang Y, Fang Z, Sun Y, Huang Q. An effective heat dissipation method for densely packed solar cells under high concentrations. Sol Energy Mater Sol Cells 2010;94:133–40. https://doi.org/10.1016/j.solmat.2009.08.014.

[70] Royne A, Dey CJ. Design of a jet impingement cooling device for densely packed PV cells under high concentration. Sol Energy 2007;81:1014–24. https://doi.org/10.1016/j.solener.2006.11.015.

[71] Royne A, Dey CJ, Mills DR. Cooling of photovoltaic cells under concentrated illumination: A critical review. Sol Energy Mater Sol Cells 2005;86:451–83. https://doi.org/10.1016/j.solmat.2004.09.003.

[72] Jakhar S, Soni MS, Gakkhar N. Historical and recent development of concentrating photovoltaic cooling technologies. Renew Sustain Energy Rev 2016;60:41–59. https://doi.org/10.1016/j.rser.2016.01.083.

[73] Reis F, Guerreiro C, Batista F, Pimentel T, Pravettoni M, Wemans J, et al. Modeling the effects of inhomogeneous irradiation and temperature profile on CPV solar cell behavior. IEEE J Photovoltaics 2015;5:112–22. https://doi.org/10.1109/JPHOTOV.2014.2358080.

[74] Siaw FL, Chong KK. A systematic method of interconnection optimization for dense-array concentrator photovoltaic system. Sci World J 2013;2013. https://doi.org/10.1155/2013/275169.

[75] Spectrolab PV Cells. Triple-Junction Terrestrial Concentrator Solar Cells 2001. http://www.spectrolab.com/DataSheets/TerCel/tercell.pdf.

[76] Schnieders J. Comparison of the energy yield predictions of stationary and dynamic solar collector models and the models' accuracy in the description of a vacuum tube collector. Sol Energy 1997;61:179–90. https://doi.org/10.1016/S0038-092X(97)00036-4.

[77] Azarkish H, Barrau J, Coudrain P, Savelli G, Collin L-M, Frechette LG. Self-adaptive microvalve array for energy efficient fluidic cooling in microelectronic systems. Proc 16th Intersoc Conf Therm Thermomechanical Phenom Electron Syst (ITherm 2017) 2017:522–9.

[78] Laguna G, Barrau J, Fréchette L, Rosell J, Ibañez M, Vilarrubí M, et al. Distributed and self-adaptive microfluidic cell cooling for CPV dense array receivers. AIP Conf. Proc., vol. 1881, 2017. https://doi.org/10.1063/1.5001444.

[79] Siaw FL, Chong KK, Wong CW. A comprehensive study of dense-array concentrator photovoltaic system using non-imaging planar concentrator. Renew Energy 2014;62:542–55. https://doi.org/10.1016/j.renene.2013.08.014.

[80] Chemisana D, Rosell JI. Electrical performance increase of concentrator solar cells under Gaussian temperature profiles. Prog Photovoltaics Res Appl 2013;21:444–55. https://doi.org/10.1002/pip.1205.

[81] Haysom JE, Jafarieh O, Anis H, Hinzer K, Wright D. Learning curve analysis of concentrated photovoltaic systems. Prog Photovoltaics Res Appl 2015;23:1678–86. https://doi.org/10.1002/pip.2567.

[82] Ekins-Daukes NJ, Sandwell P, Nelson J, Johnson AD, Duggan G, Herniak E. What does CPV need to achieve in order to succeed? AIP Conf Proc 2016;1766. https://doi.org/10.1063/1.4962072.

[83] Jakhar S, Soni MS, Gakkhar N. Historical and recent development of concentrating photovoltaic cooling technologies. Renew Sustain Energy Rev 2016;60:41–59. https://doi.org/10.1016/j.rser.2016.01.083.

[84] Barrau J, Rosell J, Chemisana D, Tadrist L, Ibañez M. Effect of a hybrid jet impingement/micro-channel cooling device on the performance of densely packed PV cells under high concentration. Sol Energy 2011;85:2655–65. https://doi.org/10.1016/j.solener.2011.08.004.

[85] Riera S, Barrau J, Perona A, Dollet A, Rosell JI, Fréchette L. Uniform temperature profile for a dense array CPV receiver under non uniform illumination profile 2014;207:207–10. https://doi.org/10.1063/1.4897062.

[86] Barrau J, Rosell J, Ibañez M. Design of a hybrid jet impingement / microchannel cooling device for densely packed PV cells under high concentration. AIP Conf. Proc., vol. 1277, 2010, p. 74–7. https://doi.org/10.1063/1.3509236.

[87] Riera S, Barrau J, Omri M, Fréchette LG, Rosell JI. Stepwise varying width microchannel cooling device for uniform wall temperature: Experimental and numerical study. Appl Therm Eng 2015;78:30–8. https://doi.org/10.1016/J.APPLTHERMALENG.2014.12.012.

[88] Cooper T, Pravettoni M, Cadruvi M, Ambrosetti G, Steinfeld A. The effect of irradiance mismatch on a semi-dense array of triple-junction concentrator cells. Sol Energy Mater Sol Cells 2013;116:238–51. https://doi.org/10.1016/j.solmat.2013.04.027.

[89] Vivar M, Antón I, Sala G. Radial CPV receiver. Prog Photovoltaics Res Appl 2010;18:353–62. https://doi.org/10.1002/pip.921.

[90] Wong C-W, Chong K-K, Tan M-H. Performance optimization of dense-array concentrator photovoltaic system considering effects of circumsolar radiation and slope error. Opt Express 2015;23:A841. https://doi.org/10.1364/oe.23.00a841.

[91] Spectrolab. C4MJ: CPV Point Focus Solar Cells 2011:2.

[92] Mellor A, Domenech-Garret JL, Chemisana D, Rosell JI. A two-dimensional finite element model of front surface current flow in cells under non-uniform, concentrated illumination. Sol Energy 2009;83:1459–65. https://doi.org/10.1016/j.solener.2009.03.016.

[93] Kinsey GS, Hebert P, Barbour KE, Krut DD, Cotal HL, Sherif RA. Concentrator Multijunction Solar Cell Characteristics Under Variable Intensity and Temperature. Prog Photovolt Res Appl 2008;16:503–8. https://doi.org/10.1002/pip.834.

[94] Spectrolab PV Cells. CPV Point Focus Solar Cells 2011. https://www.spectrolab.com/DataSheets/PV/CPV/C4MJ_40_Percent_Solar_Cell.pdf.

[95] Tuckerman DB, Pease RFW. High-performance heat sinking for VLSI. IEEE Electron Device Lett 1981;2:126–9. https://doi.org/10.1109/EDL.1981.25367.

[96] Fernández Vilella Á. Analysis of the effects of non-uniform irradiance and temperature on a CPV dense array output power cooled by microchannels and microfluidic cells 2017.

[97] Amnache A, Collin LM, Laguna G, Vilarrubi M, Hamel S, Barrau J, et al. Thermoregulated Microvalve for Self-Adaptive Microfluidic Cooling. THERMINIC 2018 - 24th Int Work Therm Investig ICs Syst Proc 2018;2018:1–6. https://doi.org/10.1109/THERMINIC.2018.8593280.

[98] Sharma CS, Tiwari MK, Michel B, Poulikakos D. Thermofluidics and energetics of a manifold microchannel heat sink for electronics with recovered hot water as working fluid. Int J Heat Mass Transf 2013;58. https://doi.org/10.1016/j.ijheatmasstransfer.2012.11.012.

[99] Kandlikar SG, Bapat A V. Evaluation of jet impingement, spray and microchannel chip cooling options for high heat flux removal. Heat Transf Eng 2007;28:911–23. https://doi.org/10.1080/01457630701421703.

[100] Fernández Á, Laguna G, Rosell J, Vilarrubí M, Ibañez M, Sisó G, et al. Assessment of the impact of non-uniform illumination and temperature profiles on a dense array CPV receiver performance. Sol Energy 2018;171:863–70. https://doi.org/10.1016/j.solener.2018.07.001.